

NATIVE ION MOBILITY-MASS SPECTROMETRY TECHNIQUES FOR
CHARACTERIZING THE STRUCTURE AND LIPID BINDING OF BACTERIAL
PORE-FORMING TOXINS.

by

JESSE WILLIAM WILSON

A DISSERTATION

Presented to the Department of Chemistry and Biochemistry
and the Graduate School of the University of Oregon
in partial fulfillment of the requirements
for the degree of
Doctor of Philosophy

June 2020

DISSERTATION APPROVAL PAGE

Student: Jesse William Wilson

Title: Native Ion Mobility-Mass Spectrometry Techniques for Characterizing the Structure and Lipid Binding of Bacterial Pore-Forming Toxins.

This dissertation has been accepted and approved in partial fulfillment of the requirements for the Doctor of Philosophy in the Department of Chemistry and Biochemistry by:

Michael Harms	Chairperson
James Prell	Advisor
Cathy Wong	Core Member
Philip Washbourne	Institutional Representative

and

Kate Mondloch	Interim Vice Provost and Dean of the Graduate School
---------------	--

Original approval signatures are on file with the University of Oregon Graduate School.

Degree awarded June 2020

© 2020 Jesse William Wilson
This work is licensed under a Creative Commons
Attribution 4.0 International (CC BY 4.0)



DISSERTATION ABSTRACT

Jesse William Wilson

Doctor of Philosophy

Department of Chemistry and Biochemistry

June 2020

Title: Native Ion Mobility-Mass Spectrometry Techniques for Characterizing the Structure and Lipid Binding of Bacterial Pore-Forming Toxins.

Membrane proteins constitute a large portion of the protein and protein complexes found across life and perform a diverse range of critical functions such as transport of molecules and signaling across lipid bilayers. However, due to the instability of membrane proteins in solution without a membrane-like environment and the heterogeneity of such samples, study of these types of complexes can be incredibly challenging using conventional techniques such as X-ray crystallography, nuclear magnetic resonance, or electron microscopy.

In the last couple of decades, native mass spectrometry with electrospray ionization has emerged as an alternative technique in structural biology for the study of soluble and membrane protein complexes alike. The unique advantage of native mass spectrometry is that non-covalent interactions can be retained from solution to the gas-phase environment of the mass spectrometer. Meaning that stoichiometry information from membrane proteins such as the oligomeric state and small molecule and lipid binding can be investigated based on the mass distributions of these complexes. When coupled with ion mobility spectrometry, not only is stoichiometry information obtained, but also size and shape information that can be utilized to better understand the structures

of biomolecules from solution and compared to structures determined using the above-mentioned techniques.

Here, studies in native mass spectrometry technique development are presented in the investigation of bacterial transmembrane pore forming toxins. As membrane proteins, these complexes pose several challenges to native mass spectrometry due to the inherent heterogeneity and polydispersity in mass caused by the associated membrane mimetic used, such as detergent micelles or lipoprotein nanodiscs. Using native mass spectrometry α HL from *Staphylococcus aureus* is found to form both hexameric and heptameric complexes in solution simultaneously, while other structural techniques had predominantly identified the heptameric complex.

CURRICULUM VITAE

NAME OF AUTHOR: Jesse William Wilson

GRADUATE AND UNDERGRADUATE SCHOOLS ATTENDED:

University of Oregon, Eugene
George Fox University

DEGREES AWARDED:

Doctor of Philosophy, 2020, University of Oregon
Bachelor of Science, Biochemistry, 2014, George Fox University

AREAS OF SPECIAL INTEREST:

Native Ion Mobility-Mass Spectrometry
Membrane Protein Biochemistry

PROFESSIONAL EXPERIENCE:

Graduate Teaching Fellowship, Chemistry, 2014-2015, 2017 to present

GRANTS, AWARDS, AND HONORS:

National Institutes of Health Molecular Biology and Biophysics Training Grant,
2015-2017

PUBLICATIONS:

Wilson, J.W.; Donor, M.T.; Shepherd, S.O.; Prell, J.S. Increasing Collisional Activation of Protein Complexes Using Smaller Aperture Source Sampling Cones on a Synapt Q-IM-TOF Instrument with a Stepwave Source. Submitted to *J. Am. Soc. Mass Spectrom.* **2020**.

Wilson, J.W.; Rolland, A.D.; Klausen, G.M.; Prell, J.S. Ion Mobility-Mass Spectrometry Reveals that α -Hemolysin from *Staphylococcus aureus* Simultaneously Forms Hexameric and Heptameric Complexes in Detergent Micelle Solutions. *Anal. Chem.* **2019**, *91*, 10204-10211.

Cunningham, R.M.; Hickey, A.; Wilson J.W.; Plakos, K.; DeRose, V.J. Pt-Induced Crosslinks Promote Target Enrichment and Protection from Serum Nucleases. *J. Inorg. Biochem.* **2018**, *189*, 124-133.

Ewing, S.A.; Donor, M.T.; Wilson, J.W.; Prell, J.S. Collidoscope: An Improved Tool for Computing Collisional Cross Sections with the Trajectory Method. *J. Am. Soc. Mass Spectrom.* **2017**, *28*, 587-596.

ACKNOWLEDGMENTS

I would like to sincerely thank Professor James Prell for being my advisor and giving me the opportunity to investigate challenging problems under his mentorship. His efforts certainly made this research possible. I would also like to thank my committee members, Professors Michael Harms, Cathy Wong, and Philip Washbourne who consistently challenged and encouraged me to keep going in my research. I would additionally like to thank all the members of the Prell lab for their input and help on my work. I have had the pleasure to work closely with several Prell lab members and it has always been a positive work and research environment. The research reported in this work was supported by the National Institute of Allergy and Infectious Diseases (award number R21AI125804-02) and the National Institute of General Medical Sciences (training grant award number 2T32GM007759-39 to J.W.W.) of the National Institutes of Health. This content is solely the responsibility of the authors and does not necessarily represent the official views of the National Institutes of Health.

TABLE OF CONTENTS

Chapter	Page
I. INTRODUCTION	1
Methods for the Study of Protein Structure	2
X-Ray Crystallography	3
Nuclear Magnetic Resonance	3
Cryo-Electron Microscopy.....	5
Mass Spectrometry.....	6
Native Mass Spectrometry as a Structural Biology Technique for the Study of Protein Complex Stoichiometry	9
Ion Mobility Spectrometry.....	11
Application of Native-MS to Membrane Proteins	12
II. ION MOBILITY-MASS SPECTROMETRY REVEALS THAT α -HEMOLYSIN FROM STAPHYLOCOCCUS AUREUS SIMULTANEOUSLY FORMS HEXAMERIC AND HEPTAMERIC COMPLEXES IN DETERGENT MICELLE SOLUTIONS	17
Introduction.....	17
Methods.....	20
Results and Discussion	21
α HL forms both hexameric and heptameric pore-like complexes in C ₈ E ₄ detergent micelles.....	21
Native mass spectra of α HL complexes embedded in FOS-14 detergent micelles confirms solution hexameric and heptameric pore-like complexes	22

Chapter	Page
α HL pore-like ion stoichiometry is consistent across mass spectrometer platforms	26
IM-MS collision cross section measurements and MD-simulated collision cross section calculations of stripped heptameric and hexameric complexes reveal compact native state	30
Conclusions.....	34
<p>III. INCREASING COLLISIONAL ACTIVATION OF PROTEIN COMPLEXES USING SMALLER APERTURE SOURCE SAMPLING CONES ON A SYNAPT Q-IM-TOF INSTRUMENT WITH A STEPWAVE SOURCE.....</p>	
	38
Introduction.....	38
Methods.....	40
Results and Discussion	40
Conclusions.....	45
<p>IV. NON-SPECIFIC BINDING OF LIPID HEAD GROUPS TO SOLUBLE PROTEINS AND α-HEMOLYSIN LIPID BINDING IN DETERGENT-LIPID MICELLES AND LIPOPROTEIN NANODISCS.....</p>	
	47
Introduction.....	47
Methods.....	51
Sample Preparation	51
Native IM-MS.....	53
Data Analysis.....	53
Results and Discussion	54

Chapter	Page
Lipid headgroups readily adduct to native transferrin protein ions in nESI	54
Mixed lipid headgroup studies reveals PS outcompetes other lipid headgroups for transferrin association	57
Only GPC removes charge when dissociated and is consistent across mixtures of headgroups	60
Lipid binding studies of α HL complexes oligomerized in C ₈ E ₄ detergent micelles	61
α HL lipoprotein nanodisc complexes	64
Conclusions.....	67
OUTLOOK	70
APPENDICES	73
A. SUPPLEMENTAL INFORMATION FOR CHAPTER II.....	73
B. SUPPLEMENTAL INFORMATION FOR CHAPTER III.....	89
C. SUPPLEMENTAL INFORMATION FOR CHAPTER IV.....	100
REFERENCES CITED.....	106

LIST OF FIGURES

Figure	Page
1. Native mass spectrum of PA prepore complexes	10
2. Native mass spectrum of PA _x (LF _N) _y complexes.	14
3. Native mass spectra of αHL hexamer and heptamer complexes	22
4. Native mass spectrum of αHL micelle-embedded complexes in FOS-14 detergent	25
5. Native mass spectrum from the Orbitrap instrument of αHL micelle-embedded complexes in FOS-14 detergent.....	27
6. Comparison between collision cross section measurements in both detergents and computationally derived CCSs.....	30
7. Compilation of all measured and computationally predicted CCS values for αHL hexamers and heptamers.....	33
8. GroEL desalting and unfolding with each source sampling cone aperture size	41
9. Simulated ion heating of BSA ¹⁵⁺	43
10. Mass spectra of αHL complexes in FOS-14 micelles with each source sampling cone.....	44
11. Native mass spectra of transferrin and common lipid headgroups	55
12. Deconvolved native mass spectra of transferrin with common lipid headgroups	56
13. Selected deconvolved mass spectra of transferrin ¹⁹⁺ with phosphoserine.....	59
14. Weighted average loss of charge of isolated transferrin ¹⁹⁺ as lipid headgroups are dissociated.....	61
15. αHL complexes oligomerized in C ₈ E ₄ detergent micelles with 1 mM DMPC lipids added	62
16. αHL complexes oligomerized in C ₈ E ₄ detergent micelles with 200 μM of the designated lipid added to solution.....	63

Figure

Page

17. α HL complexes inserted into POPC MSP1D1 nanodiscs and ejected using 5% glycerol carbonate.....	65
--	----

CHAPTER I

INTRODUCTION

While determining the primary structure of a protein is often performed by gene sequencing or proteomic analysis where the protein can be analyzed before translation or as peptide fragments,¹ determining higher levels of structure including the stoichiometry of protein complexes requires preservation of not only the covalent bonding between amino acids but also the plethora of non-covalent interactions.²⁻⁵

Membrane proteins present even further opportunities for investigating non-covalent interactions between proteins and small molecules due to their association with or insertion into lipid bilayers.⁶ Biological membranes are composed of several different types of lipids and membrane proteins that are laterally heterogeneous.⁷ A focus of structural biology of biological membranes is understanding the biophysical basis for this lateral heterogeneity and the physiological role heterogeneity plays at the few-nanometer size scale between membrane proteins and lipids. The membrane raft hypothesis has been proposed as a model to describe the preferential association between cholesterol, saturated lipids, and certain membrane proteins.^{8,9} However, the physiological role of such order remains unclear and direct detection of such organization between membrane proteins and lipids on the nanoscale is a subject of investigation by structural biology.⁷

Transmembrane proteins are unstable outside of lipid bilayers due to the hydrophobic character of the transmembrane region. While primary and secondary structural studies of membrane proteins can be performed under denaturing solution

conditions and through modeling.^{10,11} Understanding membrane protein tertiary and quaternary structures and their association with lipids at the nanoscale level requires lipid bilayers or membrane mimetics (detergent micelles or lipoprotein nanodiscs for example) to preserve native-like structures.¹²⁻¹⁴ The inherent heterogeneity and polydispersity these systems creates in terms of the types and number of protein subunits, lipids, and detergents is challenging to study by the traditional techniques used in structural biology. Many membrane proteins have been shown to have specific protein-lipid interactions that have a functional role.^{7,13,15,16} Thus, broadening the tool set of structural biology to handle the preservation of non-covalent interactions between membrane proteins and lipids at the nanoscale is of importance.

Several biophysical techniques have been developed to probe not only the primary structure, but the non-covalent interactions proteins form in their folded forms and with small molecules, including membrane proteins with lipids. The focus of this dissertation is the technique development of native mass spectrometry as an emerging tool in structural biology for both soluble and membrane proteins, but before this discussion, other structural techniques should be discussed as they relate to soluble and in particular membrane proteins and complexes.

Methods for the Study of Protein Structure

Several techniques have been established to probe protein structure; four of the most common techniques include X-ray crystallography¹⁷, nuclear magnetic resonance (NMR),¹⁸ single particle cryo-electron microscopy (cryo-EM)^{19,20}, and mass spectrometry (MS).²¹

X-Ray Crystallography. The high resolution achievable by X-ray crystallography has made this technique the standard-bearer for structural biology for many years.²² The structures for thousands of soluble proteins have been solved at atomic resolution and deposited in the Protein Data Bank, which includes structures from other biophysical techniques as well (NMR, cryo-EM).²³

Determining the structure of a membrane protein by X-ray crystallography is notoriously difficult due to the challenge of forming membrane protein crystals and resolving clear protein-lipid interactions is additionally challenging.²⁴⁻³⁰ Annular lipids that surround the surface of the transmembrane region of membrane proteins are often disordered, and thus difficult to resolve the identities of lipids surrounding the membrane protein. Of the membrane protein examples with crystal structures, only a few structures have resolved lipids.^{16,27,28,31,32} Recently, there have been advances in crystallization methods for membrane proteins using smaller sized crystals than would previously be feasible,^{25,26} and more structures are being produced with resolved lipids bound to membrane proteins, such as ammonia channel from *E. coli* with bound phosphatidylglycerol lipids.¹⁶ However, X-ray crystallography alone is incapable of producing structures for every protein complex where disorder (such as protein-lipid interactions or intrinsically disordered proteins (IDP)) may be of importance for understanding protein function.

Nuclear Magnetic Resonance. Nuclear Magnetic Resonance (NMR) is another commonly used technique in structural biology and has been applied to both soluble and membrane proteins. In contrast to X-ray crystallography NMR is typically a solution based structural determination method that more readily allows for the study of ensemble

properties of biomolecules meaning that protein dynamics can be probed as well as structure.^{33,34} The isotopes ^1H , ^{13}C , ^{15}N and ^{31}P are the typical atoms probed in protein NMR due to their high abundance in biological molecules and isotope labeling of molecules aids analysis of protein-lipid interactions.³⁵

The versatility of NMR is exemplified in the range of sample types amenable to this technique as a tool for characterizing the structures, dynamics, and small molecule binding of proteins.^{13,36} NMR has been used to determine high-resolution structures of monomeric proteins^{18,37,38} and has been applied to small membrane proteins in detergent micelles, detergent-lipid micelles, and lipoprotein nanodiscs.^{36,39-41} These studies allow for NMR to probe structural and dynamical changes in membrane proteins based on the lipid environment and the identities of included lipids.^{40,42} Recently, solid-state NMR has advanced significantly as a technique to study membrane proteins in lipid-bilayers without detergents or other restrictions based on the membrane mimetic used for solubility in solution based NMR.⁴²⁻⁴⁴ For instance, solid-state NMR has even been used to determine an atomic-resolution structure of *Anabaena* sensory rhodopsin in a mix of phosphocholine and phosphatidic acid liposomes.⁴⁵

NMR of biological samples is hampered by limitations in the protein size that can be studied, and the high protein concentrations necessary for detection.^{2,46} The typical current size limit for high-resolution NMR structural determination is about 35 kDa,⁴⁷ but example structures from larger proteins have been produced (up to ~80 kDa).^{45,48} NMR also struggles to determine the range of stoichiometries possible for a protein complex. Another major hurdle for structural characterization with NMR is the concentration of protein necessary. Protein NMR often requires 0.5 mM or greater protein concentrations

that can lead to solution instability and significant challenges in protein purification for large complexes. Additionally, these high concentrations may lead to the spurious association of molecules in NMR that have no physiological relevance.

Cryo-Electron Microscopy. Electron microscopy (EM) as a technique has been applied to biological samples for several decades with single-particle cryo-EM, more specifically, emerging as a method for protein structural characterization in the 1980's.^{49,50} Rather than determining structures from diffraction of proteins arranged in crystal structures, single-particle cryo-EM computationally combines images of individual complexes arranged in random orientations to produce three-dimensional structures.

With this approach, purified proteins or complexes in buffer solutions are applied to holey carbon film coated EM grids. These prepared grids are then plunged into liquid ethane cooled by liquid nitrogen to produce a thin layer of vitreous ice that kinetically traps native structures and prevents dehydration of samples in the vacuum chamber of the electron microscope. An electron beam and camera are then used to image individual particles. For high resolution structures, often hundreds of thousands of images of particles are collected and classified based on orientation and/or conformational state and combined to form a Coulomb potential density map that can be interpreted similarly as electron density maps from X-ray crystallography.⁵⁰

Due to the imaging of single particles with cryo-EM and ever-increasing resolution capabilities, this method has emerged as a revolutionary tool in structural biology.^{19,51,52} Several recent atomistic structures of membrane proteins have been produced in various membrane mimetics such as detergent micelles and lipoprotein

nanodiscs that would not be feasible by crystallography or NMR.^{50,53–58} Many of these reports assign electron density to lipids binding to specific sites in these structures that are thought to have a functional role.^{54,56,59} Additionally, through classification of particle images in varying conformations, cryo-EM has also taken steps towards understanding protein dynamics, including for transmembrane ion channels.^{55,60}

The instrumentation costs and instrumental/computational times associated with cryo-EM can be limiting factors for structure determination.⁶¹ Another major limitation to cryo-EM is that protein complexes must be of sufficient size for a high-resolution structure to be determined, typically ~100 kDa, which is larger than the average size protein.⁶² To counter these size restrictions, fragment antigen binding (Fab) as a method to add mass and aid image alignment by formation of a stable and rigid complex between a Fab and a target protein.^{55,63} These size limitations are the opposite problem in comparison to NMR, where large complexes are intractable, but small proteins can have structures determined at high-resolution. Additionally, while some tightly bound lipids can be resolved with cryo-EM determining protein-lipid interactions out to a few nanometers remains intractable.

Mass Spectrometry. Broadly, MS has been applied to the study of proteins at all levels of structure, from determining the primary amino acid sequence and post translational modifications of proteins in proteomics, to studying non-covalent interactions of large multisubunit transmembrane complexes.^{15,64} MS fundamentally relies on the ionization of analyte molecules, including intact proteins, and measures mass as a ratio of the mass of a molecule (m) divided by the molecule's charge (z). Hence in MS, raw mass spectra are collected with analyte ions measured in m/z , from which if

the charge is known (usually determinable from the mass spectrum) the mass of an analyte is measured.⁶⁵

As mentioned, ionization of compounds is a prerequisite for mass analysis. There are several ionization methods that are commonly divided into two groupings based on whether the ionization process causes fragmentation of covalent bonds. Electron impact (EI) for example, bombards molecules with high energy electrons that often fragment molecules. EI is commonly applied to analysis of samples containing small molecule organics because these molecules fragment in reproducible patterns, and samples containing mixtures of organics can be separated using gas chromatography before ionization and analysis with MS.⁶⁵ The “soft ionization” methods of matrix assisted laser desorption ionization (MALDI) and electrospray ionization (ESI) do not tend to fragment molecules upon ionization, thus allowing for analysis of intact biomolecules and complexes.⁶⁵ Both MALDI and ESI will be further explained below because these ionization methods are the most used methods for analysis of biomolecules, including proteins.

With MALDI biomolecules are mixed with a matrix compound that is often a weak acid and dried on a plate.⁶⁶ This plate is then sealed in a vacuum chamber with the mass spectrometer source. A pulsed laser is focused on the sample and the matrix absorbs the laser radiation and transfers a proton to the analyte of interest. The ionized analyte molecules then enter the mass spectrometer for mass analysis. MALDI is a very simple and fast method for protein characterization because the protein ions produced are typically singly charged, thus in the mass spectrum peaks appear at the mass of the protein being analyzed as long as the mass spectrometer is properly calibrated (this can

be difficult beyond a few 10s of kDa). MALDI can also be a useful method for looking at mass distributions of heterogenous samples that vary in the base mass, such as therapeutic proteins that have been labelled with polyethylene glycol groups,⁶⁷ or polymers with various size distributions.⁶⁸ With MALDI however, non-covalent interactions are often too weak to withstand the sample desiccation and ionization process, thus protein complexes and ligand binding are not typically observed with MALDI.⁶⁹ The potential loss of non-covalent interactions limits the application of MALDI to structural biology.

With ESI biomolecules are ionized and transferred directly from solution to the gas phase of the mass spectrometer instrument.⁷⁰ This is done by applying a voltage difference from a thin metal or glass capillary with solutions containing the analyte to the source of the mass spectrometer. The voltage difference pulls solution out of the capillary to form charged droplets that are rapidly de-solvated and kinetically trapped on the microsecond timescale as these droplets are accelerated through gas at atmospheric pressure and into vacuum. As the droplets evaporate charges are transferred to the analyte molecules forming ions that can be analyzed with the mass spectrometer. Solutions are normally composed of polar solvents that keep bio-analytes soluble. In comparison to MALDI where proteins are typically singly charged, in ESI proteins will have multiple charges that can vary to form a charge state distribution. Liquid chromatography is often combined with ESI such that complex mixtures in samples can be separated before ionization and mass analysis. ESI solution conditions and flow parameters can be setup to denature proteins and other biomolecules for simple measurement of the base mass of molecules (similar to MALDI experiment), or as will be described in the next section and

throughout this dissertation, can be applied to proteins under native conditions with the goal to maintain non-covalent interactions.

Native Mass Spectrometry as a Structural Biology Technique for the Study of Protein Complex Stoichiometry.

The goal of native-MS is to maintain the non-covalent interactions of biomolecules from solution into the gas phase of the mass spectrometer,⁷¹ Ideally this means biomolecules like proteins remain compact and the stoichiometry of protein complexes and associated ligands can be measured in native-MS.

Native-MS commonly uses a version of ESI known as nano-ESI (nanoliter/minute flow rates) to ionize proteins from solution.⁷⁰ Nano-ESI is done with capillaries that have small openings of a few micrometers, and is sometimes coupled to ultra-high performance liquid chromatography (UPLC). However, most commonly the nanoliter/minute flow rate can be established simply due to the potential difference between the capillary and the entrance of the instrument. Nano-ESI greatly improves the ionization efficiency of proteins in solution over other solution components and uses significantly less sample due to the low flow rates such that a few-microliters of sample can be sprayed for multiple hours.⁷²

The combination of native-MS with other structural techniques can be a powerful union. An example of a native mass spectrum is shown in Figure 1 of protective antigen (PA) heptameric and octameric complexes. PA is a component of anthrax toxin from *Bacillus anthracis*. Anthrax toxin is a tricomponent pore forming toxin (PFT). PA oligomerizes to form a prepore complex that undergoes a conformational change to form a transmembrane β -barrel pore structure.⁷³

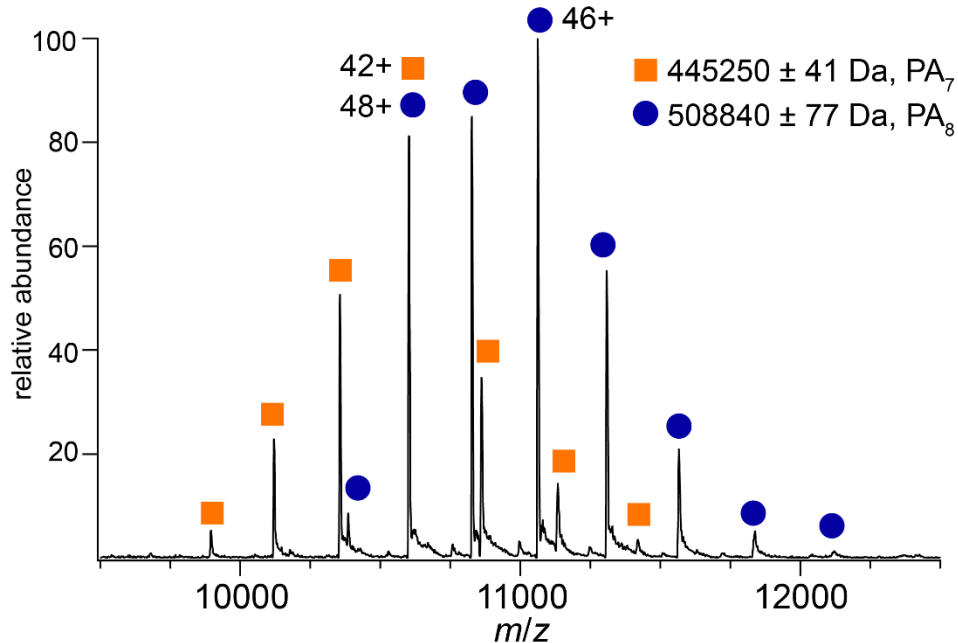


Figure 1. Native mass spectrum of PA prepore complexes at pH 8.0 collected on a Thermo Exactive Extended Mass Range Orbitrap instrument. From this spectrum heptameric and octameric complexes are clearly identified based on the measured masses. Additionally, the difference in the measured masses between the identified heptamers and octamers corresponds to the mass of a PA monomer (63.6 kDa). For each oligomer a narrow charge state distribution is formed that is typical of native-MS suggesting a compact native-like state.

X-ray crystallography had identified that PA forms heptameric rings in the prepore conformation and this protein complex was thought to only form as a heptamers for many years.⁷⁴ However, cryo-EM and native-MS experiments of PA prepores identified an octameric complex in solution simultaneously with the heptamer.^{75,76} These experiments also found that the octameric complex played a functional role. PA heptamers convert to the transmembrane pore form at pH ~ 7.2 and below. Outside of a membrane environment the pore complex is very unstable and prone to aggregation. It was found using native-MS, that octameric complexes resist pore formation at lower pH in comparison to the heptameric complexes. This greater pH stability for the octamer

could be important for PA oligomerization in blood plasma, with octameric complexes less likely to prematurely form pore complexes.⁷⁶ Crucially, this example demonstrates that X-ray crystallography acted as a purification method, allowing for only detection of the heptameric structure while excluding the octamer, while native-MS detects both forms simultaneously in solution.

Ion Mobility Spectrometry. Ion mobility spectrometry (IMS) is an allied technique to mass spectrometry that is often combined in native and non-native MS to measure size and shape information about analyte ions in the gas phase, or as a separation technique to aid analysis of congested mass spectra.⁷⁷⁻⁷⁹ IMS is a gas-phase electrophoretic technique where ions are pulled with an electric field through a drift cell filled with a neutral gas such as nitrogen or helium. Collisions with these gas particles creates a drag force on ions that correlates with their size and charge, such that more compact or higher charge ions move faster through the drift cell than extended or lower charge ions. This allows for ions with the same m/z ratio to be separated by IMS before mass analysis.

Additionally, the time an ion takes to traverse the drift cell can be measured accurately and precisely. This is called the drift time (DT), and the DT can be converted to a collision cross section (CCS) value, which is somewhat like the “surface area” of the ion and has units of area. Because ions rapidly tumble as they drift through the IM cell, CCS measurements are rotationally averaged values.⁷⁷ A CCS measurement from IMS can be compared to computed CCSs from structures determined from X-ray crystallography, NMR, or cryo-EM to report on the compactness or conformational state of protein complexes in native-MS.⁸⁰⁻⁸³ Thus the combination of IMS with MS (IM-MS)

under native conditions constitutes a powerful toolset for the study of protein complexes, including membrane proteins, in concert with the more traditional techniques in structural biology of X-ray crystallography, NMR, and cryo-EM.^{84,85} Although in native-MS a high-resolution atomic structure for a protein complex cannot be obtained, native-IM-MS can provide stoichiometry and structural information for proteins and protein complexes that are very difficult to study by the other techniques mentioned, even when tens of hundreds of different analytes are present in the same sample.⁸⁶⁻⁹¹ For instance intrinsically disordered proteins (IDP), which are notoriously difficult to study due to their heterogenous structures, can be probed with IM-MS to gain understanding of the structural dynamics of these proteins.⁹²⁻⁹⁴ Additionally, chemical cross-linking MS analysis of protein complexes has been combined with native-MS as a method to gain further understanding of how protein subunits may be arranged and to identify contact surfaces.⁹⁵⁻⁹⁷

Application of Native-MS to Membrane Proteins. Many studies highlight the power of native-MS to preserve solution structure and study non-covalent interactions in the gas phase of mass spectrometers.^{21,72,85,98-101} Over the last decade and a half native-MS has been applied to the study of membrane proteins and protein-lipid interactions in several types of membrane mimetics. These studies include membrane proteins solubilized in detergent micelles,^{15,16,102-108} bicelles,¹⁰⁹ amphipoles,¹⁰⁹ lipoprotein nanodiscs,^{89,90,109-112} and vesicles formed from native membranes.^{113,114} From these studies, native-MS has been used to define the oligomeric state and stoichiometry of protein complexes,¹¹³ measure binding constants between membrane proteins and lipids,^{16,107,108,115,116} and inform other structural studies such as X-ray crystallography

with resolved lipids bound to a membrane protein.¹⁶ The majority of these studies were performed with membrane proteins that are relatively small with most complexes under ~120 kDa (ammonia channel trimer from *E. coli*). However, many transmembrane complexes are larger and have greater variability in the stoichiometry of protein subunits.

Although the native mass spectrum in Figure 1 is well-resolved and readily interpretable, this is not always the case in native-MS,^{87,91,117-119} especially with membrane protein complexes that have heterogenous mass populations due to the membrane mimetic used. Figure 2 below builds upon the spectrum in Figure 1 and highlights some of the complexities that can occur in native-MS. PA prepore complexes bind another protein named lethal factor (LF, note: non-toxic N-terminal binding domain denoted as LF_N), which is one of the cytotoxic effectors of anthrax toxin. The spectrum in figure 2 was collected with a sample of PA_x(LF_N)_y prepore complexes that were treated with high concentrations of urea to transition to the pore form for insertion into 1,2-dimyristoyl-sn-glycero-3-phosphocholine (DMPC) lipid nanodiscs.¹²⁰⁻¹²² The goal of this spectrum is to resolve lipid association on pore form PA_x(LF_N)_y complexes, but most of the mass spectrum is poorly resolved. Between ~10000-15000 *m/z* distinguishable peaks are seen allowing for charge state and mass assignment (see expansion of this region as the top portion of Figure 2). Three of these distributions can be assigned to octameric PA complexes with 2-4 LF_N proteins bound. None of the identified distributions correspond to a possible mass distribution of the PA heptamer with LF_N bound suggesting that the octameric complexes are in the prepore conformation and that the heptameric complexes have converted to the pore form and have either aggregated or are nanodisc embedded and are poorly resolved. Additionally, there are identified charge state and mass

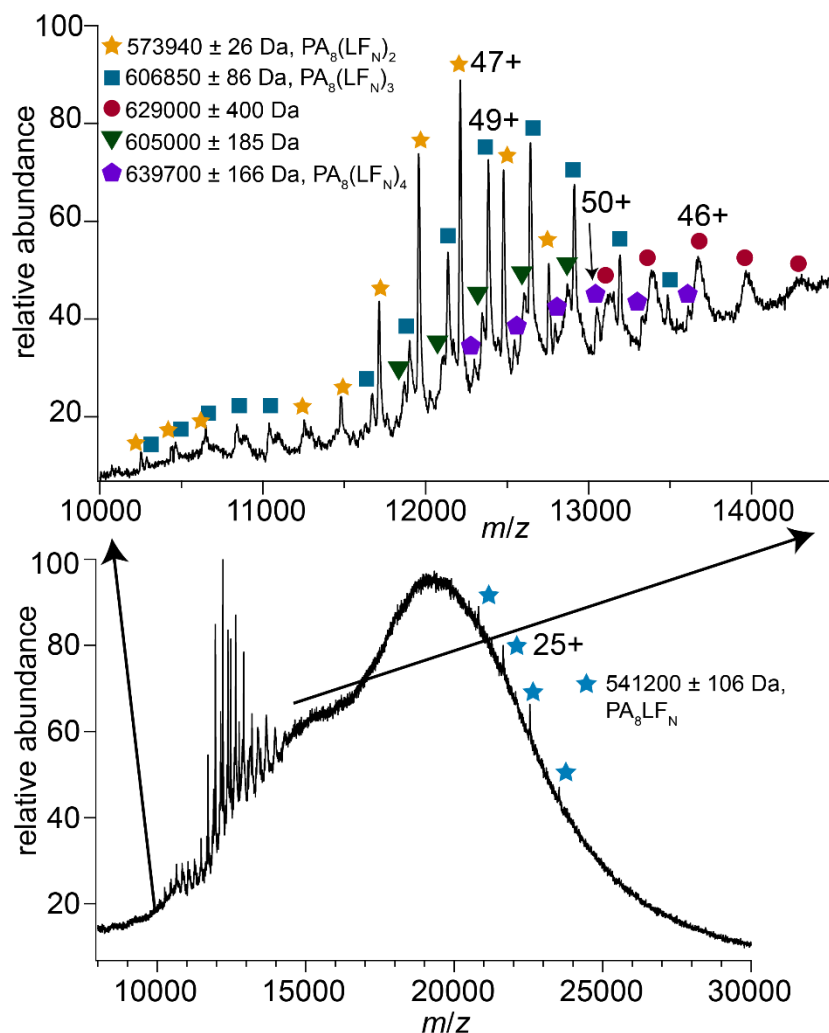


Figure 2. Bottom: Native mass spectrum of PA_x(LFN)_y complexes that could be nanodisc embedded. The top spectrum is an expansion of the resolved complexes from the bottom spectrum. In this expansion of the spectrum octameric complexes with LFN are identified based on the measured masses. Further gas-phase collisional activation would be unhelpful since collisional induced dissociation of PA₈(LFN)₂ complexes to form PA₈LFN complexes are already detected at ~20000 *m/z* (Bottom spectrum blue stars). Thus, increased activation would further dissociate complexes without obtaining new information.

distributions that cannot be readily assigned based on a known stoichiometry of PA_x(LFN)_y complexes. This could be caused by the association of lipids and/or the membrane scaffold protein (MSP) from the nanodiscs, but further analysis is hampered by the low spectral resolution caused by the overlap of multiple distributions.

In mass spectrometry, ions can be accelerated within a collision cell in the mass spectrometer instrument that is filled with neutral gas particles where the ions collide with the gas. These collisions slowly heat ions leading to the breaking of non-covalent interactions and the dissociation of adducts (salts, detergents, lipids etc.). This process termed “collisional activation” can “clean ions” such that they have narrower mass spectral peaks that are easier to analyze, but this process also leads to the gas-phase unfolding and collision induced dissociation (CID) of protein subunits in a protein complex.²¹ The mass spectrum in Figure 2 was obtained under instrumental conditions with significant collisional activation such that CID of octameric complexes are already observed. Thus, further activation would not aid mass spectral quality and the ability to observe lipid binding on any pore form toxin complexes. This dissertation is focused on the further development of native-MS approaches to better handle the types of difficult-to-study large membrane protein-lipid complexes exemplified in Figure 2 and the complications that arise with increased size (several hundred kDa) of membrane protein complex studied.

In Chapter 2, I will discuss native IM-MS experiments to study the structure and pore formation of α -hemolysin (α HL), another β -barrel PFT similar in structure to the PA pore formed in anthrax toxin that again highlights the power of IM-MS as a structural biology technique. This Chapter includes co-authored material from Amber D. Rolland, Grant M. Klausen, and James S. Prell. In Chapter 3, I discuss mass spectrometer instrumental modifications to extend the range of collisional activation achievable in the source region of Synapt “Stepwave” based mass spectrometer instruments and how these modifications aid analysis of membrane protein complexes. This chapter includes co-

authored material from Micah T. Donor, Samantha O. Shepherd, and James S. Prell. Lastly in Chapter 4, I discuss the possibility of non-specific association of lipids to proteins in native-MS due to the gas-phase basicity and polar nature of common lipid headgroups and the ramifications of such associations, as well as present studies of lipid binding to α HL pores in detergent-lipid micelles and lipoprotein nanodiscs. This chapter will include co-authored material from Micah T. Donor, Samantha O. Shepherd, Amber D. Rolland, and James S. Prell.

CHAPTER II

ION MOBILITY-MASS SPECTROMETRY REVEALS THAT α -HEMOLYSIN FROM STAPHYLOCOCCUS AUREUS SIMULTANEOUSLY FORMS HEXAMERIC AND HEPTAMERIC COMPLEXES IN DETERGENT MICELLE SOLUTIONS

Includes co-authored material from:

Wilson, J.W.; Rolland, A.D.; Klausen, G.M.; Prell, J.S. Ion Mobility-Mass Spectrometry Reveals that α -Hemolysin from *Staphylococcus aureus* Simultaneously Forms Hexameric and Heptameric Complexes in Detergent Micelle Solutions. *Anal. Chem.* 2019, *91*, 10204-10211.

Introduction

At least half of all known soluble and membrane-associated proteins form multimeric complexes, with many of these complexes forming as homooligomers.^{123–125} Most homooligomers display some form of symmetry, and evolution favors larger complexes due to the increased stability afforded by minimizing solvent exposure of hydrophobic regions and functionality constraints that require large structures.^{3,123–126} However, determining the functional oligomeric form of protein complexes can be difficult, especially for transmembrane proteins that require suitable environments not easily amenable to traditional structural elucidation techniques (e.g. x-ray crystallography, electron microscopy, analytical ultracentrifugation, and electrophoretic techniques). Both oligomeric state heterogeneity^{127–129} and oligomeric state dependence on solution conditions^{76,130} have been reported and can further increase the difficulty of structure characterization.

An example of a large homooligomer protein complex with more than one observed oligomeric state is alpha-hemolysin (α HL) from *Staphylococcus aureus* (*S.*

aureus).¹³¹ *S. aureus* is a common human pathogen that can cause severe skin and respiratory tract infections leading to extensive disease burdens in the US and internationally.¹³² α HL is a key virulence factor for *S. aureus* which forms a transmembrane β -barrel pore complex. This pore structure permeabilizes cell membranes in many types of host cells as well as causes a broad range of other toxic cellular insults.^{133,134} Beyond the medical relevance of studying the role of α HL pores in *S. aureus* infections, the ability of α HL to form stable transmembrane pore complexes *in vitro* has led to its development as a nanopore tool¹³⁵ for molecular sensing of small molecules,¹³⁶ nucleotide sequencing,^{137–139} and directed movement of nanometer-sized cargo within α HL pores.¹⁴⁰

Early experiments using electron microscopy (EM),^{141–143} atomic force microscopy,¹⁴⁴ electrophysiology,¹⁴⁵ and solution-based size-exclusion chromatography and analytical ultracentrifugation¹⁴⁶ indicated α HL can form a hexameric complex. However, the first high-resolution x-ray crystal structure of α HL was heptameric,^{147,148} and several other crystal structures of α HL pore complexes solved since then are heptameric.^{149–151} The heptameric state is also supported more indirectly by other solution studies, such as photobleaching of fluorescently-labeled α HL subunits in pore complexes,¹⁵² pore conductivity measurements made using electrophysiology,¹⁴⁵ and experiments with covalently-linked α HL subunit dimers.¹⁵³ Over the course of the last couple decades, with these combined studies, the consensus view has been that α HL forms only functional heptameric pore complexes.^{131,153,154} It has been proposed that the identification of a hexameric complex may have been due to the image processing techniques used in EM and that previous size-exclusion chromatography and analytical

ultracentrifugation studies may have lacked sufficient resolution to distinguish between hexamer and heptamer forms.¹⁴⁶

Native ion mobility mass spectrometry (native IM-MS) using nano-electrospray ionization (nESI) has proven a useful tool in structural biology for identifying oligomeric states of biological complexes due to its ability to maintain native non-covalent interactions upon ionization of protein complexes.¹⁵⁵ For example, native IM-MS was used to determine the oligomeric states populated by anthrax toxin prepore at different solution pH^{76,130} and by the lysenin pore,¹⁵⁶ both of which form β -barrel pore complexes similar to α HL. Native IM-MS has also been shown to be a powerful tool for studying small-molecule association with high chemical specificity and without the need for crystallization of membrane protein complexes.^{15,16,157,158} Here, we use native IM-MS of α HL pore-like complexes formed in two different detergent solutions (tetraethylene glycol monoethyl ether (C₈E₄) as an ether-like detergent, and *n*-tetradecylphosphocholine (FOS-14) as a lipid-like detergent), to show that α HL forms both hexameric and heptameric complexes simultaneously in both detergent solutions. Under the tested solution conditions, the heptameric complex is the dominant species, but a sizable population of hexameric complexes is detected, and this result was verified on two different mass spectrometer platforms (an IM-time-of-flight instrument and an Orbitrap instrument without IM). Using the phospholipid-like detergent FOS-14, α HL complexes embedded in nearly-intact detergent micelles are resolved enough in the native IM-MS data to characterize both their stoichiometry and collision cross section (CCS). These native mass spectra are highly congested due to hundreds of overlapped mass spectral peaks, but Fourier transform (FT) and Gábor transform (GT) are used to deconvolve both

the charge state and stoichiometry distributions of associated detergent molecules.^{87,88,118}

The ability of α HL to form hexameric and heptameric pore-like complexes has ramifications for the mechanism of α HL pore formation and the use of α HL as a nanopore tool.

Methods

Expanded method and experimental details can be found Appendix A. Briefly, lyophilized monomers of α HL from *S. aureus* were purchased from Millipore Sigma (St. Louis, MO, USA) and were resuspended in deionized water to a concentration of 0.5 mg/mL. 150 μ L of this 0.5 mg/mL α HL monomer solution was centrifugally concentrated to \sim 4x in the presence of either C₈E₄ (32 mM, CMC = 8 mM) or FOS-14 (2mM, CMC = 0.12 mM) detergent micelles in 200 mM ammonium acetate pH 7.5 to induce oligomerization and pore formation.¹⁴⁶ A portion of this sample (10 μ L diluted to 30 μ L with more detergent solution) was then used to buffer exchange into 200 mM ammonium acetate at pH 7.5 with 2x the CMC of the appropriate detergent for mass analysis. Oligomer formation was also checked using SDS-PAGE (Figure A1 in Appendix A). As part of a detergent screen, the detergents *n*-dodecyl- β -D-maltopyranoside (DDM) and *n*-dodecyl-N,N-dimethylamine-N-oxide (LDAO) were additionally tested, but under similar instrumental conditions no oligomers of α HL were detected. Mass spectra were acquired on either a Waters Synapt G2-Si Quadrupole–Ion-Mobility–Time-of-Flight (University of Oregon, Eugene, OR) or Thermo Scientific Exactive Plus extended mass range Orbitrap (University of California, San Francisco, CA) mass spectrometer, and all ion mobility-mass spectra were acquired on a Waters Synapt G2-Si. Both instruments were equipped with a nESI source, and tuning

parameters can be found in the Appendix A methods. Gas-phase compaction of model structures for native-like pores were simulated using GROMACS v. 2016.4, and theoretical collision cross sections were computed using Collidoscope.^{82,83}

Results and Discussion

α HL forms both hexameric and heptameric pore-like complexes in C₈E₄ detergent micelles. In order to characterize effects of detergent on α HL oligomerization, we initially obtained a mass spectrum of α HL in detergent-free solutions. A typical native mass spectrum of α HL monomers ($\sim 5 \mu\text{M}$) formed by nESI from detergent-free solutions using a Waters Synapt Q-IMS-ToF mass spectrometer is shown in Figure 3A. α HL monomer ions form a narrow charge state distribution from 10-12+ indicating that the monomer ions are compact. For each charge state there are two peaks of similar abundance attributed to the presence of the α HL monomers ($33,259 \pm 1 \text{ Da}$) and an unknown protein present in the commercial α HL sample ($34,126 \pm 1 \text{ Da}$; see Figure A2 in Appendix A for more information). The measured α HL monomer mass matches well with the theoretical sequence mass of 33,248 Da for the mature 293 amino acid protein. At higher m/z (~ 4500 -5000) there is a low-abundance distribution attributed to another contaminant protein with a mass that is inconsistent with any oligomeric state of the α HL monomers. No oligomers of α HL monomers are detected at this concentration and under these detergent-free solution conditions. nESI of α HL monomers concentrated in the presence of C₈E₄ detergent micelles at a concentration above the critical micelle concentration (CMC) (32 mM for concentration step, CMC = 8 mM) yields two higher-order oligomeric states with masses of $199,553 \pm 15 \text{ Da}$ and $232,806 \pm 16 \text{ Da}$ and charge state distributions of 25-33+ and 25-37+, respectively (Figure 3B). C₈E₄ was chosen

initially for its compatibility with native nESI and ease of removal in the gas phase of the

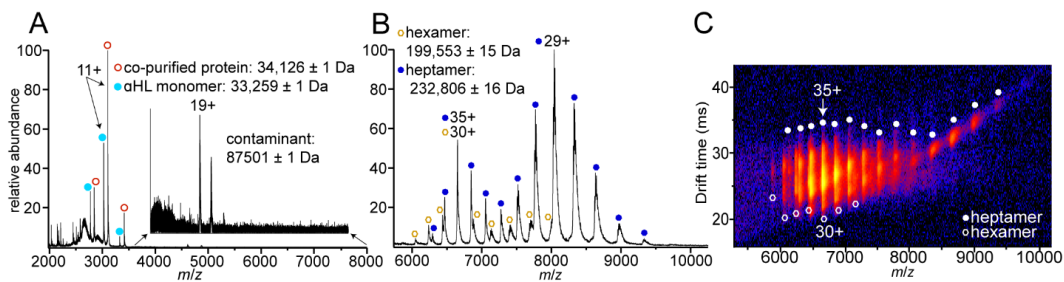


Figure 3. Native mass spectra of α HL hexamer and heptamer complexes. (A) Mass spectrum of α HL monomers in detergent-free solutions of 200 mM ammonium acetate. The presence of α HL monomers and an unidentified co-purified protein are seen while no oligomers are present. Inset shows the small abundance of a second contaminant. (B) Mass spectrum of α HL oligomerized complexes formed in C_8E_4 detergent solutions with 200 mM ammonium acetate and under the instrumental conditions of sample cone at 50 V and trap at 75 V. (C) IM-MS spectrum under the same instrumental conditions as in (B) showing multiple unfolding states.

mass spectrometer instrument.^{16,104,109} These measured masses match the expected masses for the hexameric (199,554 Da) and heptameric (232,813 Da) oligomeric states based on the measured monomer mass. By contrast, there is no evidence for the incorporation of the heavier (34 kDa) unidentified protein in the observed hexamers or heptamers.

Native mass spectra of α HL complexes embedded in FOS-14 detergent micelles confirms solution hexameric and heptameric pore-like complexes. In order to clearly resolve the two α HL oligomeric distributions in the above experiments, moderately activating instrumental conditions (sampling cone 50 V, trap 75 V, transfer 5 V) were used to strip off nearly all the detergent, as is done in the majority of native IM-MS studies to date of transmembrane proteins embedded in detergent micelles. Figure 3C shows the IM-MS data under the same instrumental conditions used to obtain the mass spectrum in Figure 3B. Under these instrumental conditions, most of the charge states for

both the hexamer and heptamer have multiple unfolded conformational states. Non-native monomers are detected in low abundance (Figure A3 in Appendix A) that, in principle, could have been ejected from activated heptameric complexes, resulting in the hexameric distribution. To eliminate this possibility, 37+ heptamer ions were first isolated under conditions where the ions remained compact and folded (sampling cone 50 V, trap 25 V) and then these ions were activated in the trap (125 V) to dissociate them into high-charge monomers (14-25+) and stripped hexamers (15-24+) (Figure A4 in Appendix A). The drastically different drift time and charge state distributions for the collision-induced hexamers show that the hexameric series in Figure 3B does not arise from gas-phase activation of the heptamers. We also tested whether the the formation of hexamer is a result of early activation in the electrospray process as protein ions are transferred to the gas phase. Increasing the sample capillary voltage does not increase the abundance of hexamer ions relative to heptamer ions but does significantly diminish signal quality (Figure A5 in Appendix A). These combined experiments demonstrate that the hexameric complex is indeed an oligomeric state formed in solution.

To more directly confirm the presence of native heptamers and hexamers in detergent solution, we acquired mass spectra under conditions where the detergent micelles surrounding the ions are largely preserved. However, obtaining resolved mass spectra of micelle-embedded α HL complexes in C₈E₄ was difficult. Detergent resolution was only obtained on protein complex ions under relatively high-activation conditions for which only a small number of detergent molecules remained adducted to protein complex ions (Figure 3B). α HL has been co-crystallized with each subunit bound to glycerol phosphocholine in a groove between the rim and stem domains of the complex.¹⁴⁹ This

evidence for phosphocholine binding has been used to reason why α HL appears to bind and form pores preferentially to membranes containing phosphocholine lipids.¹⁵⁹ The detergent FOS-14 is a lipid-like detergent with a phosphocholine headgroup, and thus it might be expected to form strong interactions with α HL pores that encourage more native-like oligomer formation than C₈E₄. We reasoned that detecting the hexameric and heptameric oligomeric states in a more phospholipid-like detergent would remove doubt about the hexameric state being artefactual due to the ether-based C₈E₄ detergent. FOS-14 and other phospholipid-like detergents have not been reported previously as a vehicle for transmembrane protein native IM.

Following a similar procedure for oligomer formation in C₈E₄, α HL monomers were concentrated in FOS-14 detergent solutions at a FOS-14 concentration (2 mM) well above the CMC (~0.12 mM). Under the same gentle nESI conditions, native mass spectra of these samples indicate oligomerized complexes associated with large FOS-14 micelles and much less stripping of detergent than for C₈E₄ (Figure 3A-D). At lower *m/z* a large distribution of protein-free detergent micelles is present at much higher abundance than that of the α HL micelle-embedded ions (Figure A6 in Appendix A). Due to the polydispersity of detergent stoichiometry in the micelles, the α HL ions embedded in detergent micelles have complicated distributions of peaks in the mass spectrum (Figure 3A-B) with overlapping charge state and detergent distributions that are difficult to assign. However, these overlapping distributions lend themselves well to Fourier transform (FT) and Gábor transform (GT) based analysis developed by our laboratory (iFAMS software) to deconvolve the charge state and detergent distributions.^{87,88,118}

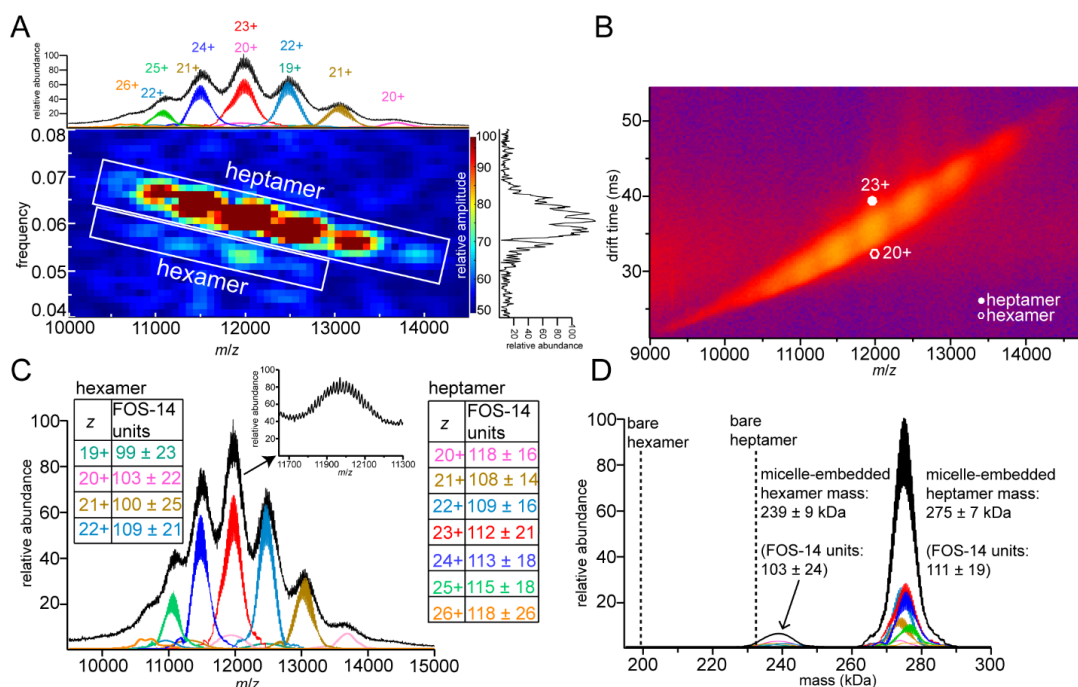


Figure 4. Native mass spectrum of α HL micelle-embedded complexes in FOS-14 detergent with 200 mM ammonium acetate with the sample cone at 150 V and trap at 50 V from the Synapt Q-IMS-ToF instrument. (A) GT spectrogram is shown with the IM-MS mass spectrum cutout across the top and FT spectrum down the right. Each individual point in the spectrogram corresponds to a charge state that is then reconstructed on the mass spectrum above (colored traces). For the heptameric series, secondary harmonics were resolved and included in the reconstruction, resulting in higher resolution than for the hexameric series. (B) IM-MS spectrum of α HL micelle-embedded complexes showing drift time overlap of hexamer and heptamer distributions that remain compact and folded. (C) Detailed stoichiometry analysis of mass spectrum shown in (A). Inset tables provide the detergent stoichiometry distributions for each individual charge state from the GT with the \pm representing the standard deviation in the detergent stoichiometry. The inset shows the repeating peaks from detergent association. Colors in table match with their respective detergent distribution for each charge state. (D) Zero-charge spectrum of the combined charge state data from the GT. Dashed vertical lines correspond to the masses calculated for detergent-stripped bare hexamer and heptamer oligomers based on the measured monomer mass.

Under the moderately-activating instrumental conditions used to collect the mass spectrum in Figure 4A-D, both hexameric and heptameric oligomeric states of α HL are detected and separated in the GT spectrogram, which have highly overlapped distributions that are not easily separated or characterized using IM-MS without

deconvolution (Figure 4B). The GT also allows for the analysis of detergent stoichiometry distributions for each charge state. The charge state distributions are plotted with the mass spectrum in Figure 4C and as a combined “zero-charge” spectrum in Figure 4D. The nearly Gaussian total mass distributions in the zero-charge spectrum indicate that the α HL hexamer associates with 103 ± 24 FOS-14 detergent molecules while the heptameric complex associates with 111 ± 19 molecules of FOS-14 in these mass spectra, consistent with a roughly oligomer size-proportional micelle stoichiometry. The IM-MS spectrum in Figure 4B indicates that the α HL pore-like complexes are compact under these conditions, demonstrating that GT can be used to deconvolve and characterize these overlapped distributions without the need to strip the ions of detergent as in Figure 1C where concomitant protein unfolding is observed.

α HL pore-like ion stoichiometry is consistent across mass spectrometer platforms. To demonstrate that the observed α HL oligomeric states are reproducible across mass spectrometer platforms, these samples were studied with nESI on an Orbitrap EMR instrument, which uses a heated ESI capillary to transfer ions into the low-pressure region of the instrument rather than a gentler “StepWave” ion guide as in the Synapt platform (Figure 5A-C). In contrast to the above-described Synapt instrument, mass spectra acquired on the Orbitrap instrument do not exhibit a large population of FOS-14 only micelles on the Orbitrap instrument, which is consistent with the Orbitrap having a harsher source. Also, on the Orbitrap more α HL complexes completely stripped of FOS-14 are detected under these conditions with peaks that are about half as wide in full-width at half-maximum compared to C_8E_4 detergent-stripped pore-like complexes on the Synapt instrument at ~ 7500 m/z (Figure A7 inset in Appendix A).¹¹⁸ The signal for stripped

complexes clearly indicates both hexamer and heptamer oligomeric states for α HL pore-like complexes with masses that closely match the detergent stripped complexes in C_8E_4 (hexamer: $199,577 \pm 4$ Da, heptamer: $232,845 \pm 6$ Da).

Under the least activating conditions we used on the Orbitrap instrument, detecting signal for the hexameric micelle-embedded complexes is difficult in comparison to the heptamer (Figure A7 A-C in Appendix A). When the mass spectrum in Figure A8A in Appendix A is processed with FT in iFAMS using only charge states 23-25+, which are well separated in the frequency domain, signal of hexameric complexes in detergent micelles is more clearly observed. Under these instrumental conditions, the

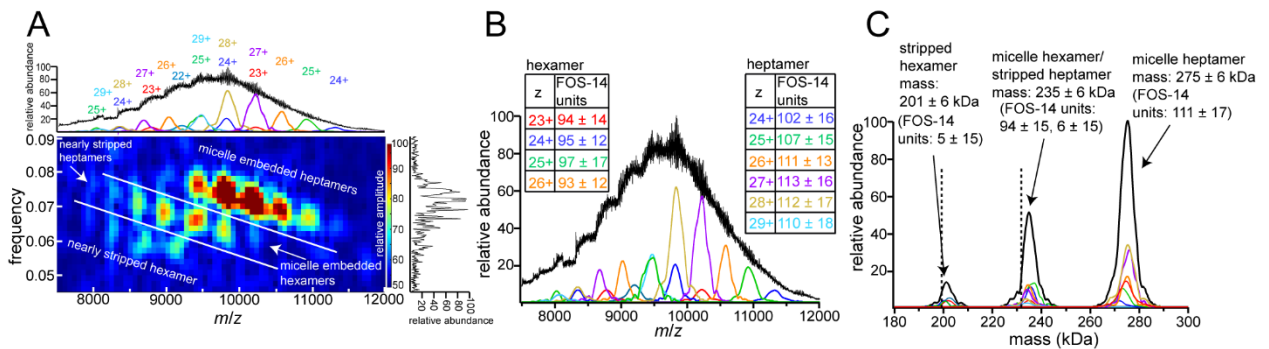


Figure 5. Native mass spectrum from the Orbitrap instrument of α HL micelle-embedded complexes in FOS-14 detergent with 200 mM ammonium acetate and under the instrumental conditions of source CID 100 V and HCD at 50 V. (A) GT spectrogram is shown with the mass spectrum across the top and the FT down the right. (B) Detailed stoichiometry analysis of mass spectrum shown in (A). Tables provide the detergent stoichiometry distributions for each individual charge state pulled from the GT with the \pm representing the standard deviation in the detergent stoichiometry. (C) Zero-charge spectrum of the combined charge state data from the GT. Dashed vertical lines correspond to the masses calculated for detergent-stripped bare hexamer and heptamer based on the measured mass of the monomer. For the middle overlapped distribution, the number of FOS-14 units associating with the micelle-embedded hexamers and the nearly detergent-stripped heptamers is given.

hexameric ions are determined to contain 112 ± 32 detergent molecules while the heptameric ions associate with 121 ± 30 , which is consistent with the number of

detergent molecules associating with the heptamer on the Synapt instrument under the least activating instrumental conditions used (Figure A9 A-D in Appendix A). Increasing the degree of in-source activation removes a small number of detergent molecules (~ 10) and significantly increases peak resolution yielding the mass spectrum and GT spectrogram seen in Figure 5A-C. The GT spectrogram contains three distinct distributions of α HL pore-like complexes that are hard to separate using FT alone and would be extremely difficult to analyze by conventional methods. In the GT, the most abundant distribution with the highest overall frequency values represents the heptameric α HL complexes embedded in detergent micelles that associate on average with 111 ± 17 FOS-14 molecules. The middle distribution corresponds to two strongly-overlapped distributions of nearly detergent-stripped heptamers and micelle-embedded hexamers with overlapped charge states and very similar mass distributions that are difficult to distinguish from the GT spectrogram. (Coincidentally, the 25+ micelle-embedded hexamer and 29+ micelle-embedded heptamer distributions have nearly identical abundance and m/z ranges and would be exceptionally difficult to deconvolve with other methods.) Based on the mass distribution width and average for each charge state in the middle series of Figure 5A, charge states 23-26+ are predominantly micelle-embedded hexamers, while charge states 27-29+ are attributed mostly to nearly detergent-stripped heptamer complexes. Under these conditions the micelle-embedded hexamers associate with 94 ± 15 FOS-14 molecules. The third, lowest-frequency distribution is attributed to nearly detergent-stripped hexameric complexes that on average have ~ 5 remaining detergent molecule adducts. Overall, these values for the masses of the stripped α HL pore-like complexes and the detergent stoichiometries for the micelle-embedded

complexes are highly consistent with data acquired on the Synapt instrument and further corroborate the existence of both hexameric and heptameric pore-like complexes in solution.

Due to the size of these complexes and the similarity in molecular identity, it is unlikely the nESI ionization efficiencies of the hexamer and heptamer are drastically different. Thus, the abundance ratios seen from the mass spectrum likely reflect the abundance ratios of the hexameric and heptameric complexes in solution. The heptameric state is clearly favored at a measured ratio of detergent-stripped heptamer to hexamer of ~5:1 in both FOS-14 and C₈E₄ detergents as determined by fitting Gaussian detergent stoichiometry distributions to each charge state in Figure 3B and Figure A7A in Appendix A and totaling the abundances of each oligomer, or by using Unidec (a Bayesian deconvolution algorithm) to estimate the abundances of each oligomer population.^{90,160,161} Determining the abundance ratios for each oligomeric state for the micelle-embedded α HL complexes on the Synapt and Orbitrap instruments is more complicated. From the zero-charge spectrum acquired on the Synapt (Figure 4D) the ratio of micelle-embedded heptamer to hexamer is ~10:1 in comparison to that of the Orbitrap (Figure 4C) of ~2:1 (including signal for detergent-stripped heptamers). This difference is likely due to the significantly better resolution of the mass spectra acquired on the Orbitrap instrument, which should result in more reliable reconstructed relative abundances. Based on this we conclude the abundance ratios of heptamer to hexamer in the micelle-embedded complexes are likely closer to that of the detergent-stripped complexes, i.e., ~5:1 heptamer : hexamer. Therefore, as has been previously reported by multiple techniques, the heptameric oligomer is the predominant species under these

conditions, but α HL also forms a large population of hexameric complexes in detergent solutions.

IM-MS collision cross section measurements and MD-simulated collision cross section calculations of stripped heptameric and hexameric complexes reveal compact native state. The native mass spectra of FOS-14 micelle-embedded α HL pore-like complexes show that both the hexameric and heptameric oligomers are native

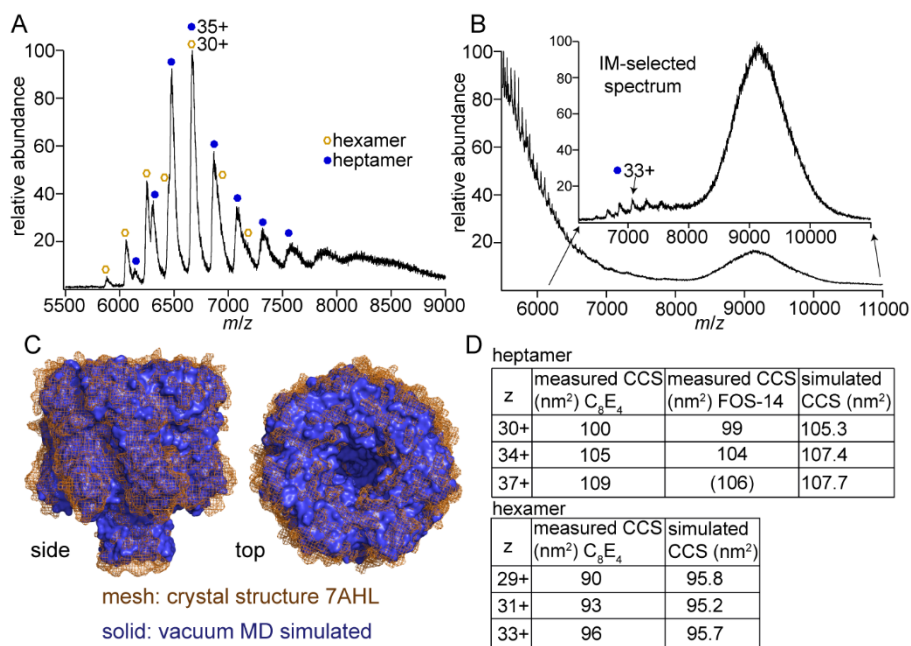


Figure 6. Comparison between collision cross section measurements in both detergents and computationally derived CCSs. (A) IM-MS spectrum of nearly-detergent-stripped α HL pore-like complexes in C_8E_4 detergent micelle solutions under instrumental conditions (sampling cone 50 V, trap 25 V) where no unfolding is seen. (B) Same as in (A) except using FOS-14 as the detergent (sampling cone 25 V, trap 50 V, transfer 25 V). (C) α HL heptameric pore crystal structure (orange mesh, PDB: 7AHL) and vacuum MD simulated structure showing gas-phase compaction (solid blue surface). (D) Comparison between measured CCSs for α HL heptamer and hexamer ions in C_8E_4 and FOS-14 detergent and for CCSs predicted from MD structures. The measured CCS value in parentheses for FOS-14 is the 36+ charge state which was the highest charge state observed.

oligomeric states for α HL complexes in detergent solutions, but these data alone do not reveal much about the structure or conformation of the oligomeric complexes.⁸²

To determine whether the α HL oligomers survive in pore-like structures upon transfer to the gas-phase, triplicate IM-MS measurements of α HL hexamer and heptamer complexes formed with C_8E_4 were collected under activation conditions for which each charge state for both oligomers remained compact. Under these instrumental conditions more C_8E_4 molecules remain attached to each oligomer and the hexameric and heptameric ion distributions partially overlap both in m/z and drift time (Figure 6A, Figure A10 in Appendix A). α HL hexameric complexes were determined to have CCS values ranging from 90-96 nm² for charge states 29-33+, while the heptamers had CCS values ranging from 100-109 nm² for charge states 30-37+ indicating that the hexamer is $\sim 6/7$ the size of the heptamer. Together these results suggest that these detergent-stripped hexameric and heptameric complexes have globally similar compact structures.

IM-MS experiments on compact α HL pore-like complexes formed with FOS-14 resulted in similar CCS values to complexes formed in the detergent C_8E_4 . Using IM-MS, signal for stripped heptameric complexes could be detected and separated from FOS-14 clusters that overlap in m/z , but have different drift time distributions (Figure 6B). For the heptameric series with charge states 30-36+ the measured CCS is 99-106 nm², indicating there is no significant difference in the size of the stripped heptamer ions formed using either of the two detergents tested.

It is well-known that native-like protein and protein complex ions often compact (by as much as 22%) in native IM-MS during the nESI process in comparison to their condensed-phase structures⁸² but that much tertiary and even secondary structure can be preserved.¹⁶² We recently showed that performing vacuum MD simulations using the GROMOS96 43a2 force field results in ion structures having calculated CCSs within 4%

on average of experimental IM-MS data for a set of globular and transmembrane proteins and protein complexes commonly used as IM-MS calibration standards.⁸² To enable more confident comparison of experimental IM-MS data presented here for the putative hexameric and heptameric α HL pore-like complexes, vacuum MD simulations were performed at 300 K with the GROMOS96 43a2 force field for both the crystal structure of the heptameric pore (PDB: 7AHL) and a model of the hexameric pore produced by Furini et al.¹⁴⁵ Figure 6C shows the crystal structure 7AHL as a mesh surface with the aligned vacuum MD simulated structure as a solid surface. These vacuum MD simulated structures were then used to calculate CCS values in N₂ gas using the Trajectory Method in Collidoscope. After MD relaxation in vacuum, a small degree of compaction (~12%

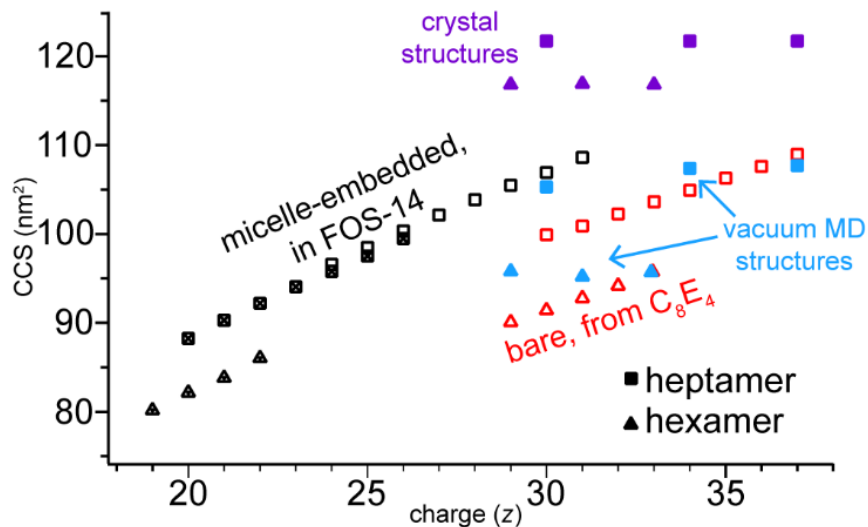


Figure 7. Compilation of all measured and computationally predicted CCS values for α HL hexamers and heptamers. Vacuum MD CCS for the 33+ hexamer and the measured CCS for the 33+ hexamer are slightly offset because they are nearly identical. CCSs for α HL micelle-embedded complexes in FOS-14 determined from Fig. 4B and A7 in Appendix A. CCSs for α HL bare complexes formed in C₈E₄ determined from Fig. 6A.

for the heptamer and ~18% for the hexamer) is predicted. Figure A11 in Appendix A shows models of the hexameric pore and vacuum MD-simulated structures.

Figure 6D compares the measured and computed CCS values. The calculated CCS for the hexamer averaged 96 nm^2 for charge states 29+, 31+, and 33+ and 107 nm^2 for the 30+, 34+, and 37+ heptamer. These simulated CCSs fall inside the range of experimentally measured CCSs for both the bare hexameric and heptameric pore-like complexes and are within the expected range of error ($\pm 4\%$) of the charge-state-averaged experimental CCSs for both oligomers ($93/105 \text{ nm}^2$ for the hexamer/heptamer). Figure 7 summarizes all the native IM-MS CCS measurements and the computationally-derived CCS values for the uncompact and MD compacted hexamer and heptamer structures. The detergent-stripped bare pore-like complexes and the micelle-embedded complexes overall have linear CCS trends as a function of charge state with similar slopes and differ by only a few nm^2 , which we attribute to the presence or absence of the detergent micelles. Although CCS measurements do not provide direct evidence of a “pore” in the physiological sense (i.e., a channel capable of permeabilizing lipid bilayers), these results indicate that the native IM-MS conditions used here preserve not only the stoichiometry but also structure consistent with the crystal and model structures of the heptameric and hexameric pores from solution into the gas phase.

Conclusions

Here, αHL from *S. aureus* is observed to adopt two oligomeric states, a hexamer and a heptamer in solution that are preserved upon transfer to the gas phase, using two different types of detergent and two different types of mass spectrometer platforms. For both the ether-based and phospholipid-like detergent used, both hexameric and heptameric detergent-stripped complexes are detected at a ratio of $\sim 5:1$ heptamer to hexamer. Based on native IM-MS results, these detergent-stripped complexes have CCSs

within 4% of their respective vacuum MD simulated structure. All these observations and measurements point to the coexistence of hexameric and heptameric pore-like complexes of α HL in the condensed phase.

The native mass spectra of micelle-embedded pore-like complexes reported here illustrate the powerful capabilities of FT and GT to deconvolve charge state and mass information to allow for interpretation of these types of challenging samples without requiring detergent removal. These results also demonstrate the utility of FOS-14 as a detergent in native mass spectrometry, which has the same phosphocholine headgroup as many of the most common physiological lipids. With FOS-14, intact membrane protein micelle complexes could be transferred to the gas phase with high enough resolution for analysis with FT and GT to determine the charge state, mass, and stoichiometries of associated detergent and protein oligomeric state. The results also illustrate advantages of FT- and GT-based deconvolution methods for CCS and structure determination based on IM data, for which accurate charge states and mass determination are prerequisites. These same methods could be used to aid oligomeric state determination of other membrane protein complexes for which resolving oligomeric states may be difficult. FT and GT analysis can as well be extended to other applications that inherently produce complicated mass spectra with repeating subunits. In this case, detergent is the repeating subunit, but this type of analysis could be extended more generally, for example, to lipid-containing complexes, proteins with multiple bound isobaric glycans, and polymers.

The propensity for intact FOS-14 micelle-embedded membrane protein complexes to be transferred to the gas phase of mass spectrometer instruments highlights the significant differences in gas phase behavior between FOS-14 and C₈E₄. As observed

here, C₈E₄ has been demonstrated to be readily removable from protein complexes in the gas phase, in contrast to other detergent groups such as maltosides (e.g. DDM).¹⁶ Reading et al. argued that the ease of detergent removal may relate to the protein stability within the detergent micelle and may suggest that the ease of a detergent's release is inversely correlated with its ability to substitute for lipid association.¹⁰⁴ Here, with FOS-14 being a phospholipid-like detergent, once the micelle-embedded pore-like complexes reach the gas phase of the mass spectrometer instrument, it is more difficult to remove all the detergent with tuning conditions available on the Synapt instrument. Only minimal detergent loss and charge stripping are seen under a wide range of activation conditions (Figure A12A-C in Appendix A), suggesting these micelle-embedded pore-like complexes are indeed highly stable.

In these experiments, α HL pore-like complexes are made through direct association with detergent micelles. *In vivo*, α HL monomers have specific cell surface binding interactions with the protein ADAM10 at nanomolar concentrations of toxin.^{163,164} At higher concentrations ($\sim 1 \mu\text{M}$) α HL monomers have been shown to associate with phosphocholine lipids and to oligomerize and form pores in an analogous fashion to how pore-like complexes were formed in detergent in these experiments.^{159,163,165} An exciting future direction of research is to use native IM-MS techniques similar to those described here to investigate effects of protein receptor models or lipid headgroups on the oligomeric state distribution of α HL complexes or other pore forming toxins (such as anthrax toxin). Additionally, different oligomeric states of α HL pores almost certainly have different pore diameters and thus different channel conductance properties.^{145,153} Tailoring the oligomeric state of α HL pores by

manipulating solution conditions or membrane environment, informed by IM-MS studies, could therefore enable broader control of pore diameter and conductance in applications.

In comparison of the FOS-14 micelle-embedded α HL complexes between the Synapt and the Orbitrap mass spectrometer instruments it became clear that the Orbitrap instrument not only has higher resolution due to the nature of its ion detection system, but is also better at desalting or stripping detergent from protein ions in the source region. This can be clearly seen in comparing the α HL complexes in Figure 4 to Figure 5 as well as Figure 6B to Figure A7 inset in Appendix A. In both cases the Orbitrap instrument is more activating in the source region allowing for easier interpretation of the complicated data due to the high level of polydispersity in the micelle-embedded complexes. While the Synapt has a less activating source, the key advantage of this instrument is the power of IM-MS such that the compactness or unfolding of protein complexes can be monitored and overlapped ion distributions in m/z can be filtered. The ideal scenario is combining the more activating source of the Orbitrap with the IM-MS capability of the Synapt.

In Chapter III I discuss simple instrumental modifications to the Synapt that increase the range of collisional activation achievable in the source region. This was done by using source sampling cones that have smaller apertures and therefore increase ion heating as ions are transferred from atmospheric pressure to the vacuum of the instrument. I demonstrate that these smaller aperture source cones reproducibly increase desalting of soluble protein complexes and strip FOS-14 detergents from α HL without drastically decreasing the total ion abundances for these complexes or causing premature protein unfolding. Swapping these source cones is a facile process that does not require

venting of the instrument and allows for the source activation characteristics to be tuned in a controllable fashion based on the aperture size.

CHAPTER III

INCREASING COLLISIONAL ACTIVATION OF PROTEIN COMPLEXES USING SMALLER APERTURE SOURCE SAMPLING CONES ON A SYNAPT Q-IM-TOF INSTRUMENT WITH A STEPWAVE SOURCE

While the material included here is primarily my own work, Micah T Donor and Samantha O. Shepherd aided analysis with protein ion simulations and James S. Prell contributed to experimental design and interpretation. This work was recently submitted as an Application Note to the *Journal of the American Society for Mass Spectrometry* for publication with the above named as co-authors.

Introduction

A significant challenge of native ion mobility-mass spectrometry with nano-electrospray ionization is that cosolutes from solution adduct to protein ions.^{21,72,166,167} This causes peak broadening that can obscure ligand binding and hinder accurate mass determination.²¹ Typically, native-like protein ions are accelerated into neutral buffer gases either in the relatively high-pressure instrument source or in a collision cell within the instrument to aid desalting or to cause unfolding/dissociation. Previous generations of the Waters Q-IM-TOF Synapt instruments used a source “extraction cone” for nozzle-skimmer activation, which can be very effective for desalting and detergent removal from membrane proteins.^{168,169} More recent generations of the Synapt instrument replaced the extraction cone with a wide-diameter traveling wave “Stepwave” ion guide between the source region and quadrupole. The Stepwave, which operates in standard configuration at a pressure of ~3.0 mbar for the first segment and ~9.0e-3 mbar at the source turbo pump,

is used in combination with a larger sampling cone (SC) than in earlier Synapt series instruments to increase sensitivity at the expense of decreasing the maximum degree of ion activation and desalting for large ions.

It is known that ions generated by ESI can undergo collisional heating, cooling, or both upon transfer into the vacuum of the instrument interior.^{170,171} Acceleration into the decreasing gas pressure gradient between the exterior and source converts kinetic energy of collisions into internal energy, whereas solvent and salt evaporation can remove internal energy from the ion. The pressure of the source region is a key determinant of the extent of collisional cooling or heating ions experience.^{72,168,171–173} High pressures (low mbar) in the instrument source increase collisional cooling to slow protein ions for efficient transfer.^{172,173} However, excessive collisional cooling leads to increased salt adduction.^{72,168} Thus, a balance must be struck such that pressure is sufficient to transmit large ions, but not so high as to prevent adduct removal. Figure 8A shows a theoretical scenario where low and medium pressures (red and green) would completely desalt the protein (and could begin unfolding the protein in the case of the red curve line) in the source region while high pressure (blue) would not. Desalting a protein in the source region prior to the quadrupole may aid experiments performed in the collision or IMS cells. For example, a protein could be fully desalted prior to an unfolding and dissociation experiment, allowing the full range of collision cell voltages to be accessed that would otherwise be necessary to first desalt before substantial unfolding and dissociation.

Landreh et al. demonstrated that reducing the source pressure on the Synapt G1 HDMS with an adjustable valve between the source region and its dedicated pumping line reduces collisional cooling to aid activation of membrane proteins.¹⁶⁸ This method

typically also raises the pressure throughout the instrument, therefore efficacy is limited by the operating pressure of the TOF region. The Synapt G2-Si does not have a dedicated source pump line. Thus we sought a facile, “hot-swappable” approach to increase ion heating in the source of a Waters Synapt G2-Si instrument by reducing the pressure with smaller aperture source SCs, that do not affect pressures in the rest of the instrument (see Table A1 in Appendix B for SC-specific instrument pressures).

Methods:

GroEL was purchased from Millipore-Sigma and prepared using established protocols.¹⁶⁹ α HL monomers were purchased from Millipore-Sigma and oligomerized in n-tetradecylphosphocholine (FOS-14) detergent solutions as described previously in Chapter II and the supplemental methods in Appendix A. Waters Synapt G2-Si instrumental parameters are listed in the Supplemental Methods in Appendix B.⁹¹ GroEL mass spectral peaks were analyzed using Igor Pro (WaveMetrics) to determine excess mass, peak fwhm, and integrated abundances for each charge state. Mass spectra for α HL heptamers were deconvolved using iFAMS.^{87,88,118}

Ion heating and cooling simulations were performed as previously described.¹⁷⁴ A pressure (from 3.0 mbar to 9.0e-3 mbar for the large SC) exponential decay length of 2.5 mm was assumed as ions are accelerated from the Stepwave through a differential aperture into an ion guide in the source. Because the exact pressure decay length is not known, we also modeled results for shorter (1.25 mm) and longer (5 mm) decay lengths (see Figure A1 in Appendix B). Simulation details are further described in the Supplemental Methods in Appendix B.

Results and Discussion:

GroEL 14-mer (sequence mass 800,770 Da) is a common protein complex in native MS for assessing instrumental figures of merit for transmission of large ions and

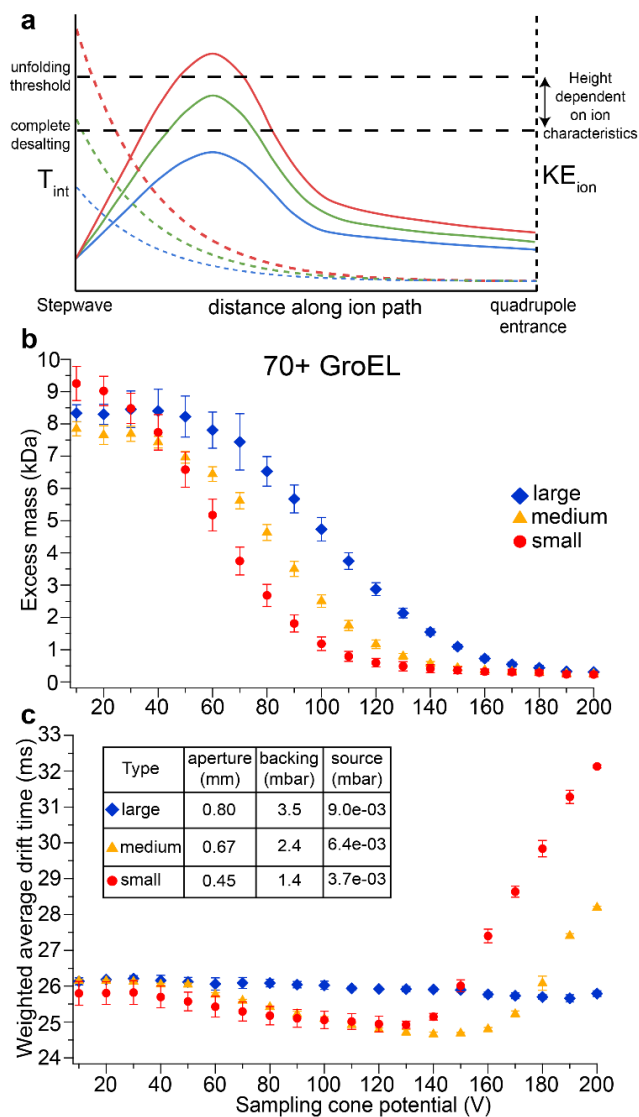


Figure 8: GroEL desalting and unfolding with each source sampling cone aperture size. (A) Simple model of protein ion heating/cooling (effective ion vibrational temperature, T_{int} (solid lines) after ions are accelerated in the instrument source (with initial laboratory-frame kinetic energy KE_{ion} (dashed lines)) under varying source pressures to demonstrate the balance between ion heating, desalting, and unfolding/dissociation at low (red), medium (green), and high (blue) pressures (note: not to scale). Excess mass (B) and weighted average DT (B) for GroEL⁷⁰⁺ as the SC potential is raised with each SC size. Data were collected in triplicate on separate days with error bars representing one standard deviation. Inset table for (B) provides aperture size for each cone and corresponding instrument pressure readbacks.

various types of ion activation.^{21,72,99,175} We used GroEL to benchmark effects of ion activation in the instrument source with each SC diameter. The “large” cone refers to the standard 0.8 mm i.d. cone for the Synapt G2-Si, while the “medium” and “small” cones refer to 0.67 and 0.45 mm i.d. SCs from Waters Xevo instruments to reduce the backing and source pressures. Instrument pressures beyond the source are unaffected (Table A1 in Appendix B). Experimentally determined excess mass (Figure 8B), drift time (DT) (Figure 8C), peak width (Figure A2A in Appendix B), and ion abundance (Figure A2B in Appendix B) were used to assess GroEL activation with each SC as the cone potential was incrementally raised from 10-200 V. At low cone potentials, little difference is measured between the cone sizes. Above 60 V, ion activation increases as the cone aperture decreases, with the small cone the most activating and the large cone the least. Selected mass spectra of the GroEL 14-mer for each cone are shown in Figure A3 in Appendix B. The greatest difference in excess mass between the large and small cone is ~4 kDa at 90 V, whereas the medium cone at 100 V leads to ~2 kDa less excess mass than the large cone. Thus, the small cone provides the equivalent of an extra 50 V cone potential beyond the standard configuration (large cone), and the medium cone 30 V. These trends are paralleled in the peak width measures (Figure A2A in Appendix B), with the smaller cones leading to narrower peaks (more desalted) at lower potentials. The smaller cone leads to 20-30% reduction in GroEL ion signal as compared to the standard cone (Figure A2B in Appendix B) but greatly improves adduct removal capabilities.

The DT distributions (Figure 8C) for GroEL activation with each SC exhibits the same trend with aperture size. The potential at which unfolding begins with each SC decreases with decreasing cone aperture (large: 190 V, medium: 150 V, small: 130 V).

Independent of aperture size, GroEL unfolding begins with ~400 Da of excess mass remaining,^{72,169} suggesting that the smaller SCs do not cause such rapid heating that a different unfolding pathway is followed. At high SC potentials (170-200 V) the medium and small cones can cause dissociation of GroEL (Figure A4 in Appendix B) without additional activation in the trap, whereas the large cone does. Interestingly, the DT distributions for GroEL with each SC indicate aperture-dependent maximal degrees of ion compaction before the unfolding onset voltage (Figure 8C).⁸² Together, these GroEL experiments demonstrate that the “hot-swappable,” smaller aperture SCs improve desalting in the source region of the Synapt instrument.

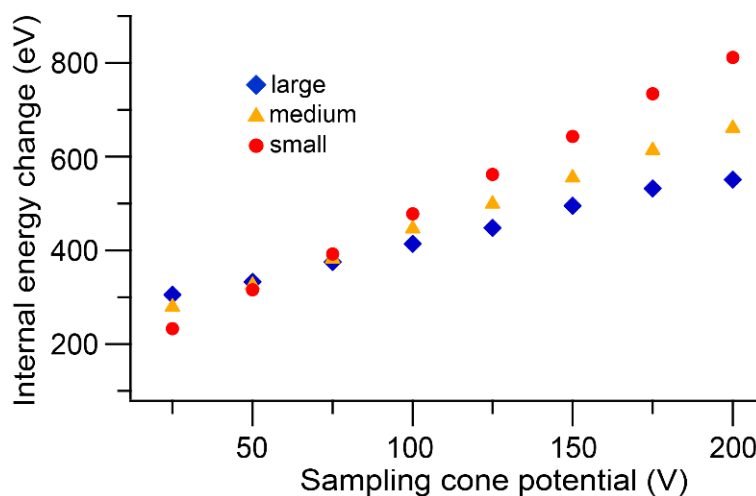


Figure 9: Simulated ion heating of BSA¹⁵⁺ under pressure conditions that match those produced by each SC diameter (pressures indicated in inset table Figure 8C) as a function of acceleration potential.

Lower pressure in the instrument source can decrease the amount of collisional cooling ions undergo upon transfer from atmospheric pressure to vacuum.^{72,168,171,173} To further explore increased ion activation at lower pressures, protein ion heating and cooling simulations were performed at pressures and potentials that replicate those produced at the exit of the Stepwave as ions are accelerated across a differential aperture

into a conjoined ion guide. From these simulations (Figure 9) of bovine serum albumin (BSA^{15+}) ions, little difference in effective ion internal temperature is predicted as a function of pressure at low cone potentials. However, the slopes of the ion heating trends increase as the pressure is reduced with the medium (slope 1.5x large) and small (slope 2.25x large) cones. This means as the cone potential is raised at lower pressures, a higher percentage of collisions are net heating leading to a more efficient conversion of kinetic to internal energy, consistent with the GroEL experiments.

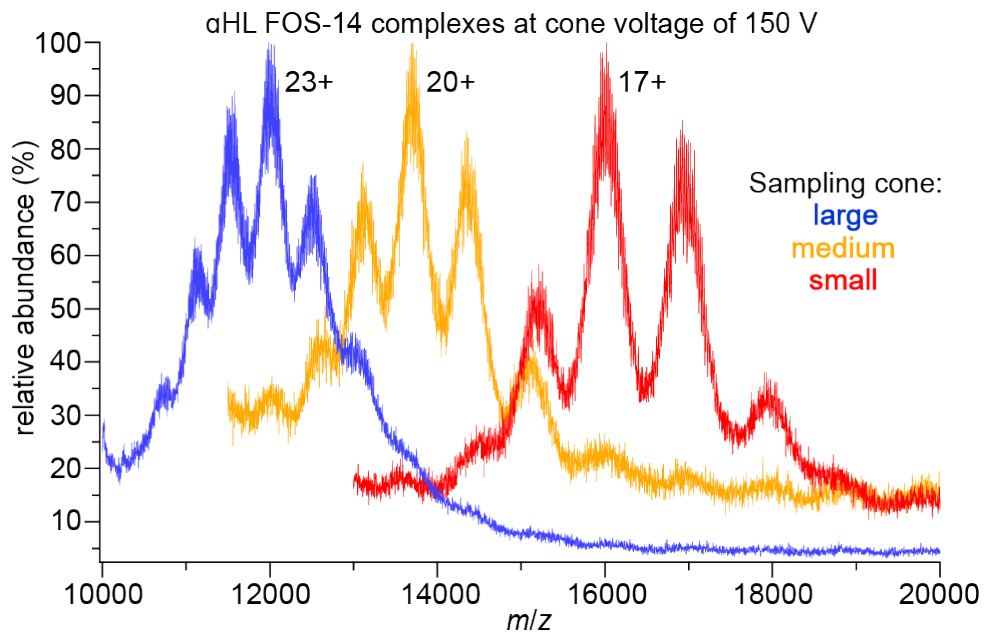


Figure 10: Overlaid mass spectra of α HL complexes in FOS-14 micelles with each source sampling cone at a cone potential of 150 V. Lower m/z portions of the mass spectra are truncated for clarity due to increasing signal from empty FOS-14 micelles. The highest-abundance charge state for each spectrum is indicated.

To demonstrate the advantages of smaller SCs when working with a membrane protein complex that requires significant collisional activation for analysis, we used α HL heptamers formed in FOS-14 detergent.⁹¹ We previously demonstrated that stripping the lipid-like detergent FOS-14 from α HL complexes is difficult, and that dramatic charge

reduction occurs when FOS-14 molecules are removed. For each SC, mass spectra were collected at cone potentials of 25 V (Figure A5A in Appendix B), 100 V (Figure A5B in Appendix B), and 150 V (Figure 10). Mass spectra of α HL FOS-14 micelle-embedded complexes are highly congested and require deconvolution using Gábor Transform analysis in iFAMS.⁸⁸ The average mass, charge, and number of associated FOS-14 molecules are reported in Table A2 in Appendix B. At 25 V the mass spectra for α HL complexes in FOS-14 micelles heavily overlap. By 100 V the charge and FOS-14 distributions for α HL complexes with each cone are shifted relative to one another, with the medium and small cone removing more FOS-14 and charge. At 150V, the large cone produces an average charge state of 23.4+ with 116 ± 23 FOS-14 molecules associating with α HL heptamer complexes, while the medium cone has an average charge of 19.8+ with 108 ± 23 FOS-14 molecules, and the small cone strips the most FOS-14 and charge to 16.7+ and 104 ± 19 FOS-14 molecules. These experiments are consistent with the GroEL data, showing that the medium and small SCs are more activating than the large cone, and that this increase in collision energy can be useful for removing adducts like detergents and lipids from membrane proteins without altering pressures in other regions of the instrument.

Conclusions:

Here, we demonstrated and quantified the collisional activation effects of using source SCs with smaller apertures on protein ions on a Waters Synapt G2-Si instrument. Protein ion activation follows the trend of increasing activation with decreasing SC aperture size, with only a modest reduction in total ion signal. The increase in activation is caused by the concomitant decrease in source pressure with the smaller SCs, which

reduces collisional cooling of protein ions in the instrument source.^{72,168,171–173} Based on excess mass and DT measurements of GroEL, the medium and small cones provide ~30 and ~50 V additional SC potential than the large cone, respectively. This increase in collision energy can be used to strip difficult-to-remove adducts such as detergents and lipids from membrane proteins with the Synapt G2-Si's otherwise very gentle ESI source, as demonstrated here with α HL heptamer complexes in FOS-14 micelles. Distinct additional advantages of these smaller SCs are that they are inexpensive, can be quickly exchanged without venting the instrument, and do not significantly affect pressures beyond the instrument source.

The ability of FOS-14 to significantly strip charge away from α HL micelle-embedded ions in the gas phase as well as the salt or zwitterionic character of lipid headgroups lead us to investigate the possibility of lipids to adduct non-specifically to protein complexes in the gas-phase. As mentioned in Chapter II and this chapter, FOS-14 detergent has a phosphocholine headgroup that is the same as any other phosphocholine lipid found in nature. Since FOS-14 readily strips charge from protein ions, this suggests phosphocholine lipids may also strip charge from membrane proteins in the gas phase when activated from detergent-lipid micelles or lipoprotein nanodiscs. This may have significant ramifications for native-MS studies of membrane protein-lipid binding interactions where the strength of such interactions is of interest, and leads to the important question of, to what extent does the abundance and strength of these gas-phase interactions reflect membrane protein-lipid binding affinities in solution?

CHAPTER IV

NON-SPECIFIC BINDING OF LIPID HEAD GROUPS TO SOLUBLE PROTEINS AND α -HEMOLYSIN LIPID BINDING IN DETERGENT-LIPID MICELLES AND LIPOPROTEIN NANODISCS

While the material included here is primarily my own work, Micah T. Donor, Amber D. Rolland, and Samantha O. Shepherd assisted with sample preparation and analysis. James S. Prell contributed to experimental design and interpretation. This work will form portions of manuscripts to be submitted in the future, with the above named as co-authors.

Introduction

Over the last decade native-MS has expanded dramatically to the application of membrane protein systems.^{21,85} Using native-MS to determine the strength of interactions between membrane proteins and various lipids is of particular interest to structural biology due to the difficulty of studying these interactions by the more traditional techniques mentioned in Chapter I, and the importance these interactions have on some membrane proteins.^{15,16,54,56,106,176} The key advantage of native-MS in this respect is that membrane protein-lipid interactions can be studied from solutions that contain biologically relevant concentrations of components and the native-like structure and stoichiometry of these interactions can be maintained.

The Robinson, Laganowsky, Marty, Klassen, and Wysocki groups have pioneered native-MS techniques to study membrane protein-lipid interactions in a broad range of

membrane mimetic systems such as detergent-lipid micelles,^{16,102,106,157,177,178} lipoprotein nanodiscs,^{89,90,109,112,179–181} and even from native membrane vesicles.^{113,114} In several of these studies, based on relative abundances of apo or ligand bound states collected from native mass spectra, apparent dissociation constants or mole fraction binding affinities were measured between membrane proteins and lipids or other small molecules or peptides.^{16,106,108,116,182} These measurements are then used to demonstrate solution-based phenomena such as allostery between lipid binding events or propose gating mechanisms in ion channels based on lipid binding.^{108,182}

However, as exemplified in Chapter III, there may not be an exact correlation between association of molecules measured in the gas phase with solution phase interactions. Non-specific association between two species can be an artefact of the nano-electrospray ionization (nESI) process as species in the same droplet form a complex as the droplet evaporates, when the concentrations of species is sufficiently high.^{183–185} This is commonly seen between proteins and salts in nESI experiments. Even though native-MS typically uses the volatile salt ammonium acetate in solution to suppress non-volatile salt adduction, sodium ions are almost always detected on compact native-like proteins. As shown in Chapter III the strength of interaction between native-like protein complexes and salts in the gas-phase can prove to be robust, requiring significant gas-phase activation for removal of these non-specific interactions.

The non-specific association between lipids and membrane proteins in detergent micelle solutions should be considered as a possibility in nESI experiments due to the μM concentrations of proteins and lipids used. Landreh et al. considered this possibility when they compared nESI lipid binding between a membrane protein and bovine serum

albumin (BSA, a soluble protein that should not readily bind lipids in solution) from detergent-lipid micelle solutions.¹⁸⁶ They found significantly higher levels of lipid binding with the membrane protein in comparison to BSA using nESI and concluded the association between the membrane protein and lipids was located at sites along the transmembrane region and not along unrelated charge sites where lipid headgroups could non-specifically adduct. While this experimental framework does support that non-specific association between proteins and lipids is unlikely to be a considerable contribution to initial binding in nESI experiments, it does not however, account for the relative strength of protein-lipid binding interactions in the gas phase and the significant amount of gas-phase activation typically required to remove the detergent micelle from membrane proteins. The ideal scenario for translating observed gas-phase association in terms of physiologically-relevant protein-lipid interactions is that trends in lipid binding in the gas phase mimics solution phase binding affinities and is not merely a gas-phase phenomenon due to the chemistry of the lipid headgroup.^{16,89,106,116,182}

Common lipid tails have no readily ionizable bonds, but lipid headgroups are polar and either negatively charged or zwitterionic in solution at neutral pH. The acidic phosphate and/or basic amine groups of the common biological lipids could form shared-proton bonds with basic residues on the protein surface where proteins are thought to be typically charged in the ESI process.¹⁸⁷ The strength of these shared proton bonds relies upon the gas-phase basicity (GB) values of both species, with stronger interactions forming when the GB values of each species are similar, than when one species is more basic than the other. A recent study of the GB of common biological lipids from my colleagues in the Prell and Donald groups demonstrated that the phosphatidylcholine and

sphingomyelin lipids are the most basic in the gas phase (highest GB value) of any small biomolecule measured to date and significantly more basic than arginine.¹⁸⁸ They also found that phosphatidylserine and phosphatidylethanolamine have GB values very similar to the basic amino acids lysine and histidine, and that phosphatidic acid and phosphatidylglycerol are the least basic, but still more basic than alanine. This means that, for protein-lipid complex ions with a net positive charge, phosphatidylcholine and sphingomyelin should form rather weak shared proton bonds with acidic amino acids, while the other lipids should form stronger interactions in the gas phase, with phosphatidylserine and phosphatidylethanolamine the strongest. Another prediction from these studies is that lipids with a phosphocholine headgroup (i.e., sphingomyelin and phosphatidylcholine) should act as charge reducing reagents upon gas-phase activation, such that if phosphatidylcholine associates with a protonated site on a protein using ESI, upon gas-phase dissociation, the phosphatidylcholine lipid should dissociate as a protonated species.

To experimentally test these predictions for the gas-phase behavior of protein-lipid complexes, I used soluble proteins and lipid headgroups (without acyl chains in order to increase their solubility) aqueous solutions. This experimental framework allows for the interrogation of only non-specific interactions between proteins and lipid headgroups without the need for detergents or nanodiscs required with membrane proteins and full lipids. In this chapter I demonstrate that lipid headgroups can indeed non-specifically associate with proteins through nESI and that the general extent and strength of binding follows the outlined predictions with phosphoserine and phosphoethanolamine strongly binding to proteins in the gas phase and the ability of

phosphocholine to act as a charge reducing reagent. These results demonstrate the importance in considering the GB of lipid headgroups when studying membrane protein-lipid interactions with native-MS and indicate that current protocols for identifying physiologically relevant interactions with native-MS may be insufficient.^{106,107,115,176,189} I also include α HL lipid binding experiments in detergent-lipid micelle solutions and lipoprotein nanodiscs with the goal of how these complexes can continue to be studied based in light of solution experiments that predict the preference for phosphocholine lipid binding by α HL complexes.

Methods

Sample preparation. The lipid headgroups phosphoserine (PS), phosphorylethanolamine (PE), glycerolphosphocholine (GPC), and glycerol 1-phosphate sodium salt (PG), as well as the proteins transferrin and α HL monomers were purchased from Millipore Sigma. The soluble lyophilized protein transferrin was reconstituted in ultrapure 18 M Ω water and buffer-exchanged into 200 mM ammonium acetate pH 7.5. Lipid headgroups were similarly dissolved in the same 200 mM ammonium acetate solutions. For the transferrin experiments the final concentration of protein was 5 μ M with 0.5 mM of one lipid headgroup, or in mixed headgroup solutions, 0.5 mM of each headgroup.

α HL monomers were oligomerized in C₈E₄ micelle solutions as described in Chapter II and Appendix B. For detergent-lipid micelle solutions, lipids dissolved in chloroform were dried under a stream of dry nitrogen and weighed. The dried lipids were then reconstituted with sonication in 16 mM C₈E₄ micelle solutions as 5 mg/mL lipid

stocks. The lipid concentration could then be further diluted as needed for lipid binding experiments.

Additionally, α HL monomers oligomerized in C₈E₄ micelle solutions were attempted to be inserted into single lipid lipoprotein nanodiscs with either MSP1D1 (diameter ~10 nm) or the larger MSP1E3D1 (diameter ~ 12 nm) membrane scaffold proteins (MSP). This was done following standard protocols.^{190,191} Briefly, the membrane scaffold proteins were expressed in *E. coli* (BL21(DE3)).^{192,193} Lipid and sodium cholate stocks were made at 50 mM lipid to 100 mM sodium cholate. The nanodisc assembly mixture included 12 μ M MSP, the appropriate ratio of lipid needed based on the surface area of the lipid (for instance 80:1 DMPC to MSP1D1),¹⁹⁰ additional sodium cholate (to maintain 20 mM concentration in excess of the critical micelle concentration), and α HL complexes oligomerized in C₈E₄. The concentration of α HL complexes was assumed to be 1-2 μ M in the final assembly mixture but is difficult to measure due to protein impurities in the raw sample and the presence of α HL monomers still in solution. Assuming these concentrations of toxin complexes approximately 1:6 to 1:4 nanodiscs made are toxin embedded. After incubation for at least one hour, samples were dialyzed overnight on biobeads (at the melting point transition temperature of the lipid used) to remove the cholate in a buffer containing 50 mM Tris, 100 mM NaCl, and 0.5 mM EDTA at pH 7.5. The next day samples were then dialyzed overnight into 200 mM ammonium acetate pH 7.5. Samples were then either ready for use as is or were further purified using a size-exclusion chromatography to enrich for α HL nanodisc inserted complexes over empty nanodiscs. Control nanodiscs without α HL complexes were also made to ensure the nanodisc procedure worked accordingly. Samples were additionally

analyzed using SDS-PAGE to check for the presence of α HL and the MSP, as was done with α HL detergent micelle complexes from Chapter II and in Appendix B.

Native IM-MS. Most mass spectra were acquired using a Synapt G2-Si (Waters Corp.) quadrupole-ion mobility-time-of-flight mass spectrometer with a nESI source. Where stated, some additional mass spectra of α HL nanodisc complexes were acquired on a Thermo Scientific Q-Exactive Ultra High Mass Range (UHMR) Orbitrap mass spectrometer also with a nESI source. For both instruments, nESI emitters were pulled from 0.78 mm i.d. borosilicate capillaries to a final i.d. of \sim 1-3 μ m with a Flaming-Brown P-97 micropipette puller from Sutter instruments. Pulled emitters were filled with 3-5 μ L of sample and spray was initiated with a platinum wire inserted into the sample solution and a spray voltage of 0.7-1.0 kV.

For the lipid headgroup studies with transferrin, the Synapt source was held at ambient temperature. The nitrogen, helium, and argon gas flow rates were 50, 100, and 5 mL/min, respectively. The IMS traveling wave velocity was set to 400 m/s and a wave height of 20 V. For collision induced dissociation experiments the trap potential was incrementally raised in 10 V steps from 10-100 V while the source sampling cone potential was held at 25 V. For each transferrin-lipid headgroup combination tested the activation series was performed with isolation of the 19+ charge state at a LM resolution of 4. This allowed for charge stripping to be readily detected upon dissociation of the lipid headgroup. Some additional mass spectra were acquired without quadrupole isolation at 10, 50, 70, and 100 V of trap activation.

Data analysis. Native mass spectra of transferrin with each lipid headgroup were deconvolved using Unidec^{160,161} to determine the charge state and mass distributions.

This also aided assignments of lipid headgroup adducts across charge states.

Deconvolved mass spectra were then further analyzed using Igor Pro (Wavemetrics) in a similar way as in Chapter II and III. α HL complexes embedded in nanodiscs were analyzed with iFAMS using GT as outlined in Chapter II.^{87,88,118}

Results and Discussion

Lipid headgroups readily adduct to native transferrin protein ions in nESI.

The lipid headgroups phosphoserine (PS), phosphorylethanolamine (PE), glycerolphosphorylcholine (GPC), and glycerol 1-phosphate (PG) are some of the most common biological headgroups and their structures are shown in Figure C1 in Appendix C. GPC was used instead of phosphorylcholine (PC) because without the glycerol group PC and PS headgroups have a mass difference of ~ 1 Da and would be difficult to differentiate in mixed lipid headgroup experiments. Transferrin was selected as a model soluble monomeric protein due to its rather large size of 79.6 kDa (of the same order as many membrane protein complexes) and homogeneity in base mass with no identified isoforms. Transferrin, an iron-binding protein with homologs found in many organisms, has no known physiologically relevant interactions with lipids. Native mass spectra of transferrin are shown in Figure C2 in Appendix C at 10, 50, or 70 V of trap activation. Figure 11 depicts native mass spectra of solutions containing 5 μ M transferrin and 0.5 mM of each lipid headgroup tested individually at a low trap activation of 10 V (Figure 11A) and a moderate trap activation of 70 V (Figure 11B). At low trap activation transferrin with each headgroup forms a narrow charge state distribution of 17-21+ (most abundant charge state 19+) with ~ 1200 Da of excess mass.

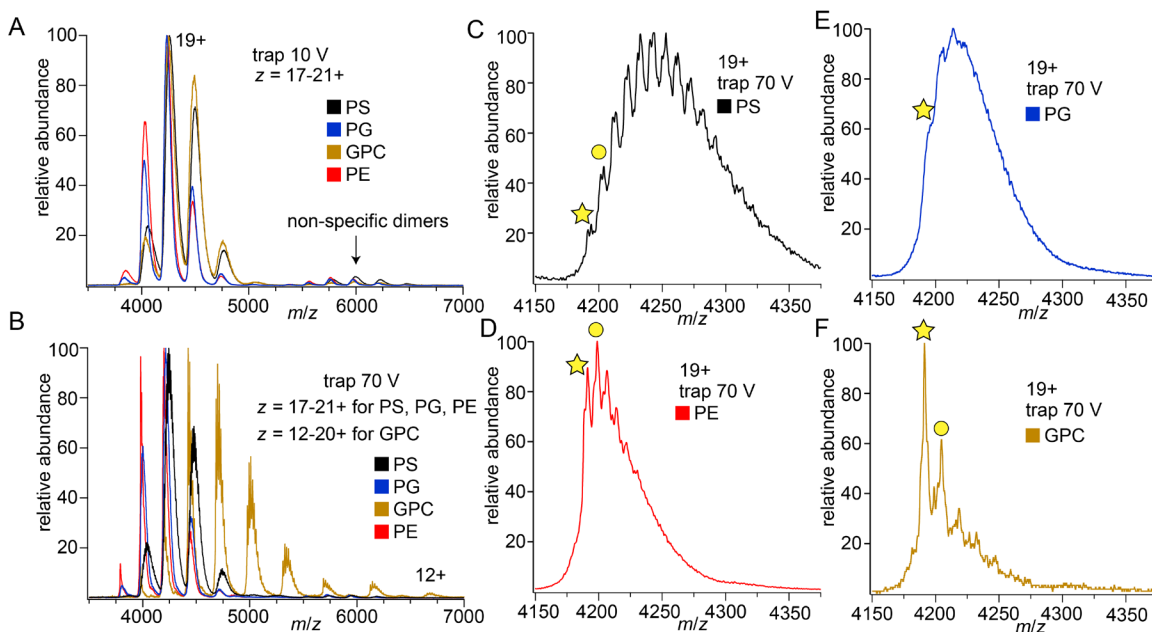


Figure 11. Native mass spectra of transferrin and common lipid headgroups. nESI of solutions containing 5 μM transferrin and 0.5 mM of either PS, PG, GPC, or PE. (A) Overlaid mass spectra with each headgroup at a low trap activation of 10 V. (B) Overlaid mass spectra with each headgroup at a moderate trap activation of 70 V. Substantial charge stripping is observed of transferrin as GPC adducts are dissociated. (C-F) Comparison of transferrin¹⁹⁺ with each lipid headgroup under the same instrumental conditions. Stars mark the transferrin¹⁹⁺ base peak with no adducts and the circles mark the first resolved adduct from a given lipid headgroup.

Distinct adducts are not resolved under these light activating conditions. Around a trap potential of 50 V, resolution of individual adduction states is detected with clear resolution by 70 V with all headgroups except for PG (Figure 11 B). At this trap activation charge stripping is seen in the mass spectra of transferrin with GPC as adducted GPC is dissociated. This supports the prediction that the GPC headgroup, with its high GB value can act as a charge reducing agent upon dissociation. No clear charge stripping is detected from the other lipid headgroups upon dissociation.

Figure 11C-F shows mass spectra of transferrin¹⁹⁺ complexed non-specifically with each type of lipid headgroup. The extent of binding at this level of trap activation on

transferrin¹⁹⁺ follows the trend PS > PE ≥ PG > GPC. Under these conditions the most abundant adduction state of transferrin¹⁹⁺ is 5 PS adducts in comparison to 1 PE adduct, while the unadducted base peak for transferrin¹⁹⁺ is the most abundant in GPC solutions. Due to the anionic character of PG, these solutions include sodium, which additionally adducts in nESI and obscures clear individual adduction states of PG. This trend in binding is again in line with the predictions made based on the GB of each lipid headgroup where the similarity in GB of PS the basic residues lysine and histidine leads to strong gas-phase interactions, while the high GB of GPC leads to weaker interactions.

To gain a better understanding of the extent and gas-phase strength of these associations, Figure 12A-D depicts charge-state deconvolved (Unidec) mass spectra of

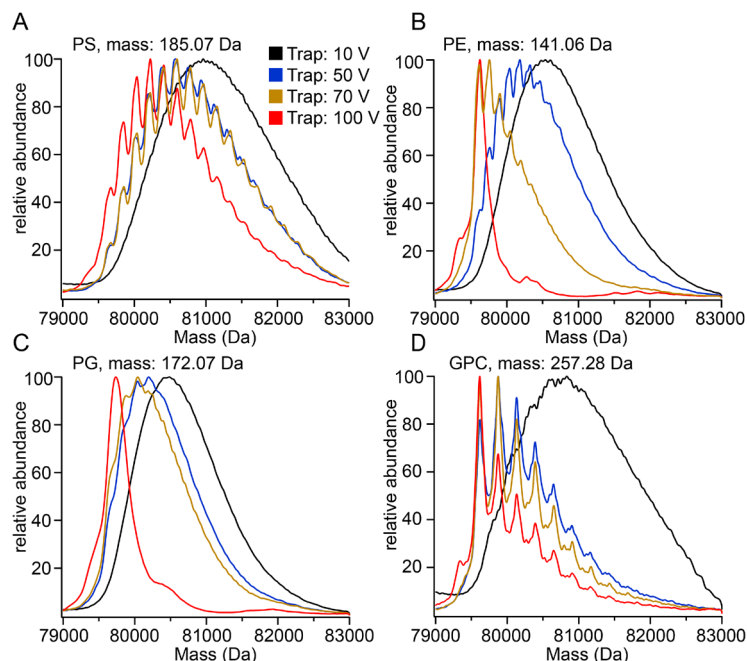


Figure 12. Deconvolved native mass spectra of transferrin with common lipid headgroups. Overlaid deconvolved (using Unidec) native mass spectra using of transferrin with (A) PS, (B) PE, (C) PG, or (D) GPC as the trap activation voltage was raised from low (10 V) to high (100 V).

transferrin with each lipid headgroup under the given trap activation voltage (10, 50, 70, and 100 V). Charge state deconvolution allows for analysis of the headgroup adduction

state across all the charge states present in each mass spectrum as the activation level is raised. PS clearly forms the strongest interactions with transferrin. At a trap potential of 100 V, several PS adducts remain bound. With transferrin alone at 100 V much of the protein has undergone dissociation (Figure C3 in Appendix C), showing that these PS adducts are very robust. Several PE adducts are resolved by 50 V, but for PG mass spectral resolution remains poor. For both PE and PG, headgroup adducts are stripped from transferrin by 100 V, while GPC adducts remain bound. At first glance these remaining GPC adducts seem to counter the predictions made that GPC should weakly associate to proteins based on GPC's high GB value. However, the observed adduction at 100 V is due to the high degree of charge stripping that occurs upon GPC dissociation. The charge-stripped ions have lower Coulomb repulsion between their remaining charge sites, which reduces the propensity to further strip GPC adducts.^{112,194,195} This observation is additionally supported by the higher degree of adduction on the lower charge state transferrin ions in Figure 11B. In the case of lipid binding studies to membrane proteins, this implies that gas-phase binding thermodynamics may dramatically affect which lipids remain bound to the protein as lipids and other adducts are removed in the gas phase, leading to the heightened possibility of incorrect interpretation of these data in terms of physiologically relevant membrane protein lipid specificity if extreme caution is not exercised. In a mixed lipid situation these observations would additionally predict that PS headgroup lipids would likely be the lipids resolved if substantial gas-phase activation is required to resolve lipid binding.

Mixed lipid headgroup studies reveals PS outcompetes other lipid headgroups for transferrin association. It is important to consider competition in lipid

headgroup binding to proteins as the gas-phase collisional activation is incrementally raised. Often in native-MS experiments of membrane proteins in nanodiscs or detergent-lipid micelles a mixture of lipids may be used with the goal of understanding which type of lipid binds more strongly to the membrane protein than others.^{89,108} In these experiments stepwise collisional activation is used to incrementally strip off excess lipids and/or detergents that are loosely bound till only a few lipids remain. These most tightly bound lipids are typically interpreted to be structural lipids bound between protein subunits or annular lipids that directly surround the membrane protein.^{16,89,106} Based on the strength of PS headgroup adducts displayed in Figures 11 and 12 it is clear that, in some cases, PS adducts can outcompete other lipid headgroups for binding in this type of gas-phase collisional activation experiment in a way that could be interpreted, according to current protocols,¹⁷⁶ as specific interactions from solution.

To test this prediction, solutions containing 5 μ M transferrin were mixed with 0.5 mM of two lipid headgroups and investigated using nESI with incremental steps in trap collisional activation. Transferrin¹⁹⁺ ions with multiple lipid headgroup adducts were isolated to additionally track charge loss upon dissociation of any lipid headgroups. Figure 13A shows deconvoluted transferrin¹⁹⁺ with PS alone as the trap collision energy is scanned from 10-100 V, while Figure 13B-D shows the combination of PS with the other lipid headgroups tested. In every combination of PS with GPC (13B), PE (13C), or PG (13D), at high collisional activation PS adducts are resolved and the other lipid headgroup is either never resolved (PE and PG) or is removed by 100 V in the trap (GPC). In the case of transferrin with PS and GPC at 80 V the deconvoluted mass

distribution shows some evidence of PS and GPC (lower abundance) binding, but at 100 V only PS adducts are resolved. With PS and PE, only PS adducts are ever resolved at 60

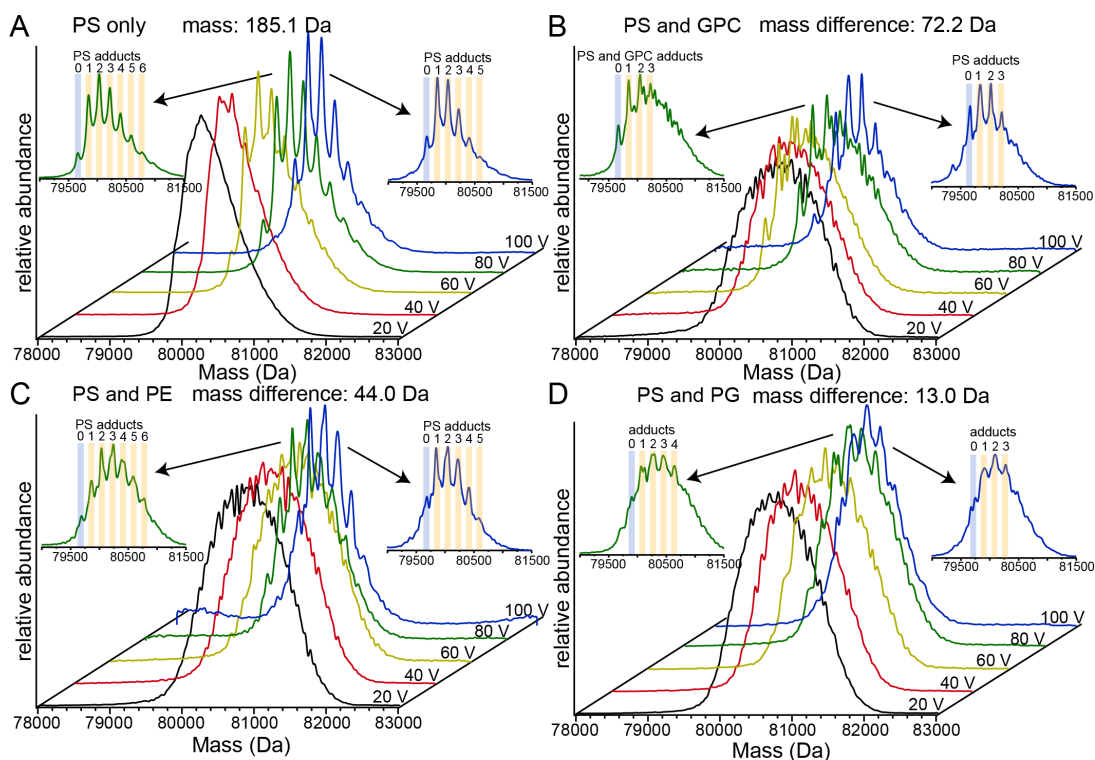


Figure 13. Selected deconvolved mass spectra of transferrin¹⁹⁺ with PS alone (A), PS and GPC (B), PS and PE (C), and PS and PG (D) as the trap is incrementally raised from 10-100 V in 10 V steps. In each case of mixed lipid headgroups, PS adducts are observed at high activation in support that PS forms the strongest shared protein bonds with proteins in the gas phase. The mass difference between the lighter and heavier lipid headgroup is given with every combination.

V and above. With PS and PG there is a small mass difference (13.0 Da) between the two headgroups and the addition of extra sodium with PG frustrates adduct resolution.

However, comparing the mass distributions of transferrin with PS alone and PG alone to the mixed combination demonstrates that the poorly resolved adducts in the PS and PG headgroup mixture are likely PS adducts at 100 V of trap activation (Figure C4 in Appendix C).

These mixed-lipid headgroup experiments demonstrate that PS forms stronger shared proton bonds with positively charged protein ions in the gas-phase than do the other lipid headgroups tested. These results indicate that extreme caution should be used in interpreting survival of PS-membrane protein interactions in native-MS collision-induced dissociation experiments as being physiologically important.^{16,106,115} By extension, these results also indicate that quantitative solution-phase lipid-binding affinities for membrane proteins as currently determined by native-MS protocols may often reflect artifacts of gas-phase binding thermodynamics.^{115,176,189,196}

Only GPC removes charge when dissociated and is consistent across mixtures of headgroups. While Figure 11 demonstrates that GPC dissociation can cause significant charge stripping, it is important to make sure that other lipid headgroups do not display the same behavior as predicted based by their respective GB values and to understand to what extent charge stripping occurs with GPC. Since the experiment described above was performed with quadrupole isolation of transferrin¹⁹⁺ with adducts, changes in the weighted average charge state and width of the charge state distribution were tracked as the trap activation was raised. Figure 14 shows the weighted average loss of charge from these isolated transferrin¹⁹⁺ ions as they are activated in the trap and lipid headgroups dissociate. Every lipid headgroup-transferrin solution tested with GPC alone or in combination with another lipid headgroup yielded charge loss as GPC dissociated from transferrin. With GPC alone at 100 V on the trap, the weighted average charge state is 16.3 ± 1.6 demonstrating a loss of 2.7 charges from transferrin¹⁹⁺ on average. In comparison to transferrin with PS at 100 V trap activation, transferrin maintained an average weighted charge state of 19.0 ± 0.57 (small amount of transferrin¹⁸⁺ detected,

likely from imperfect isolation in the quadrupole due to overlapping precursor m/z distributions). Figure 14 demonstrates that only GPC leads to charge stripping while the other lipid headgroups do not cause measurable loss of charge upon dissociation. On

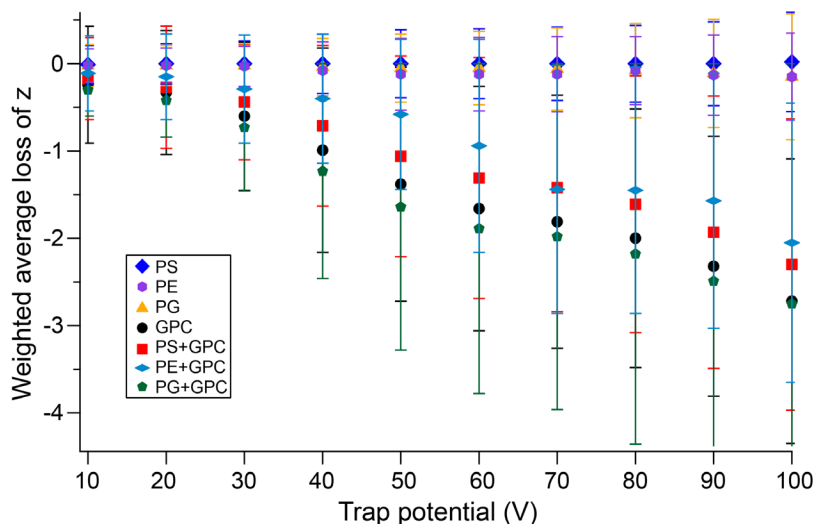


Figure 14. Weighted average loss of charge of isolated transferrin¹⁹⁺ as lipid headgroups are dissociated as the trap activation was incrementally raised in 10 V increments from 10-100 V. Error bars represent one standard deviation of the charge state distribution. Only incorporation of GPC leads to significant charge stripping and broadening of the charge state distribution as GPC is dissociated from transferrin.

average 2-3 charges are consistently lost when GPC is used along with other lipid headgroups across the range of activation tested. This experimentally confirms that the GPC lipid headgroup, which has a high GB, can effectively act as a charge reducing reagent when dissociated from protein ions in the gas phase. In contrast, the other lipid headgroups studied do not strip charge upon gas-phase ion activation.

Lipid binding studies of α HL complexes oligomerized in C₈E₄ detergent micelles. The above experiments using a non-membrane protein establish that artefactual association of lipid headgroups to proteins in the gas-phase using nESI can display patterns that can be misinterpreted according to current protocols as evidence of solution preference-phase lipid preference. We next investigated this effect using membrane

proteins and full lipids (i.e., including acyl tails). Figure 15 shows native mass spectra of α HL complexes oligomerized in C_8E_4 with 1 mM 1,2-Dimyristoyl-sn-glycero-3-phosphocholine (DMPC) lipid. Here, as the cone potential was held at 75 V and the trap

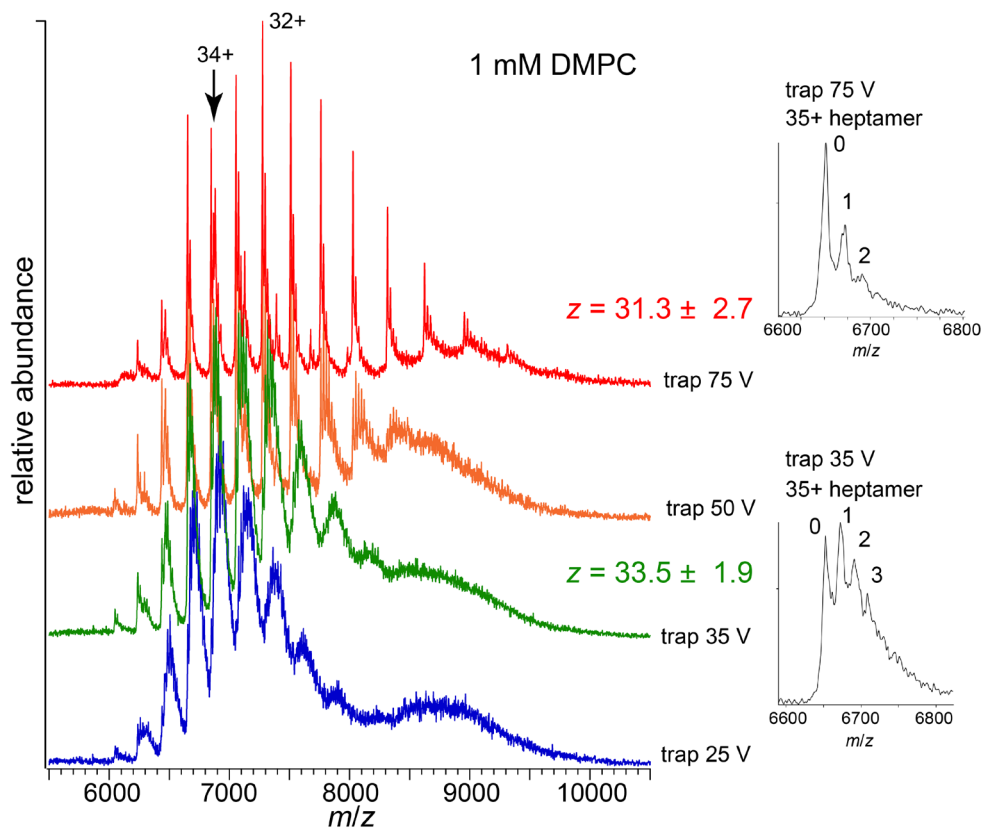


Figure 15. α HL complexes oligomerized in C_8E_4 detergent micelles with 1 mM DMPC lipids added. By a cone potential of 75 V and a trap potential of 35 V the detergent micelle is stripped leaving α HL complexes with bound DMPC lipids. Increasing the trap collisional activation to 75 V dissociates several DMPC lipids and reduces the average charge state distribution. The inset shows the 35+ heptamer ions with up to 3 DMPC lipids bound at 35 V in the trap and fewer bound lipids at 100 V.

collisional activation was raised stepwise from 25 V to 75 V. Beginning at a trap potential of 35 V, the detergent micelle has been removed revealing, up to 3 DMPC lipid adducts (see inset on right side of figure). The ions in this mass spectrum had a weighted-average charge state of $(33.5 \pm 1.9)^+$. As the trap collisional activation was raised to 75 V, DMPC lipid adducts are stripped (see inset spectrum) and the average charge state is

reduced to $(31.3 \pm 2.7)^+$. This experiment indicates that DMPC lipids, which have PC headgroups, can strip charge from a membrane protein and dissociate as positive ions. There are a few caveats to this experiment, however. Namely, the lipid concentration used here is higher than typical of native-MS experiments of detergent-lipid micelles, which are commonly done around 200 μM or below.^{16,108} Additionally, a more decisive demonstration of charge-stripping capability of DMPC and other PC headgroup lipids would to use similar isolation experiments are outlined with transferrin¹⁹⁺ ions with lipid headgroup adducts. (Such experiments were planned, but not possible to execute, due to the shelter-in-place order in Oregon in response to the 2020 COVID-19 pandemic.)

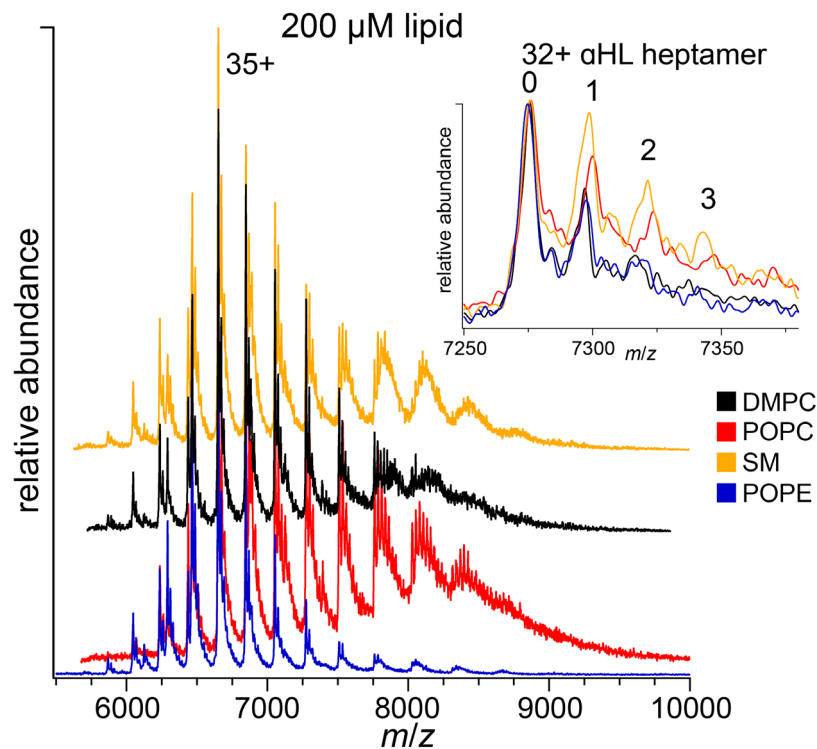


Figure 16. αHL complexes oligomerized in C_8E_4 detergent micelles with 200 μM of the designated lipid added to solution. Instrument conditions were the same for each lipid tested with 50 V collision potential applied to the cone and trap. This level of collisional activation is sufficient to remove the detergent micelle and reveal lipid binding. Each lipid tested associates with αHL , including the non-PC headgroup lipid POPE. The inset shows the 32+ heptamer with each lipid with up to 3 binding events detected.

Nevertheless, this experiment demonstrates the charge stripping potential of the PC headgroup on a full lipid when bound to a membrane protein.

Figure 16 displays four different lipid binding experiments to α HL complexes at 200 μ M lipid. Three of these lipids share the PC headgroup (1-palmitoyl-2-oleoyl-glycero-3-phosphocholine (POPC), N-stearoyl-D-erythro-sphingomyelin (SM), and DMPC), while one has the PE headgroup (1-palmitoyl-2-oleoyl-sn-glycero-3-phosphoethanolamine (POPE)). At 200 μ M lipid concentration, α HL complexes are found in these native-MS experiments to bind each of these lipids to varying extents. As mentioned in Chapter IV, α HL is thought to have lipid preference for PC headgroup lipids with specific binding sites between the rim and stem domains of the complex.^{149,159,165} Based on these mass spectra and the abundances of the lipid bound states, there is a higher degree of association between α HL complexes and the PC headgroup lipids over POPE (see inset of 32+ heptamer ions with lipids bound).

α HL lipoprotein nanodisc complexes The above-described transferrin experiments with lipid headgroups demonstrate that the GB of lipids may lead to artefactual gas-phase derived affinities in detergent-lipid micelle experiments, thus it is important to study membrane proteins with as many lipids still bound as possible and as little gas-phase activation as necessary to resolve and interpret their mass spectra. Ideally this would be achieved using lipid bilayer mimics, such as nanodiscs, rather than detergent micelles as hosts for the membrane protein complex. Further, limiting gas-phase activation can prevent loss of lipids that may be physiologically important in solution but may not bind as tightly in the gas-phase, such as lipids containing PC/SM headgroups. Interpreting mass spectra of membrane proteins with far more lipids bound

than is currently done in lipid-affinity native-MS work should therefore be a more reliable way to investigate physiologically relevant lipid-binding and -recruiting preferences.

Nanodiscs are commonly used as a membrane mimetic in condensed-phase studies, as they can often be closer to a physiological membrane environment than are detergent micelles.^{40,89,90,179} Depending on the size of the membrane scaffold protein (MSP) used, nanodiscs can contain ~100-400 lipids with membrane protein complexes,

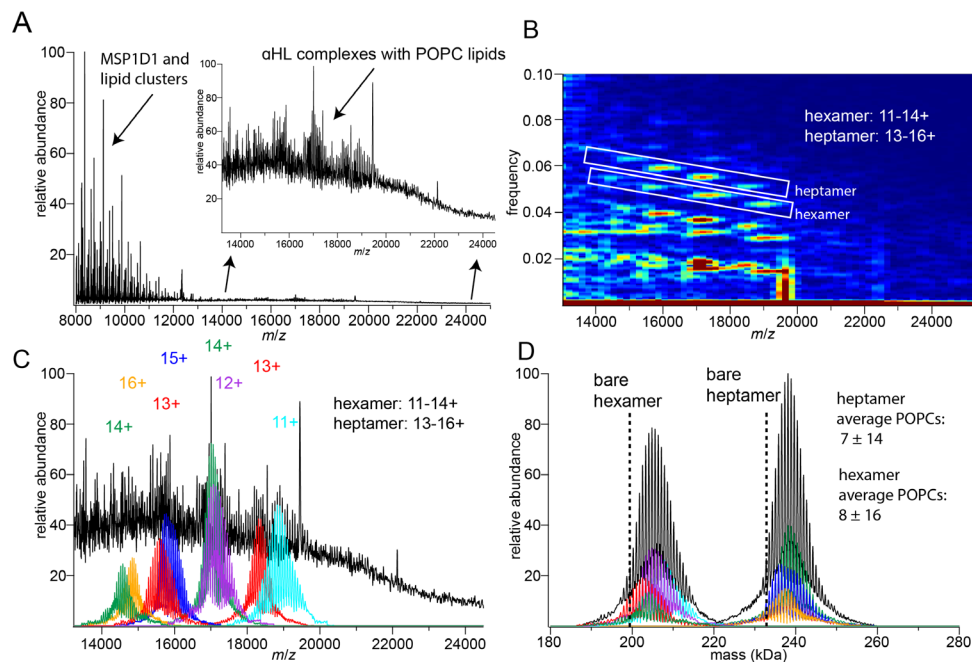


Figure 17. α HL complexes inserted into POPC MSP1D1 nanodiscs and ejected using 5% glycerol carbonate. (A) Mass spectrum collected on UHMR Orbitrap instrument with high in-source activation to strip away the MSP and most of the POPC lipids. (B) Gabor Transform of mass spectrum in (A). (C) shows the deconvolved mass distributions from the GT. (D) Zero-charge mass spectrum from the GT. Vertical dashed lines mark the mass positions of bare hexameric and heptameric complexes.

in contrast to the handful of lipids per micelle used in detergent-lipid micelle experiments. The Marty and Prell labs recently reported using chemical additives in solution that dramatically increase the charge states of proteins in ESI to destabilize membrane protein nanodisc complexes.⁹⁰ Adding 5% glycerol carbonate (GC) in positive

ionization mode resulted in ejection of intact membrane protein complexes from the nanodisc with a few bound lipids such that lipids binding directly to the membrane protein could be detected and the mass spectra were resolved enough for detailed interpretation. This method allows for the investigation of annular lipids that bind around the surface of the membrane protein.

Assembly of α HL complexes inserted into lipoprotein nanodiscs (α HL NDs) has not heretofore been reported in the literature. I developed a protocol for nanodisc insertion based around forming α HL complexes in C₈E₄ detergent solutions as in Chapter II, to which the nanodisc components solubilized in cholate detergent were added to form nanodiscs once the cholate is removed through dialysis.^{190,191} This is schematically depicted in Figure C5 in Appendix C and supported by SDS-PAGE analysis (Figure C6 in Appendix C). Importantly, this protocol produces 2-3x the number of empty nanodiscs than α HL complex-embedded nanodiscs with the goal that all α HL complexes survive the nanodisc insertion procedure leading to complications in separating mass spectral signals corresponding to empty nanodiscs from complex embedded nanodiscs

Figure 17A shows a mass spectrum of α HL ND complexes formed with POPC lipids collected on a UHMR Orbitrap mass spectrometer. To this solution 5% (vol/vol) GC was added to dissociate the nanodisc and release α HL complexes with POPC lipids bound. Most of the signal detected in Figure 17A (m/z ~8000-12000) corresponds to MSP1D1 and POPC lipid clusters that are being dissociated from the NDs. At higher m/z (~13000-20000) ejected α HL complexes are detected with bound lipids. Analyzing this portion of the mass spectrum would be very challenging by hand. Using GT (Figure 17B) as outlined in Chapter II and III allows for analysis of this congested mass spectrum. In the

GT frequency signals corresponding to the hexamer and heptamer can be separated and analyzed individually across all the charge states detected. Figure 17C shows the reconstructed mass spectrum from the inverse GT and highlights the overlap of the hexamer and heptamer distributions in the mass spectrum. Each charge state distribution is then combined in the deconvolved zero-charge spectrum in Figure 17D. From this deconvolved spectrum both the heptamer and hexamer are detected with about the same number of bound POPC lipids with an average of ~8 and up to 20 associated lipids. This mass spectrum demonstrates that α HL complexes can be inserted into lipoprotein nanodiscs with many more associated lipids than in detergent-lipid micelle solutions. The assembly protocol developed here sets the stage for future study of lipid binding using a membrane mimetic platform that may be much less prone to gas-phase artefacts than state-of-the-art protocols using detergent micelles and extensive gas-phase collisional activation.

Conclusions

The non-specific association between several of the most common biological lipid headgroups and the soluble protein transferrin was investigated in light of the GB measurements and calculations that were recently performed.¹⁸⁸ Each lipid headgroup tested readily bound to transferrin using nESI and the strength of these interactions followed the pattern $PS > PE \geq PG > GPC$. PS adducts proved to be very robust to gas-phase activation. In comparison, GPC headgroups were found to readily strip charge from transferrin upon dissociation leaving the charge stripped transferrin ions less prone to further dissociation of GPC adducts. These trends correlate well with the GB measures of each lipid headgroup. Since PS has a GB value similar to lysine, PS can form a strong

shared proton bond that resists dissociation. In comparison, the high GB value of GPC leads to rather weak shared proton bonds with amino acids, and to charge stripping upon dissociation. This leaves PE and PG headgroups in-between the two extremes. PE seems to more readily adduct to transferrin than PG, but this may be due to the difficulty of resolving PG adducts by the addition of sodium with PG.

Since the GB of lipid headgroups clearly affects the extent and strength of non-specific association with proteins in the gas phase it is important to extend these results to membrane proteins with full lipids. α HL complexes in detergent-lipid micelles provides a potential platform for these studies. With high concentrations of DMPC lipids and sufficient gas-phase activation, DMPC does seem to dissociate from α HL complexes with a positive charge, supporting the GB measures.

X-ray crystallography and solution studies suggest a preference for α HL binding to PC headgroup lipids.^{149,159,165} Experiments with α HL complexes in detergent-lipid micelles shown here demonstrates that lipids will associate with α HL in native-MS experiments, including the non-PC headgroup lipid POPE. It would be interesting to test mixed lipid binding experiments between PC and PS lipids and demonstrate which lipid stays bound upon significant gas-phase activation. If the PS lipid remains bound over the PC lipid this would indicate that membrane protein-lipid binding native-MS experiments should be interpreted with extreme caution. Additionally, this chapter outlines the potential of studying α HL lipid interactions in lipoprotein nanodiscs instead of detergent-lipid micelles. Studying membrane protein-lipid interactions using lipoprotein nanodiscs may prove to be a better membrane mimetic platform than detergent-lipid micelles due to the higher similarity between nanodiscs and biological lipid-bilayers and the possible

artefacts caused by the gas-phase activation needed to strip the detergent micelle before lipid binding is observed.

OUTLOOK

Native mass spectrometry has emerged as a powerful tool for structural biology to investigate non-covalent complexes between proteins and small molecules like lipids. The study of membrane protein interactions with lipids is a notoriously difficult problem, but specific protein-lipid interactions have been demonstrated to be of physiological importance. This dissertation presents methods and analysis to further expand the frontiers of native mass spectrometry to investigate membrane protein detergent and lipid interactions as applied to bacterial pore forming toxins.

While recent X-ray crystallography, electron microscopy, and other solution-based techniques had predominantly identified the pore forming toxin α HL from *S. aureus* to form only heptameric complexes, using native mass spectrometry as outlined in Chapter II, demonstrated that α HL forms both hexameric and heptameric complexes simultaneously. This was additionally confirmed in two very different detergent micelle solutions, including the detergent FOS-14, which is lipid-like. This work in FOS-14 solutions highlighted the power of Gábor Transformation techniques to aid interpretation of congested mass spectra, and thus reduces the need to strip away the detergent micelle in order to determine the oligomeric state of membrane proteins in native-MS experiments. This chapter also pointed to the capability of native-MS to maintain compact native-like protein structures in the gas phase using ion-mobility and demonstrated the accuracy of simple MD simulations to predict the amount of compaction protein complexes undergo upon transfer from solution to vacuum.

In Chapter III simple instrument modifications were introduced to aid desalting and detergent or lipid removal in the source region of the Synapt “Stepwave” based mass spectrometer. This work used source sampling cones with smaller apertures to reduce the source pressure, and thus increase ion heating in the source region to dissociate non-specific salts and adducts. Using these smaller sampling cones greatly reduced the cone potential needed to reach the same level of desalting, while maintaining similar signal levels, without causing higher degrees of protein ion unfolding. This work also exemplified the charge reducing capability of the phosphocholine headgroup of α HL FOS-14 detergent micelle complexes when FOS-14 is dissociated through gas-phase activation.

Chapter IV continued this work to study the non-specific association between lipid headgroups and the soluble protein transferrin as well as the association between lipids and α HL complexes in detergent-lipid micelles and lipoprotein nanodiscs. This work was grounded in predictions made based on the gas-phase basicity values of lipid headgroups. The lipid headgroups phosphoserine and phosphoethanolamine were found to form strong gas-phase interactions with transferrin, while phosphocholine weakly associated and stripped charge from transferrin upon dissociation. These observations are consistent with predictions made based on the GB values of the headgroups tested, and thus sound a note of caution to the native-MS community in interpreting the physiological role of protein-lipid interactions from gas-phase experiments. Chapter IV also outlined the potential to further probe protein-lipid interactions using α HL complexes in detergent-lipid micelles and lipoprotein nanodiscs and the role GB plays with these interactions based on solution studies that demonstrate α HL preference for

phosphatidylcholine lipids. In light of the GB of lipid headgroups using lipoprotein nanodiscs, with 100-400 lipids, is likely a better platform for native-MS experimentation to study protein-lipid interactions than detergent-lipid micelles that only contain a few lipids per a micelle.

APPENDIX A

SUPPLEMENTAL INFORMATION FOR CHAPTER II

Expanded Experimental Methods

Sample Preparation. Lyophilized monomeric alpha hemolysin (α HL) from *S. aureus* was purchased from Sigma-Aldrich (St. Louis, MO, USA). α HL monomers were concentrated in the presence of detergent micelles to induce oligomerization and pore formation.¹⁴⁶ Detergents tetraethylene glycol monoethyl ether (C₈E₄) and n-tetradecylphosphocholine (Fos-14) were purchased from Anatrace (Maumee, OH, USA). To produce α HL pores, lyophilized monomers were resuspended in water to a concentration of 0.5 mg/mL. 150 μ L of this solution was then mixed with appropriate amounts 100 mM detergent stock to reach a final detergent concentration of 32 mM in the case of C₈E₄ (64 μ L added, \sim 4x CMC) or 2 mM for Fos-14 (4 μ L added, \sim 17x CMC) and enough ammonium acetate solution to reach a total sample volume of 200 μ L. This mixture of α HL monomer and detergent was then concentrated in a 3 kDa cutoff centrifugal concentrator to an approximate volume of 35-40 μ L. After concentration, the sample was aliquoted to 10 μ L aliquots and used immediately or frozen and stored at -80 °C for future use. Before use, each 10 μ L aliquot was diluted with 20 μ L of either 32 mM C₈E₄ or 2 mM Fos-14 in 200 mM ammonium acetate, pH 7.5. Then the sample was buffer exchanged using a centrifugal desalting column equilibrated with 2x the CMC (16 mM C₈E₄, or 0.25 mM FOS-14) of the appropriate detergent in 200 mM ammonium acetate pH 7.5. MS analysis was performed immediately after buffer exchanging samples.

Instrument settings

Waters Synapt G2-Si. IM-MS spectra were acquired using a Waters Synapt G2-Si Quadrupole-Ion-Mobility-Time-of-Flight (Q-ToF) mass spectrometer. Borosilicate glass capillary emitters (1.0 mm o.d./0.78 mm i.d., Sutter Instruments) were pulled using a Flaming/Brown micropipette puller (Model P-97, Sutter Instruments) to a tip size of ~2 μm , measured using a scanning electron microscope (FEI Quanta 200 ESEM/VPSEM Microscopes). Nano-electrospray was initiated by applying a 0.6-0.9 kV potential to a platinum wire inserted into the capillary and in contact with the sample solution. Once spray was initiated, the potential was dropped to the lowest stable value between 0.6 and 0.9 kV where spray could be maintained. For C₈E₄ α HL pore samples the sample cone potentials ranged between 25 and 50 V, and a “trap” collision cell potential from 25 to 100 V was used with an Argon gas flow rate of 10 mL/min. FOS-14 α HL samples required higher levels of activation. For these FOS-14 samples the cone potential ranged from 50-150 V and the trap potential from 50-150 V. The transfer cell was held at 5 V for all experiments except for the mass spectrum in Figure 4B of 25 V. The source temperature was held at 150 °C, and the backing pressure in the source region was ~3.5 mbar. For ion mobility experiments the helium flow rate was 50 mL/min in the helium cell. Nitrogen was used as the drift gas at a flow rate of 100 mL/min. A quadrupole profile (typically set at 3,000, 6,000, and 10,000 m/z) was used to more efficiently transmit large ions and reduce signal intensity for small detergent clusters.

Ion mobility arrival time data were calibrated according to established literature procedures for each replicate using calibrant proteins alcohol dehydrogenase (ADH), pyruvate kinase (PYK), and glutamate dehydrogenase (GDH).^{78,197} For α HL pores in C₈E₄ the settings were as follows:

Trap wave velocity: 300 m/s

Trap wave height: 1.0 V

IMS wave velocity: 500 m/s

IMS wave height: 18 V

Transfer wave velocity: 100 m/s

Transfer wave height: 2.0 V

For α HL pores in FOS-14 the settings were the same except an IMS wave velocity of 400 m/s was used.

Simple Molecular Dynamics simulations to account for gas-phase collapse of protein ions on transfer to the gas phase were conducted in GROMACS using the GROMOS 43a2 force field. After a short vacuum relaxation step, 5-ns production runs were computed using a modified Berendsen thermostat at 300 K as described elsewhere.⁸² Collision cross sections for initial and collapsed structures were calculated in Collidoscope using the Trajectory Method after identifying low-energy charge state isomers with the Charge Placement algorithm.⁸¹ Nitrogen was used as the buffer gas, and all other settings were set to their default values.

Orbitrap Exactive Plus Extended Mass Range. Mass spectra of α HL pores in Fos-14 were collected on a Thermo Scientific Exactive Plus extended mass range Orbitrap with an m/z range up to 20,000 and a nanoESI source. Electrospray voltages were set between 1.2-1.5 kV for stable spray. The capillary source was heated to 250 °C to aid desolvation of analyte ions. Source CID voltages were tuned to 50-100 V. The S-lens ion guide was held at an RF level of 200 V for efficient transfer of large complexes. The voltage settings for the transport multipoles were tuned as follows to maximize

signal of large complexes (C-trap entrance lens; 0 V, bent flatapole DC; 8 V, inter-flatapole DC; 4 V, injection flatapole DC; 4 V). The HCD cell was held at 50 V with a trapping gas setting of 10.

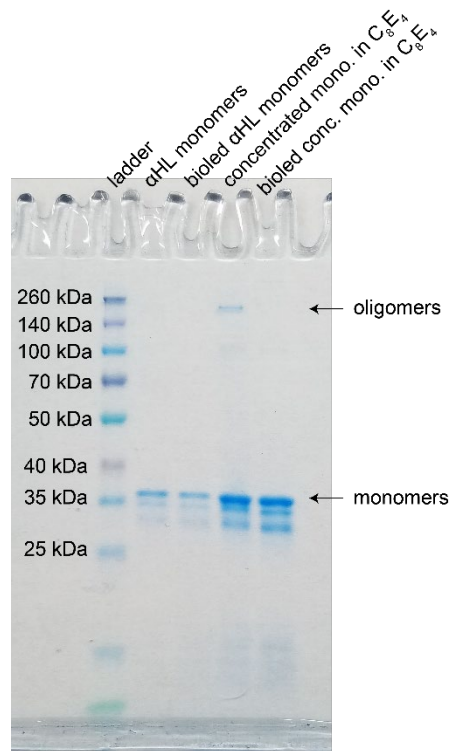


Figure A1. SDS-PAGE of α HL monomers in detergent-free solutions and oligomers formed in C_8E_4 detergent solutions. No oligomers are observed for detergent-free solutions but are observed upon concentrating in the presence of C_8E_4 detergent micelles. The high molecular weight oligomer band is SDS-resistant as long as the sample is not boiled.¹⁴⁶

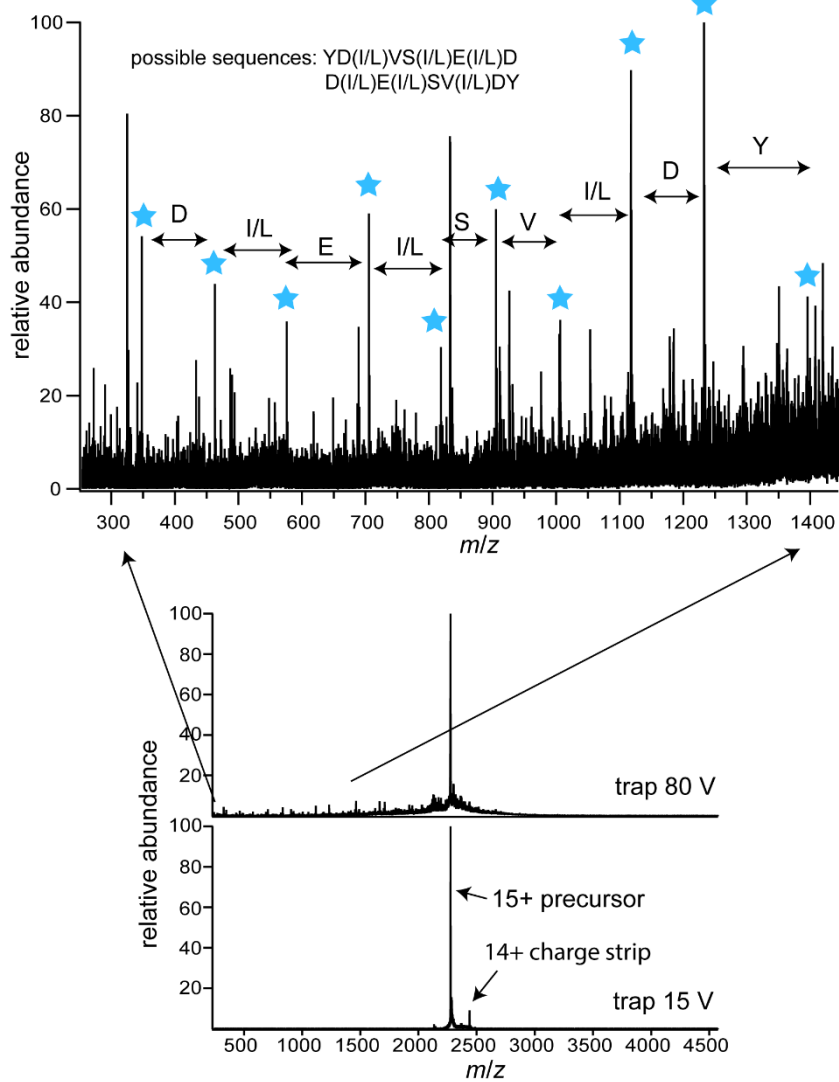


Figure A2. In order to identify the co-purified protein with α HL monomers, sample solutions were mixed with 5% sulfolane and 0.05% formic acid to cause supercharging and unfolding of proteins during ESI. The 15+ co-purified protein ion was then isolated and fragmented in the trap to sequence a portion of the protein. This yielded a series of 1+ fragment ions that allowed for the determination of a set of possible sequences. Based on the determined sequence and mass of fragment ions the co-purified protein is not a form of α HL monomer. Basic local alignment search tool (BLAST) analysis of possible sequences did not yield an obvious candidate protein.

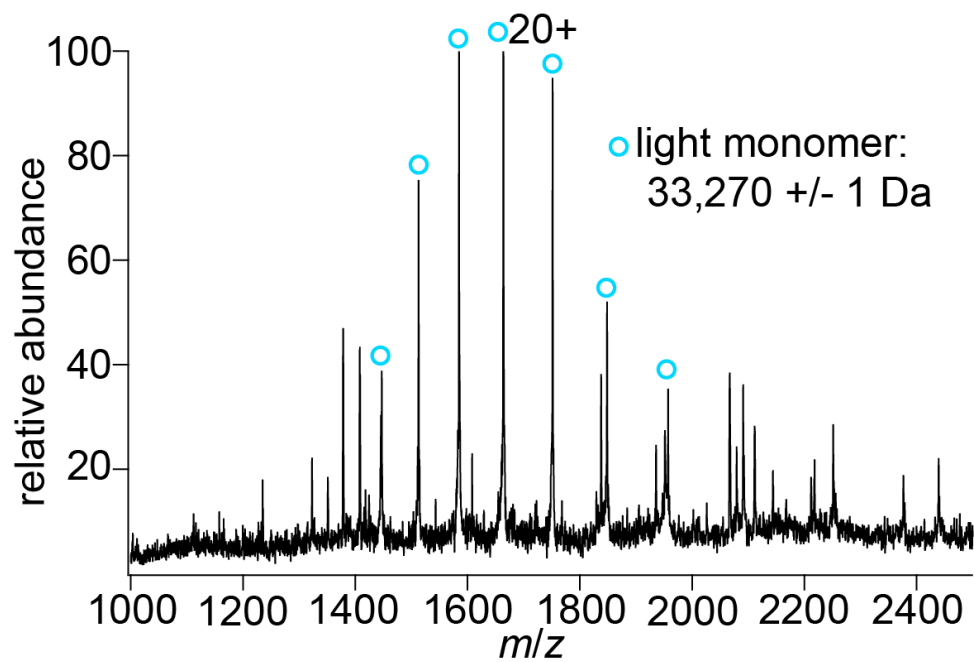


Figure A3. Mass spectrum of high-charge non-native α HL monomers formed in the process of detergent stripping in Fig. 3B and Fig. 3C.

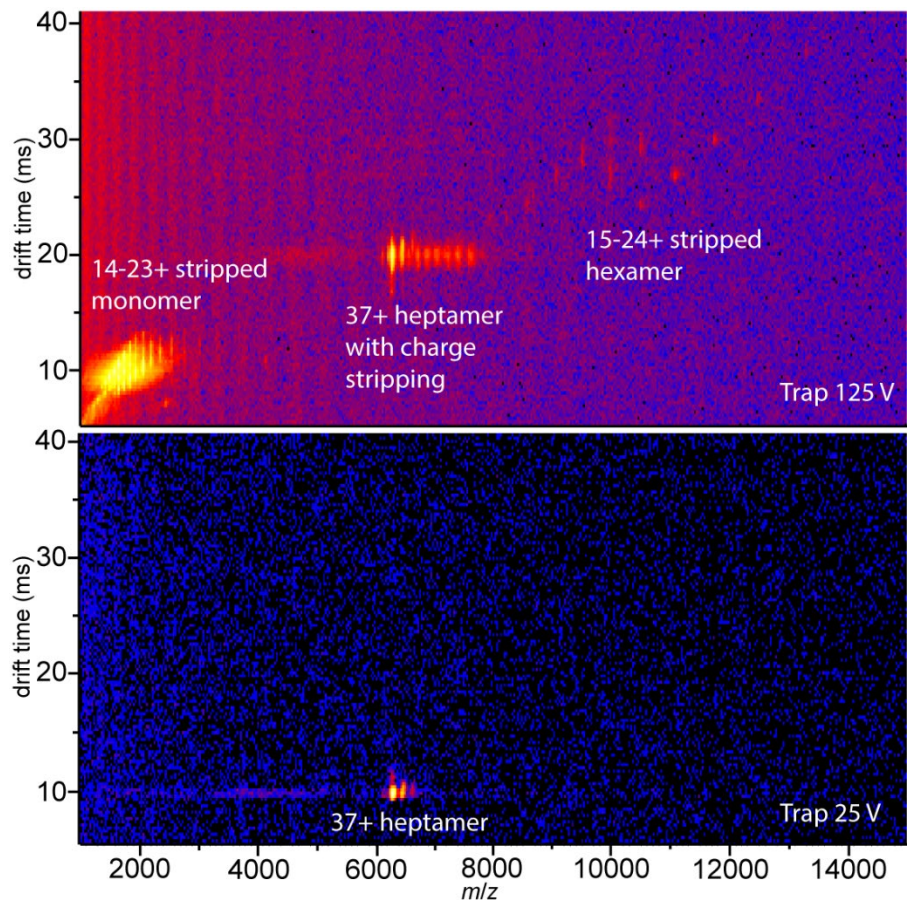


Fig A4. IM-MS of isolated 37+ α HL heptamer ions formed in C_8E_4 under light activation (sampling cone: 50 V, trap: 125 V) and high instrumental activation conditions (sampling cone: 50 V, trap: 125 V). Upon gas-phase activation by collisions with neutral argon gas, native heptamers produce hexamers with charge states complementary to those of the high-charge, unfolded monomers. These results indicate that the native hexamers (most abundant charge state 30+) are not formed by gas-phase dissociation of the heptamers.

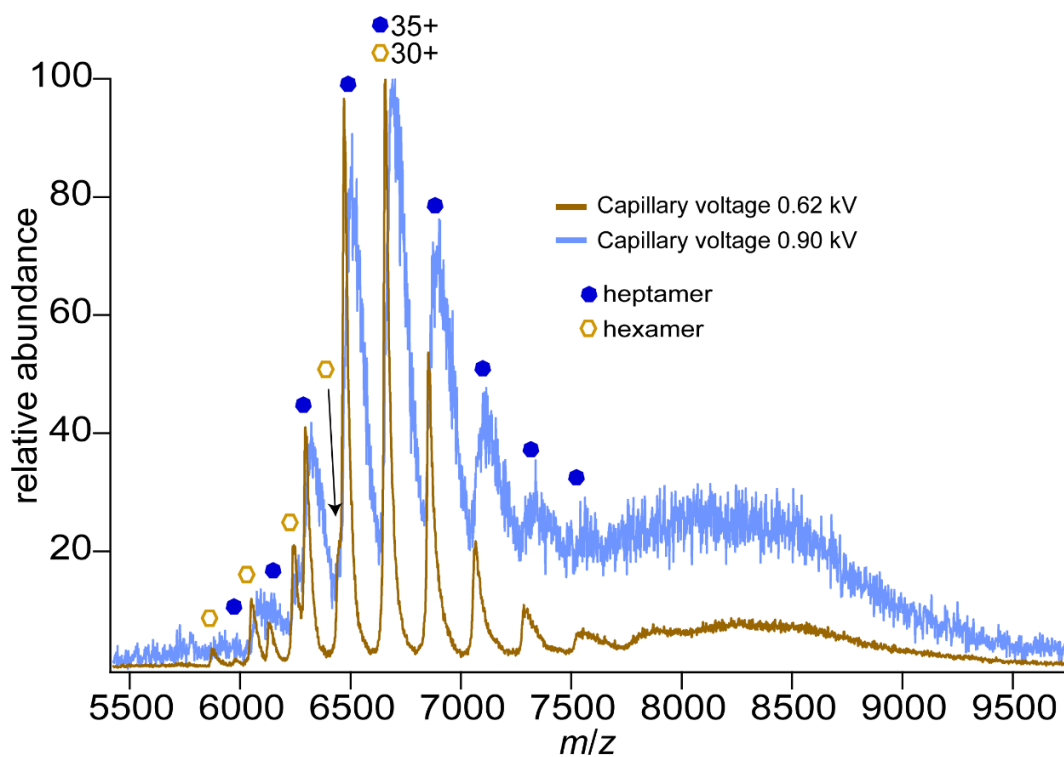


Figure A5. Native mass spectra of α HL oligomers formed in C_8E_4 detergent under typical nESI spray conditions (capillary voltage 0.62 kV) and with elevated spray conditions (capillary voltage 0.9 kV). Increasing the capillary voltage significantly diminishes signal quality and signal level for α HL oligomers but does not increase the abundance of hexamer relative to heptamer. This demonstrates that the hexamer is not a consequence of dissociation in the electrospray process before complete transfer to the gas phase.

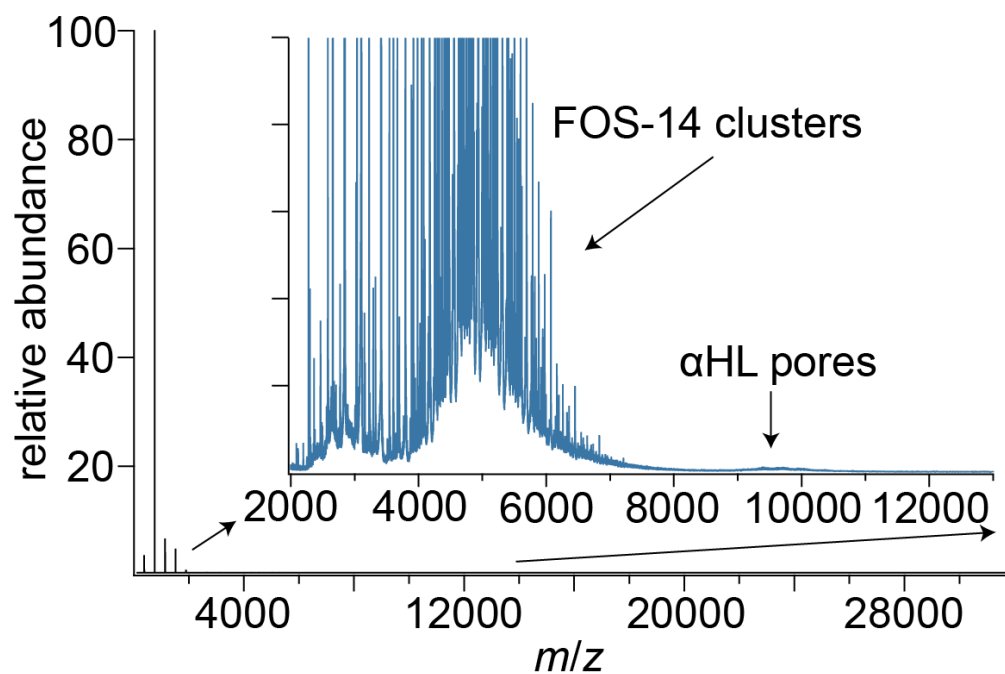


Figure A6. Representative mass spectrum showing relative abundance of (proteinless) FOS-14 cluster ions and FOS-14 micelle-embedded α HL pore ions acquired on Synapt instrument with the sampling cone at 50 V and the trap at 50 V.

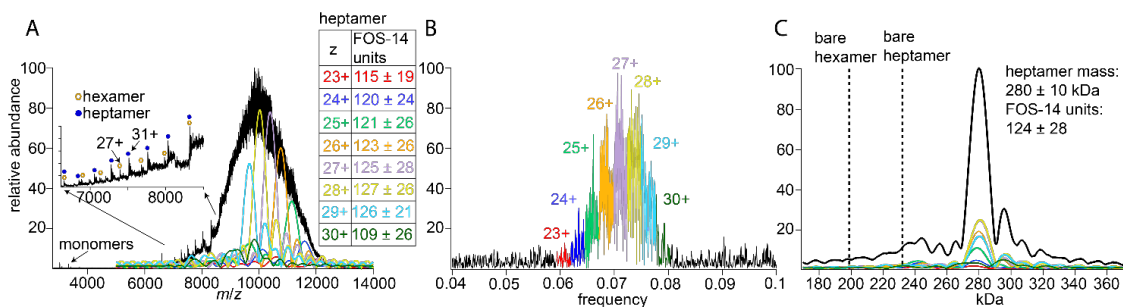


Figure A7. Native mass spectrum and Fourier transform (FT) analysis of FOS-14 embedded α HL oligomer ions acquired on the Orbitrap instrument under the least activating conditions (source CID: 50 V and HCD: 50 V). (A) Mass spectrum of α HL detergent-stripped complexes and micelle-embedded complexes. The inset shows the signal for detergent-stripped complexes that are hexameric and heptameric. The inset table provides the detergent stoichiometry distribution for each individual charge state data from the FT (B) for heptameric micelle-embedded pores with the \pm representing the standard deviation in detergent molecule stoichiometry. (C) Zero-charge spectrum of the combined charge state data. Dashed vertical lines correspond to the masses of detergent-stripped bare hexamer and heptamer pores. Overlap of charge states (26-30+) in the frequency domain (B) causes some ringing artefacts in the zero-charge spectrum, making signal of micelle-embedded hexamers difficult to detect confidently from these data.

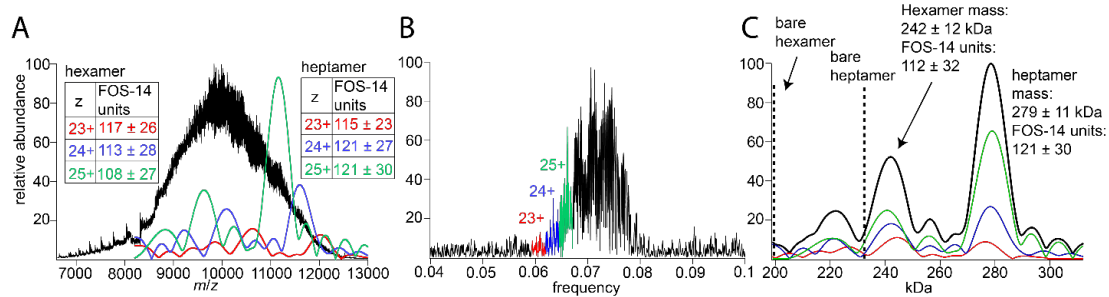


Figure A8. (A) Native mass spectrum and (B) corresponding Fourier spectrum of α HL oligomers formed in FOS-14 micelles on the Orbitrap instrument under the least activating conditions as in Fig. A4. Only charge states 23-25+ are analyzed because these charge states are well separated in the frequency domain, which allows for more confident identification of micelle-embedded hexamers in the zero-charge spectrum above the level of ringing artefacts (C).

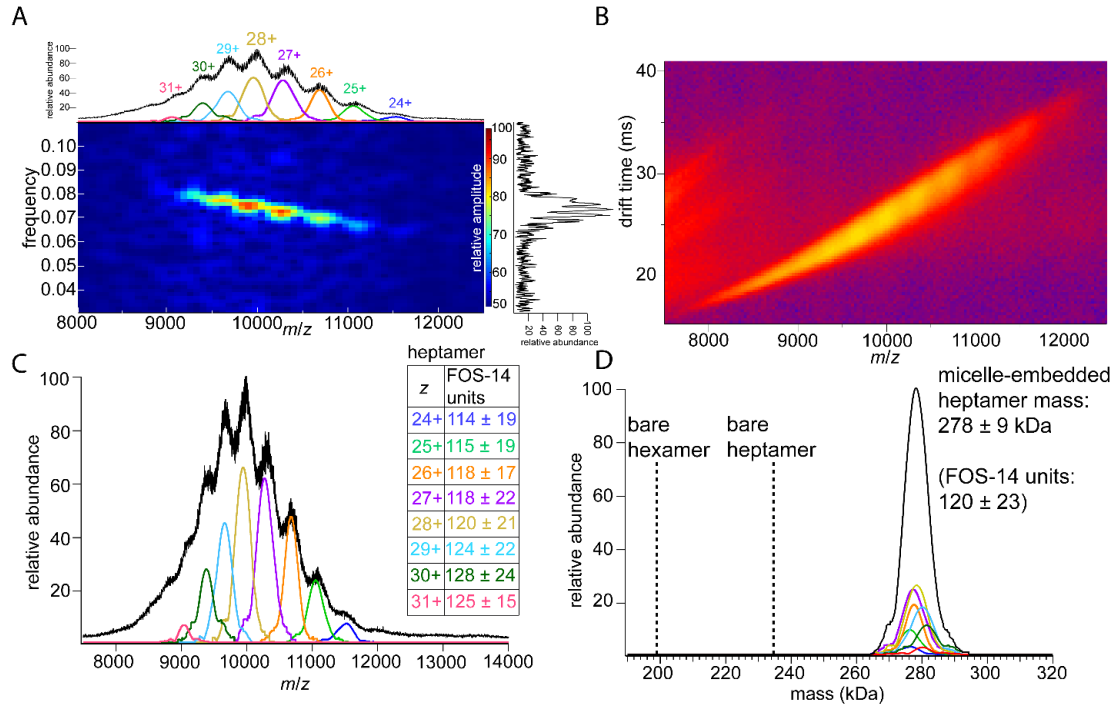


Figure A9. Native IM-MS data from the Synapt Q-IMS-ToF instrument under the least activating conditions (sampling cone: 100 V, trap: 50 V) of α HL micelle-embedded pores in FOS-14 detergent with 200 mM ammonium acetate. (A) The Gabor transform (GT) spectrogram is shown with the IM-MS cutout mass spectrum across the top and the Fourier transform down the right. Under these instrumental conditions only signal for micelle-embedded heptamers can be detected due to the strong overlap of charge state distributions. (B) IM-MS spectrum of micelle-embedded α HL. (C) Detailed stoichiometry analysis of mass spectrum shown in (A). The inset table provides the detergent stoichiometry distributions for each individual charge state pulled from the GT with the \pm representing the standard deviation of detergent molecule stoichiometry. (D) Zero-charge spectrum of the combined charge state data from the GT. Dashed vertical lines correspond to the masses of detergent-stripped bare hexamer and heptamer pores based on the measured monomer mass.

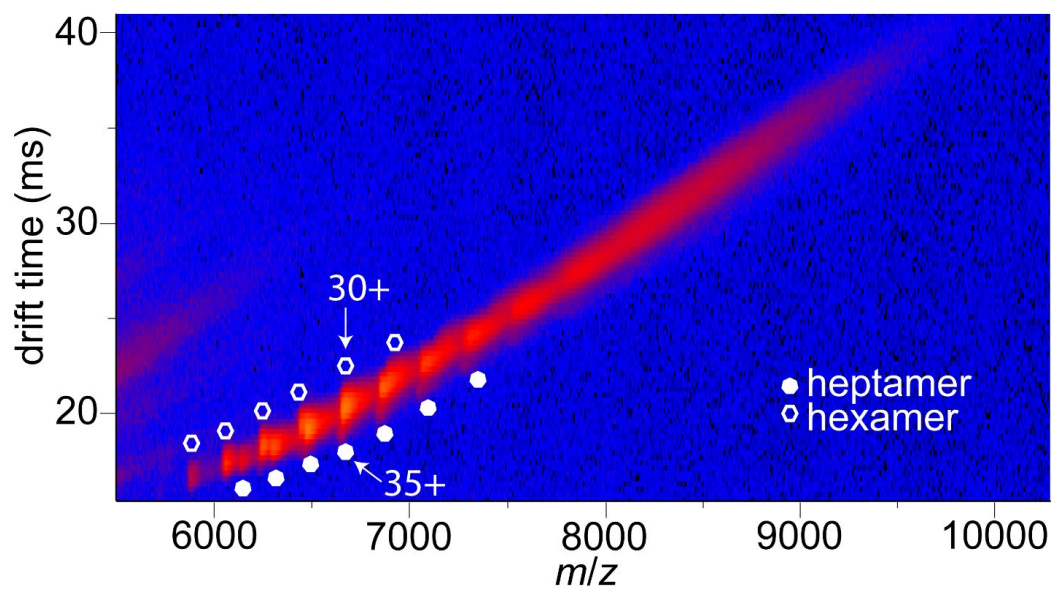


Figure A10. Native IM-MS data for α HL oligomers formed in C_8E_4 detergent micelles under minimal gas-phase activation conditions where complexes remain compact.

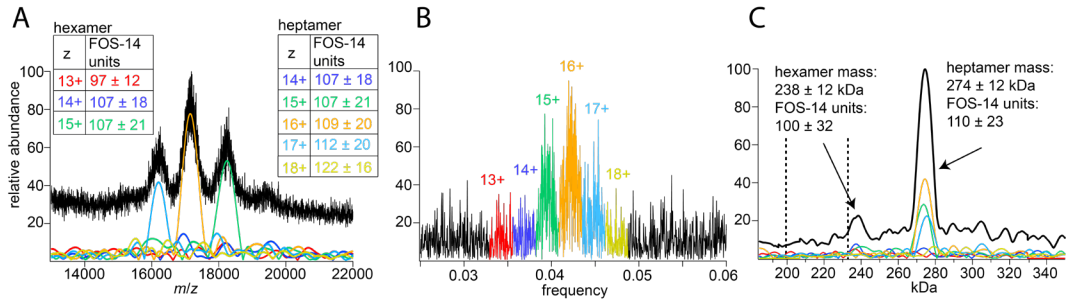


Figure A12. Native mass spectrum and FT analysis of α HL micelle-embedded pores in FOS-14 detergent acquired on the Synapt Q-IMS-ToF instrument under highly-activating conditions (sampling cone: 50 V, trap: 150 V). (A) Mass spectrum of α HL oligomers. Inset tables provide the detergent stoichiometry distributions for each individual charge state extracted from the FT (B), with \pm representing the standard deviation of detergent molecule stoichiometry. (C) Zero-charge spectrum of the combined charge state data. Dashed vertical lines correspond to the masses for detergent-stripped bare hexamer and heptamer pores. Overall, significant charge stripping with minimal detergent removal is observed from micelle-embedded pores in comparison to lower activation levels.

APPENDIX B

SUPPLEMENTAL INFORMATION FOR CHAPTER III

GroEL mass spectral acquisition and data analysis:

For each trial day (1-3), previously prepared frozen aliquots of GroEL were buffer exchanged using a centrifugal desalting column equilibrated with 200 mM ammonium acetate, pH 7.5. After sample preparation, 3 μ L of sample was loaded into a nanoelectrospray ionizations (nESI) capillary. Spray was initiated with a Pt wire inserted into the sample solution at a capillary voltage of \sim 1.0 kV. The capillary voltage was then reduced to \sim 0.65 kV for data collection. Before the start of every trial the nESI capillary was positioned such that the maximum GroEL signal was achieved for each cone. Typically, the highest signal was reached with the capillary positioned 1-2 mm from the sampling cone, and, over this range of distances, no significant effect on excess mass or desalting was observed. GroEL mass spectra were recorded for each source sampling cone (in mixed order across trial days) with the same instrumental parameters (see below), while the sampling cone voltage was raised from 10-200 V in 10 V increments. At each sampling cone voltage step, a 1-minute acquisition was acquired and summed so that GroEL signal abundances could be compared for each cone and trial day. When exchanging each sample cone for the next trial, the new cone was allowed to equilibrate temperature with the rest of the source block for \sim 5 minutes and a new nESI capillary with GroEL sample was used.

IM-MS spectra for each trial day were then analyzed with Gaussian multi-peak fitting in Igor Pro to determine the average mass, peak width (fwhm), and abundances of

each charge state. The entire drift time profile for each charge state was extracted and the average weighted drift time was calculated for a given charge state so that compaction and/or unfolding could be observed across source sampling cones and sampling cone potentials.

Synapt G2-Si instrument parameters:

Source Temperature: 100 °C

Source sampling cone voltage: 10-200 V with 10 V steps

Quadrupole profile was set to: 3000, 6000, 10000

Trap voltage: 10 V for GroEL experiments, 50 V for α HL experiments

Transfer voltage: 5 V for all experiments

Trap Argon gas flow rate: 10 mL/min

Helium cell flow rate: 50 mL/min

IMS Nitrogen flow rate: 100 mL/min

Traveling Wave settings for GroEL experiments:

Trap wave velocity: 300 m/s

Trap wave height: 1.0 V

IMS wave velocity: 400 m/s

IMS wave height: 18 V

Transfer wave velocity: 100 m/s

Transfer wave height: 2.0 V

Traveling Wave settings for α HL experiments performed in ToF mode without IM:

Trap wave velocity: 300 m/s

Trap wave height: 1.0 V

Transfer wave velocity: 100 m/s

Transfer wave height: 2.0 V

Simulations of in-source ion activation

Simulations were conducted according to the method described in Donor et al.,¹⁷⁴ with limited modifications to model the conditions in the source region. The collision physics remained the same, however, changes to the ion acceleration, pressure profile, and time step were implemented due to the different pressures for these simulations. The ions are accelerated across the ~ 1 mm gap between the exit of the Stepwave and the differential aperture, an area with gas pressure in the mbar range (estimated using the Backing pressure readback, ~ 3.0 mbar for the large SC). Thus, rather than assume that the ions reach a kinetic energy equal to the charge multiplied by the acceleration potential, the acceleration was modeled explicitly in these simulations. The ions were assumed to have an initial velocity equal to their RMS thermal velocity at 298 K (~ 10 m/s), and the change in kinetic energy for a time step was taken as the charge multiplied by the change in potential over the distance traveled during that time step. Once the ions travel 1 mm, they enter the Source ion guide (~ 9 mm in length) and experience only the traveling-wave potential (wave velocity of 300 m/s and wave height of 1 V) for the rest of the simulation. The pressure differential between the Stepwave and Source ion guides was assumed to follow an exponential profile, with a characteristic decay length equal to the diameter of the differential aperture (~ 2.5 mm). Shorter (Fig. B1a, 1.25 mm) and longer (Fig. B1b, 5 mm) exponential decay lengths of the pressure do not change the trends in the slopes of the ion heating plots, but the slopes do get closer together for the 1.25 mm decay length and further apart for the 5.0 mm decay length due to

decreased/increased cooling, respectively. The time step (t.s.) while the ions are being quickly accelerated was determined using the original method:

$$t. s. = 0.05 \cdot \frac{\textit{mean free path}}{\textit{max. velocity}}$$

In order to reduce simulation time, for the remainder of the simulations the time step was determined at each step using the current velocity:

$$t. s. = 0.05 \cdot \frac{\textit{mean free path}}{\textit{curr. velocity}}$$

Acceleration voltages of 25, 50, 75, 100, 125, 150, 175, and 200 V were simulated for each of the three pressures. Bovine serum albumin (BSA) was used as the model protein for the simulations, because, at the pressures used, GroEL may experience simultaneous collisions, which our model does not explicitly account for. A charge state of 15+ was used, corresponding to the most abundant charge state for BSA electrosprayed from native-like solution conditions.

Supplemental Figures and Tables

Instrument Pressures with each sampling cone

Normal (0.8 mm) cone instrument pressures (mbar)

	Backing	Source	Trap	Helium Cell	IMS	Transfer	ToF
ToF mode	3.5	9.0e-3	3.6e-2	8.3e-4	1.0e-3	3.7e-2	1.5e-6
IMS mode	3.5	9.2e-3	4.2e-2	1.9	1.8	4.3e-3	1.7e-6

Medium (0.67 mm) cone instrument pressures (mbar)

	Backing	Source	Trap	Helium Cell	IMS	Transfer	ToF
ToF mode	2.4	6.2e-3	3.6e-2	8.3e-4	1.0e-3	3.7e-2	1.6e-6
IMS mode	2.4	6.4e-3	4.2e-2	1.9	1.8	4.3e-3	1.7e-6

Small (0.45 mm) cone instrument pressures (mbar)

	Backing	Source	Trap	Helium Cell	IMS	Transfer	ToF
ToF mode	1.4	3.6e-3	3.6e-2	8.2e-4	1.0e-3	3.7e-2	1.7e-6
IMS mode	1.4	3.8e-3	4.3e-2	1.9	1.8	4.4e-3	1.8e-6

Table B1. Instrument pressures for each source sampling cone in TOF mode and IMS mode. Each sampling cone provides a reproducible backing and source pressure reading, while all regions beyond the source are unchanged (from Trap to TOF).

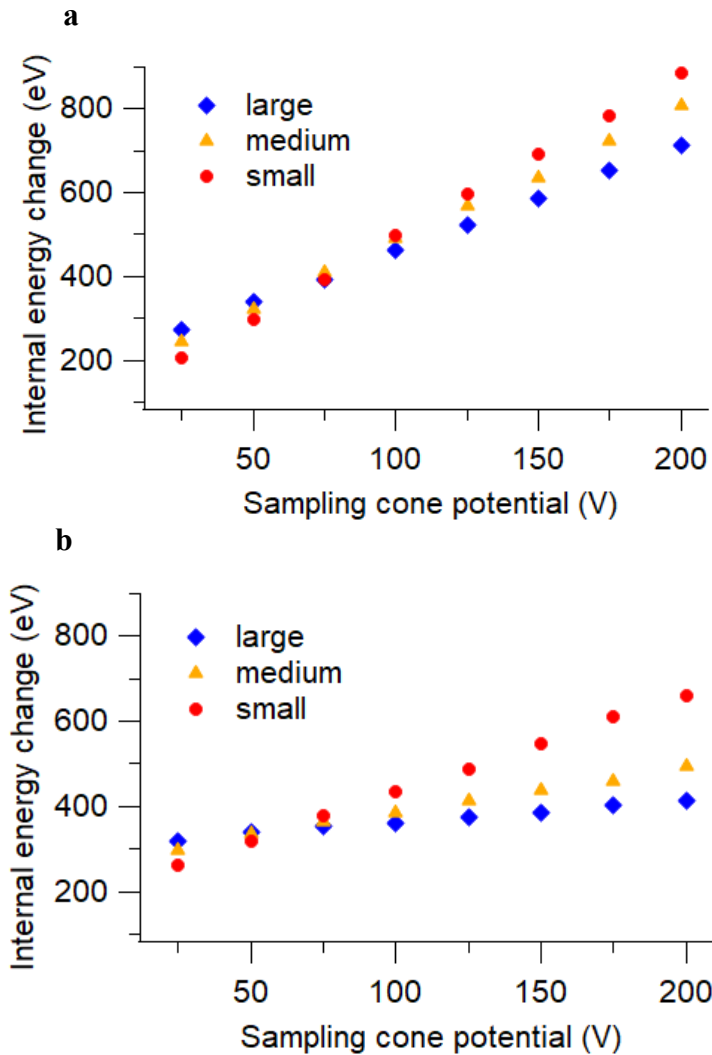


Figure B1: Simulated ion heating of BSA^{15+} under the same pressure conditions as in Fig. 2 except with shorter (a, 1.25 mm) and longer (b, 5.0 mm) pressure decay lengths as the ions are accelerated across a differential aperture from the Stepwave to the conjoined traveling-wave ion guide. At a pressure (from ~ 3.0 mbar down to $\sim 9\text{e-}3$ mbar for the large SC) exponential decay length of 1.25 mm the slopes of the ion heating trends are closer together due to increased collisional cooling, while at 5.0 mm the slopes diverge due to less collisional cooling.

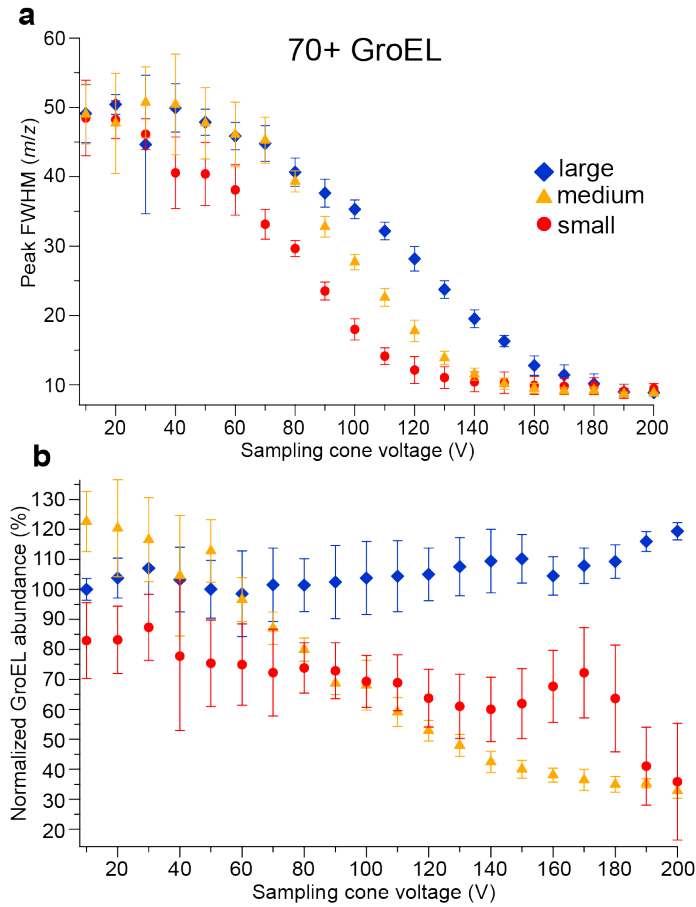


Figure B2: Peak width analysis for GroEL⁷⁰⁺ ions (a) and total GroEL signal abundances with all charge states included (b). GroEL signal abundance for each point is normalized to that when using the large sampling cone at a cone potential of 10 V. Note, with the medium and small cones, CID of GroEL 14-mers occurs from 170-200 V, which further reduces the signal.

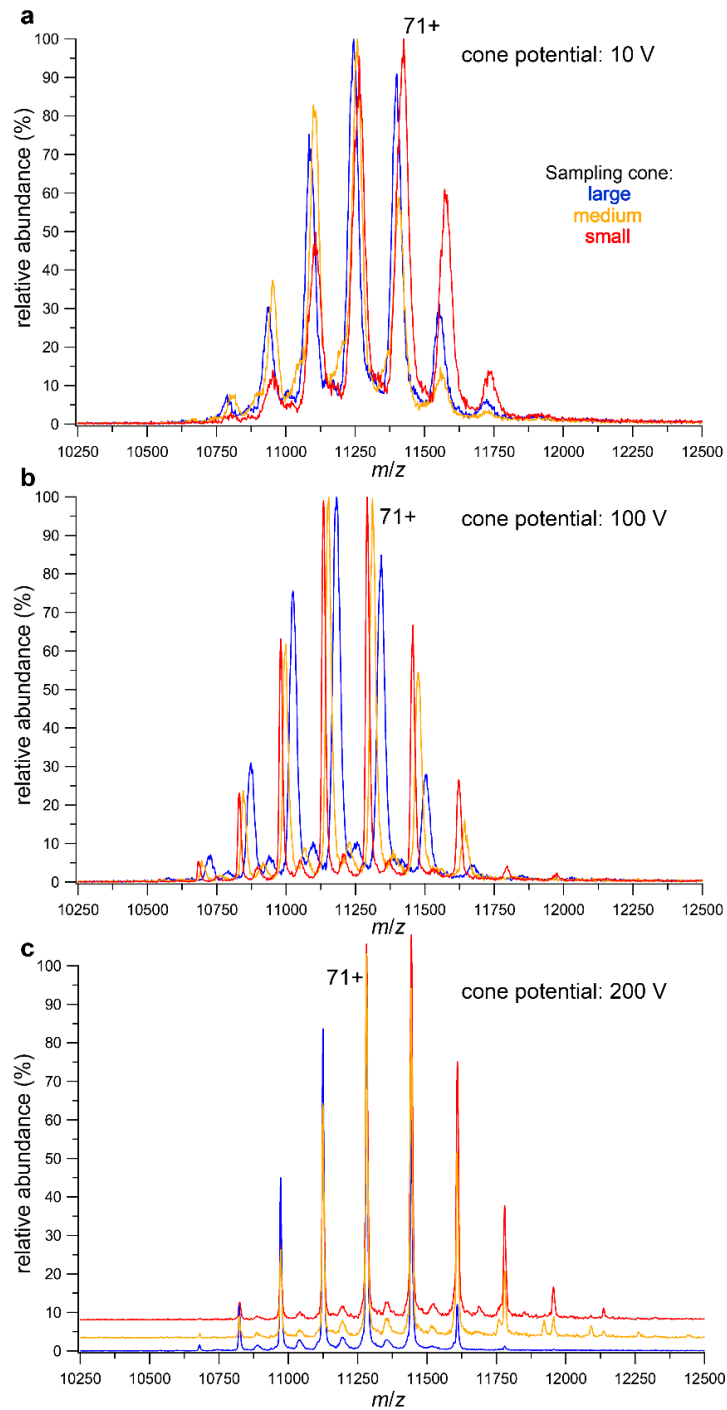


Figure B3: Selected mass spectra of GroEL 14-mers for each sampling cone overlaid at a sampling cone potential of 10 V (a), 100 V (b), and 200 V (c). Note: in (c) mass spectra slightly offset to aid differentiation.

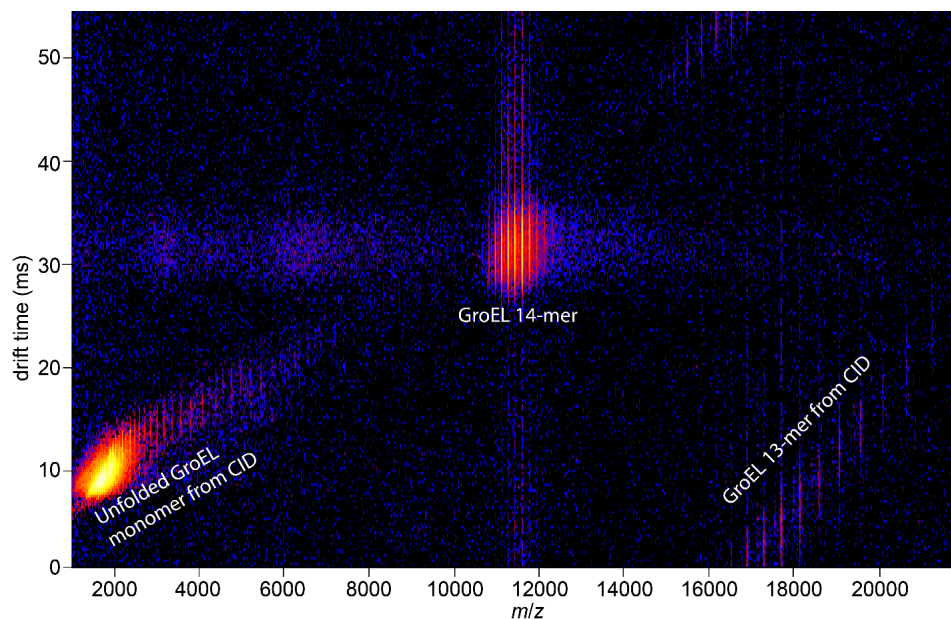


Figure B4: IM-MS spectrum of GroEL with the small cone at a cone potential of 200 V. Here activation in the source region is sufficient to cause CID of the GroEL 14-mer to produce high-charge monomer and GroEL 13-mer distributions.

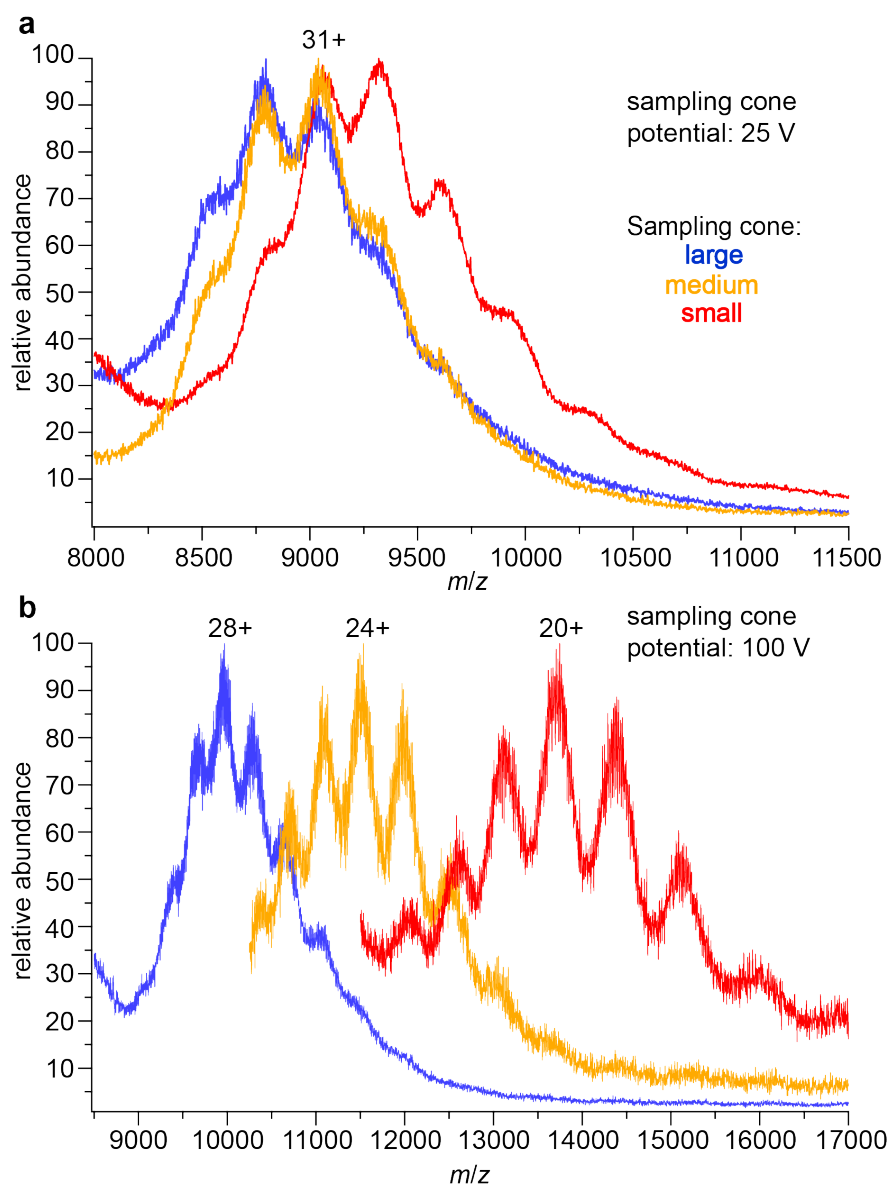


Figure B5: Overlaid mass spectra of α HL complexes in FOS-14 micelles with each sample cone size at a sampling cone potential of 25 V (a) or 100 V (b). Lower m/z portions of the mass spectra collected with the medium and small cones are truncated for clarity due to increasing signal from empty FOS-14 micelles. The highest-abundance charge state for each spectrum is indicated. At low sampling cone potentials (25 V) little difference in the charge state and FOS-14 distributions are seen. As the potential is raised (100 V) the medium and small cones are more activating (strip more FOS-14 and charge) than the large cone.

Cone Potential	Cone Size	Average Mass (kDa)	Average Charge	Bound FOS-14 Molecules	Standard Dev. FOS-14 Molecules
25V	large	279.9	31.6	124	20
	medium	280.3	30.8	125	15
	small	280.7	30.6	126	22
100V	large	279.0	27.7	122	21
	medium	276.7	24.3	116	18
	small	274.0	19.9	109	19
150 V	large	276.7	23.4	116	23
	medium	273.8	19.8	108	23
	small	272.2	16.7	104	19

Table B2. GT analysis results for α HL heptamers in FOS-14 micelles with each sampling cone.

APPENDIX C

SUPPLEMENTAL INFORMATION FOR CHAPTER IV

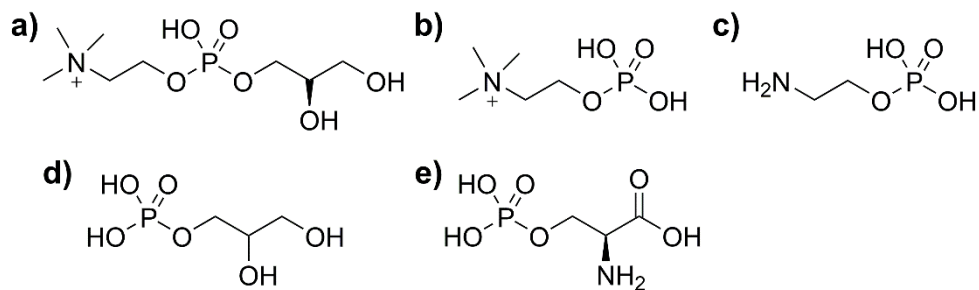


Figure C1. Structures of several common biological lipid head groups **(a)** glycerophosphorylcholine, GPC **(b)** phosphorylcholine, PC **(c)** phosphorylethanolamine, PE **(d)** glycerol 1-phosphate, PG and **(e)** phosphoserine, PS.

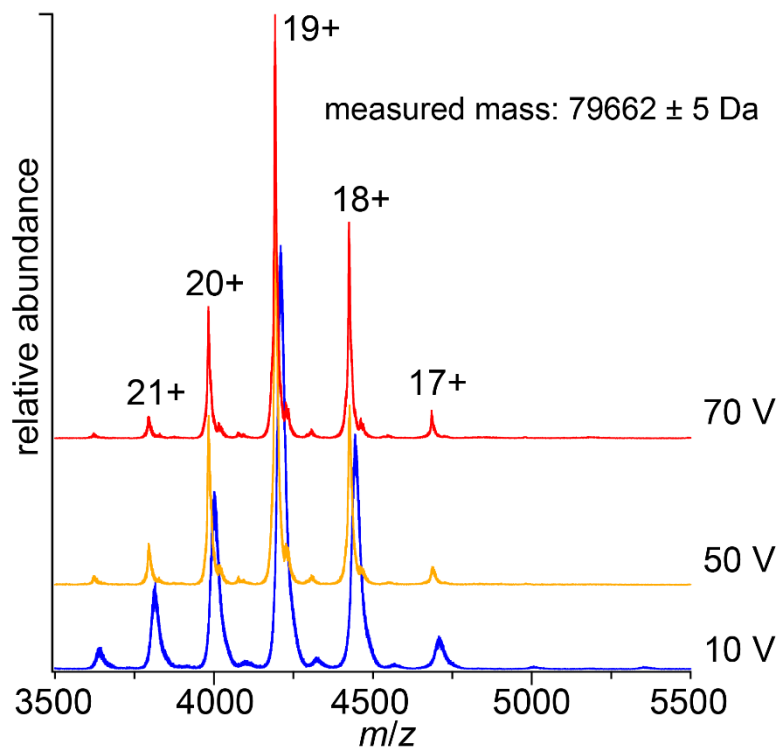


Figure C2. Native mass spectra of 5 μ M transferrin in 200 mM ammonium acetate solutions with no lipid headgroups at the given trap potentials of 10, 50, or 70 V. Transferrin produces clearly resolved mass spectra with a homogenous base mass.

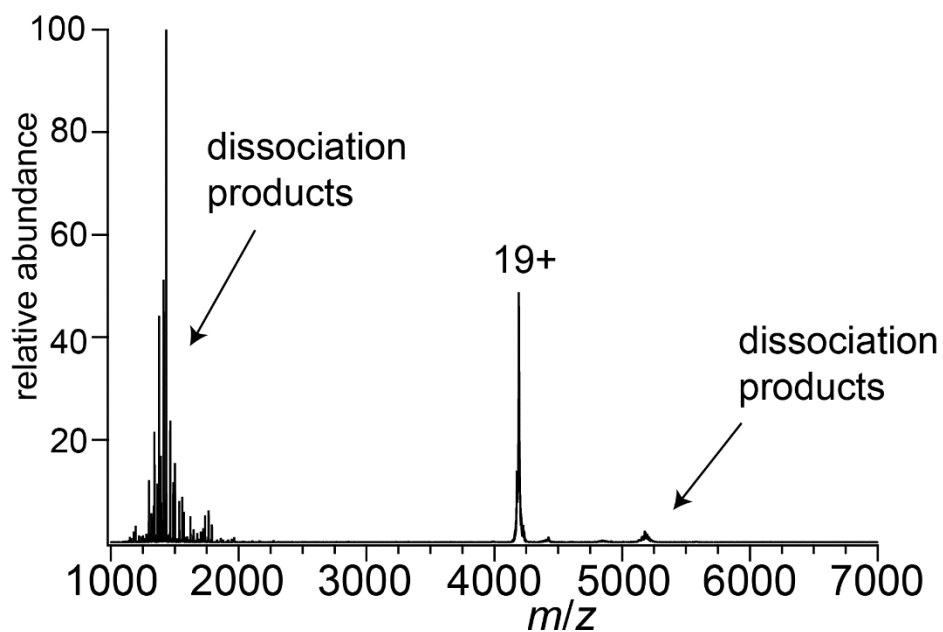


Figure C3. Quadrupole isolated transferrin¹⁹⁺ at a trap potential of 100 V without the presence of any lipid headgroups. At this high activation level significant dissociation of transferrin is produced.

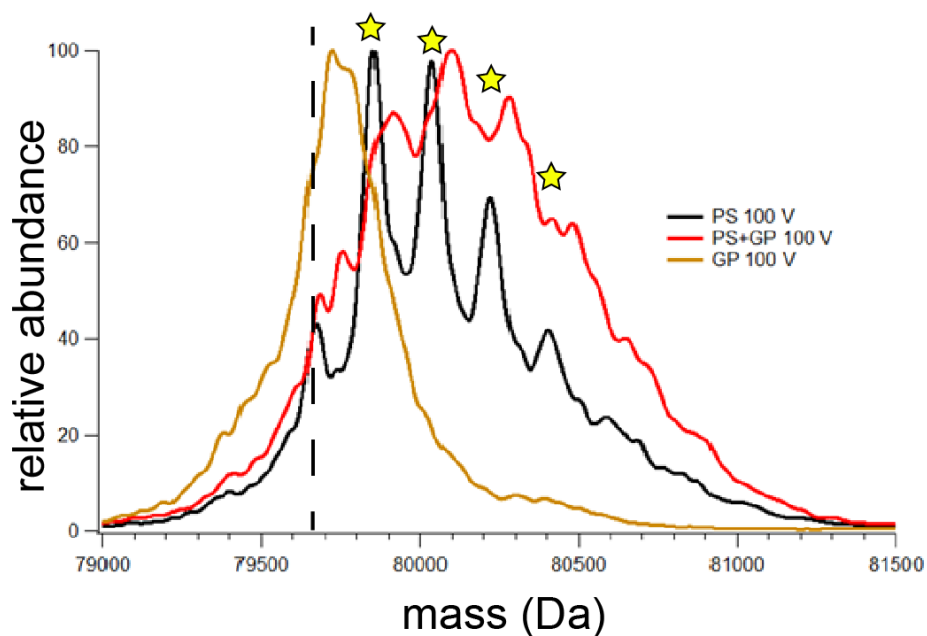


Figure C4. Comparison of deconvolved mass spectra of transferrin with PS, GP, and the mixture of PS and GP at 100 V of trap activation. The dashed line corresponds to the base mass of transferrin with no lipid headgroup adducts. With GP alone (gold) at 100 V no lipid headgroups are resolved and the mass position is near the base mass of transferrin. With PS (black) at 100 V several PS adducts are resolved on transferrin marked by the gold stars. With the mixture of the two lipid headgroups at 100 V (red) broad peaks are partially resolved that are more closely spaced with the mass of PS than GP suggesting the adducts here correspond to PS adducts and not GP adducts.

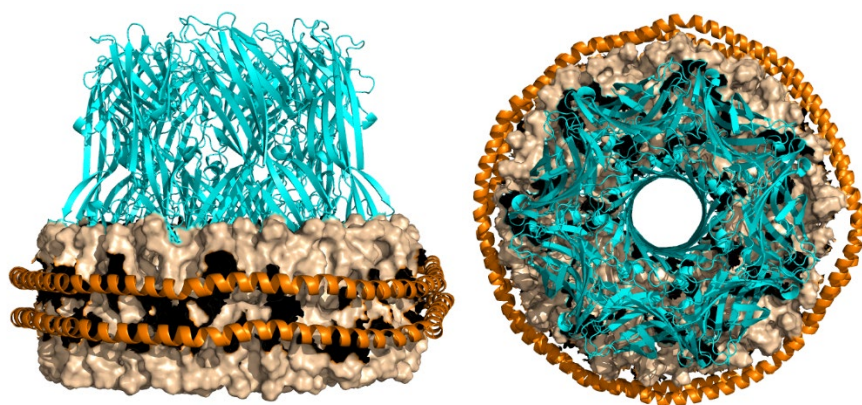
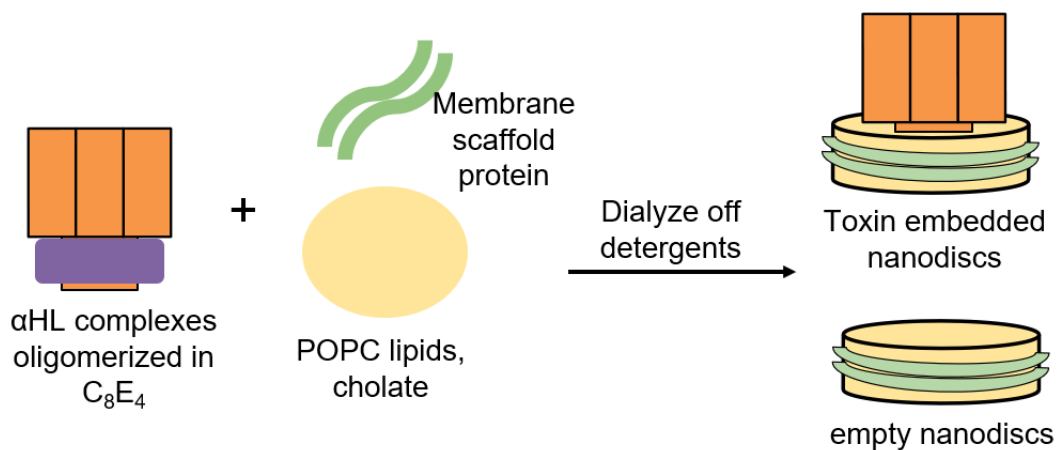


Figure C5. Brief schematic of α HL nanodisc insertion procedure. Below: CHARMM GUI model structure of the α HL heptamer embedded in a MSP1E3D1 nanodisc with 200 POPC lipids. MSP1E3D1 produces larger nanodiscs (~ 12 nm in diameter) in comparison to MSP1D1 nanodiscs (~ 9 - 10 nm in diameter).

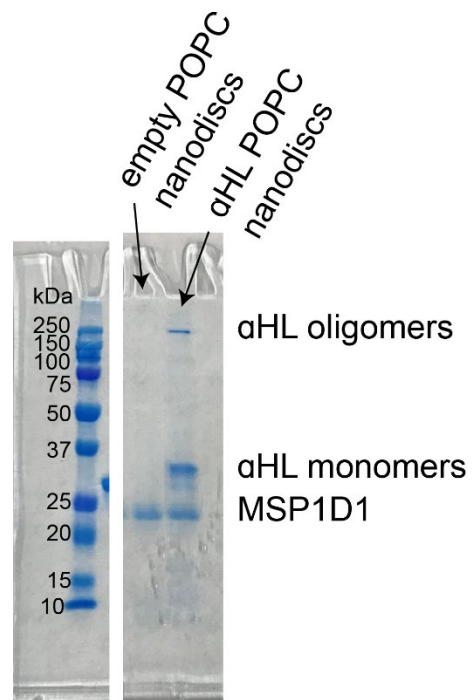


Figure C6. SDS-PAGE analysis of the sample used to produce Figure 17 in Chapter IV. The gel suggests α HL complexes remain stable through the nanodisc insertion process and are nanodisc-embedded.

REFERENCES CITED

- (1) Steen, H.; Mann, M. The Abc's (and Xyz's) of Peptide Sequencing. *Nat. Rev. Mol. Cell Biol.* **2004**, *5* (9), 699–711.
- (2) Marsh, J. A.; Teichmann, S. A. Structure, Dynamics, Assembly, and Evolution of Protein Complexes. *Annu. Rev. Biochem.* **2015**, *84* (1), 551–575.
- (3) Levy, E. D.; Erba, E. B.; Robinson, C. V.; Teichmann, S. A. Assembly Reflects Evolution of Protein Complexes. *Nature* **2008**, *453*, 1262.
- (4) Curry, S. Structural Biology: A Century-Long Journey into an Unseen World. *Interdiscip. Sci. Rev.* **2015**, *40* (3), 308–328.
- (5) Dobson, C. M. Biophysical Techniques in Structural Biology. *Annu. Rev. Biochem.* **2019**, *88* (1), 25–33.
- (6) Cournia, Z.; Allen, T. W.; Andricioaei, I.; Antonny, B.; Baum, D.; Brannigan, G.; Buchete, N.-V.; Deckman, J. T.; Delemotte, L.; del Val, C.; Friedman, R.; Gkeka, P.; Hege, H.-C.; Hénin, J.; Kasimova, M. A.; Kolocouris, A.; Klein, M. L.; Khalid, S.; Lemieux, M. J.; Lindow, N.; Roy, M.; Selent, J.; Tarek, M.; Tofoleanu, F.; Vanni, S.; Urban, S.; Wales, D. J.; Smith, J. C.; Bondar, A.-N. Membrane Protein Structure, Function, and Dynamics: A Perspective from Experiments and Theory. *J. Membr. Biol.* **2015**, *248* (4), 611–640.
- (7) Sezgin, E.; Levental, I.; Mayor, S.; Eggeling, C. The Mystery of Membrane Organization: Composition, Regulation and Roles of Lipid Rafts. *Nat. Rev. Mol. Cell Biol.* **2017**, *18*, 361.
- (8) Lingwood, D.; Simons, K. Lipid Rafts As a Membrane-Organizing Principle. *Science (80-.)*. **2010**, *327* (5961), 46–50.
- (9) Simons, K.; Gerl, M. J. Revitalizing Membrane Rafts: New Tools and Insights. *Nat. Rev. Mol. Cell Biol.* **2010**, *11* (10), 688–699.
- (10) Whitelegge, J. P. Integral Membrane Proteins and Bilayer Proteomics. *Anal. Chem.* **2013**, *85* (5), 2558–2568.
- (11) Chou, K.-C. Some Remarks on Protein Attribute Prediction and Pseudo Amino Acid Composition. *J. Theor. Biol.* **2011**, *273* (1), 236–247.
- (12) Frey, L.; Lakomek, N.-A.; Riek, R.; Bibow, S. Micelles, Bicelles, and Nanodiscs: Comparing the Impact of Membrane Mimetics on Membrane Protein Backbone Dynamics. *Angew. Chemie Int. Ed.* **2017**, *56* (1), 380–383.

- (13) Yeagle, P. L. Non-Covalent Binding of Membrane Lipids to Membrane Proteins. *Biochim. Biophys. Acta-Biomembranes* **2014**, *1838* (6), 1548–1559.
- (14) Zhou, H.-X.; Cross, T. A. Influences of Membrane Mimetic Environments on Membrane Protein Structures. *Annu. Rev. Biophys.* **2013**, *42* (1), 361–392.
- (15) Zhou, M.; Morgner, N.; Barrera, N. P.; Politis, A.; Isaacson, S. C.; Matak-Vinkovic, D.; Murata, T.; Bernal, R. A.; Stock, D.; Robinson, C. V. Mass Spectrometry of Intact V-Type ATPases Reveals Bound Lipids and the Effects of Nucleotide Binding. *Science (80-.)*. **2011**, *334* (6054), 380–385.
- (16) Laganowsky, A.; Reading, E.; Allison, T. M.; Ulmschneider, M. B.; Degiacomi, M. T.; Baldwin, A. J.; Robinson, C. V. Membrane Proteins Bind Lipids Selectively to Modulate Their Structure and Function. *Nature* **2014**, *510* (7503), 172–175.
- (17) Parker, M. W. Protein Structure from X-Ray Diffraction. *J. Biol. Phys.* **2003**, *29* (4), 341–362.
- (18) Markwick, P. R. L.; Malliavin, T.; Nilges, M. Structural Biology by NMR: Structure, Dynamics, and Interactions. *PLOS Comput. Biol.* **2008**, *4* (9), e1000168.
- (19) Fernandez-Leiro, R.; Scheres, S. H. W. Unravelling Biological Macromolecules with Cryo-Electron Microscopy. *Nature* **2016**, *537* (7620), 339–346.
- (20) Ognjenović, J.; Grisshammer, R.; Subramaniam, S. Frontiers in Cryo Electron Microscopy of Complex Macromolecular Assemblies. *Annu. Rev. Biomed. Eng.* **2019**, *21* (1), 395–415.
- (21) Marcoux, J.; Robinson, C. V. Twenty Years of Gas Phase Structural Biology. *Structure* **2013**, *21* (9), 1541–1550.
- (22) Shi, Y. A Glimpse of Structural Biology through X-Ray Crystallography. *Cell* **2014**, *159* (5), 995–1014.
- (23) Protein Data Bank: The Single Global Archive for 3D Macromolecular Structure Data. *Nucleic Acids Res.* **2018**, *47* (D1), D520–D528.
- (24) Carpenter, E. P.; Beis, K.; Cameron, A. D.; Iwata, S. Overcoming the Challenges of Membrane Protein Crystallography. *Curr. Opin. Struct. Biol.* **2008**, *18* (5), 581–586.
- (25) Hunter, M. S.; DePonte, D. P.; Shapiro, D. A.; Kirian, R. A.; Wang, X.; Starodub, D.; Marchesini, S.; Weierstall, U.; Doak, R. B.; Spence, J. C. H.; Fromme, P. X-Ray Diffraction from Membrane Protein Nanocrystals. *Biophys. J.* **2011**, *100* (1)

- (26) Parker, J. L.; Newstead, S. Membrane Protein Crystallisation: Current Trends and Future Perspectives. *Adv. Exp. Med. Biol.* **2016**, *922*, 61–72.
- (27) Lee, A. G. Lipid–Protein Interactions in Biological Membranes: A Structural Perspective. *Biochim. Biophys. Acta - Biomembr.* **2003**, *1612* (1), 1–40.
- (28) Lee, A. G. Biological Membranes: The Importance of Molecular Detail. *Trends Biochem. Sci.* **2011**, *36* (9), 493–500.
- (29) Birch, J.; Axford, D.; Foadi, J.; Meyer, A.; Eckhardt, A.; Thielmann, Y.; Moraes, I. The Fine Art of Integral Membrane Protein Crystallisation. *Methods* **2018**, *147*, 150–162.
- (30) Moraes, I.; Evans, G.; Sanchez-Weatherby, J.; Newstead, S.; Stewart, P. D. S. Membrane Protein Structure Determination — The next Generation. *Biochim. Biophys. Acta - Biomembr.* **2014**, *1838* (1, Part A), 78–87.
- (31) Hite, R. K.; Li, Z. L.; Walz, T. Principles of Membrane Protein Interactions with Annular Lipids Deduced from Aquaporin-0 2D Crystals. *Embo J.* **2010**, *29* (10), 1652–1658.
- (32) Vinothkumar, K. R. Structure of Rhomboid Protease in a Lipid Environment. *J. Mol. Biol.* **2011**, *407* (2), 232–247.
- (33) Hong, M.; Zhang, Y.; Hu, F. Membrane Protein Structure and Dynamics from NMR Spectroscopy. *Annu. Rev. Phys. Chem.* **2012**, *63* (1), 1–24.
- (34) Kay, L. E. NMR Studies of Protein Structure and Dynamics. *J. Magn. Reson.* **2011**, *213* (2), 477–491.
- (35) Dikiy, I.; Clark, L. D.; Gardner, K. H.; Rosenbaum, D. M. Chapter Two - Isotopic Labeling of Eukaryotic Membrane Proteins for NMR Studies of Interactions and Dynamics. In *Biological NMR Part A*; Wand, A. J. B. T.-M. in E., Ed.; Academic Press, 2019; Vol. 614, pp 37–65.
- (36) Opella, S. J.; Marassi, F. M. Applications of NMR to Membrane Proteins. *Arch. Biochem. Biophys.* **2017**, *628*, 92–101.
- (37) Marion, D. An Introduction to Biological NMR Spectroscopy. *Mol. & Cell. Proteomics* **2013**, *12* (11), 3006 LP – 3025.
- (38) Cavalli, A.; Salvatella, X.; Dobson, C. M.; Vendruscolo, M. Protein Structure Determination from NMR Chemical Shifts. *Proc. Natl. Acad. Sci.* **2007**, *104* (23), 9615 LP – 9620.

- (39) Liang, B.; Tamm, L. K. NMR as a Tool to Investigate the Structure, Dynamics and Function of Membrane Proteins. *Nat. Struct. Mol. Biol.* **2016**, *23* (6), 468–474.
- (40) Hagn, F.; Nasr, M. L.; Wagner, G. Assembly of Phospholipid Nanodiscs of Controlled Size for Structural Studies of Membrane Proteins by NMR. *Nat. Protoc.* **2018**, *13* (1), 79–98.
- (41) Hiller, S.; Wagner, G. The Role of Solution NMR in the Structure Determinations of VDAC-1 and Other Membrane Proteins. *Curr. Opin. Struct. Biol.* **2009**, *19* (4), 396–401.
- (42) Huster, D. Solid-State NMR Spectroscopy to Study Protein–Lipid Interactions. *Biochim. Biophys. Acta - Mol. Cell Biol. Lipids* **2014**, *1841* (8), 1146–1160.
- (43) Park, S. H.; Das, B. B.; Casagrande, F.; Tian, Y.; Nothnagel, H. J.; Chu, M.; Kiefer, H.; Maier, K.; De Angelis, A. A.; Marassi, F. M.; Opella, S. J. Structure of the Chemokine Receptor CXCR1 in Phospholipid Bilayers. *Nature* **2012**, *491* (7426), 779–783.
- (44) Ladizhansky, V. Applications of Solid-State NMR to Membrane Proteins. *Biochim. Biophys. Acta - Proteins Proteomics* **2017**, *1865* (11, Part B), 1577–1586.
- (45) Wang, S.; Munro, R. A.; Shi, L.; Kawamura, I.; Okitsu, T.; Wada, A.; Kim, S.-Y.; Jung, K.-H.; Brown, L. S.; Ladizhansky, V. Solid-State NMR Spectroscopy Structure Determination of a Lipid-Embedded Heptahelical Membrane Protein. *Nat. Methods* **2013**, *10* (10), 1007–1012.
- (46) Campbell, I. D. The March of Structural Biology. *Nat. Rev. Mol. Cell Biol.* **2002**, *3* (5), 377–381.
- (47) Yu, H. Extending the Size Limit of Protein Nuclear Magnetic Resonance. *Proc. Natl. Acad. Sci.* **1999**, *96* (2), 332 LP – 334.
- (48) Saio, T.; Guan, X.; Rossi, P.; Economou, A.; Kalodimos, C. G. Structural Basis for Protein Antiaggregation Activity of the Trigger Factor Chaperone. *Science* (80-.). **2014**, *344* (6184), 1250494.
- (49) Kourkoutis, L. F.; Plitzko, J. M.; Baumeister, W. Electron Microscopy of Biological Materials at the Nanometer Scale. *Annu. Rev. Mater. Res.* **2012**, *42* (1), 33–58.
- (50) Cheng, Y. Single-Particle Cryo-EM at Crystallographic Resolution. *Cell* **2015**, *161* (3), 450–457.

- (51) Bai, X.; McMullan, G.; Scheres, S. H. W. How Cryo-EM Is Revolutionizing Structural Biology. *Trends Biochem. Sci.* **2015**, *40* (1), 49–57.
- (52) Rawson, S.; Davies, S.; Lippiat, J. D.; Muench, S. P. The Changing Landscape of Membrane Protein Structural Biology through Developments in Electron Microscopy. *Mol. Membr. Biol.* **2016**, *33* (1–2), 12–22.
- (53) Gao, Y.; Cao, E.; Julius, D.; Cheng, Y. TRPV1 Structures in Nanodiscs Reveal Mechanisms of Ligand and Lipid Action. *Nature* **2016**, *534* (7607), 347–351.
- (54) Autzen, H. E.; Myasnikov, A. G.; Campbell, M. G.; Asarnow, D.; Julius, D.; Cheng, Y. Structure of the Human TRPM4 Ion Channel in a Lipid Nanodisc. *Science* (80-.). **2018**, *359* (6372), 228–232.
- (55) Coleman, J. A.; Yang, D.; Zhao, Z.; Wen, P.-C.; Yoshioka, C.; Tajkhorshid, E.; Gouaux, E. Serotonin Transporter–Ibogaine Complexes Illuminate Mechanisms of Inhibition and Transport. *Nature* **2019**, *569* (7754), 141–145.
- (56) Duan, J.; Li, J.; Chen, G.-L.; Ge, Y.; Liu, J.; Xie, K.; Peng, X.; Zhou, W.; Zhong, J.; Zhang, Y.; Xu, J.; Xue, C.; Liang, B.; Zhu, L.; Liu, W.; Zhang, C.; Tian, X.-L.; Wang, J.; Clapham, D. E.; Zeng, B.; Li, Z.; Zhang, J. Cryo-EM Structure of TRPC5 at 2.8-Å Resolution Reveals Unique and Conserved Structural Elements Essential for Channel Function. *Sci. Adv.* **2019**, *5* (7).
- (57) Wang, L.; Zhou, H.; Zhang, M.; Liu, W.; Deng, T.; Zhao, Q.; Li, Y.; Lei, J.; Li, X.; Xiao, B. Structure and Mechanogating of the Mammalian Tactile Channel PIEZO2. *Nature* **2019**, *573* (7773), 225–229.
- (58) Jiang, J.; Pentelute, B. L.; Collier, R. J.; Zhou, Z. H. Atomic Structure of Anthrax Protective Antigen Pore Elucidates Toxin Translocation. *Nature* **2015**, *521* (7553),
- (59) Gao, Y.; Cao, E.; Julius, D.; Cheng, Y. TRPV1 Structures in Nanodiscs Reveal Mechanisms of Ligand and Lipid Action. *Nature* **2016**, *doi: 10.10*.
- (60) Bonomi, M.; Vendruscolo, M. Determination of Protein Structural Ensembles Using Cryo-Electron Microscopy. *Curr. Opin. Struct. Biol.* **2019**, *56*, 37–45.
- (61) Alewijnse, B.; Ashton, A. W.; Chambers, M. G.; Chen, S.; Cheng, A.; Ebrahim, M.; Eng, E. T.; Hagen, W. J. H.; Koster, A. J.; López, C. S.; Lukoyanova, N.; Ortega, J.; Renault, L.; Reyntjens, S.; Rice, W. J.; Scapin, G.; Schrijver, R.; Siebert, A.; Stagg, S. M.; Grum-Tokars, V.; Wright, E. R.; Wu, S.; Yu, Z.; Zhou, Z. H.; Carragher, B.; Potter, C. S. Best Practices for Managing Large CryoEM Facilities. *J. Struct. Biol.* **2017**, *199* (3), 225–236.

- (62) Liu, Y.; Huynh, D. T.; Yeates, T. O. A 3.8 Å Resolution Cryo-EM Structure of a Small Protein Bound to an Imaging Scaffold. *Nat. Commun.* **2019**, *10* (1), 1864.
- (63) Wu, S.; Avila-Sakar, A.; Kim, J.; Booth, D. S.; Greenberg, C. H.; Rossi, A.; Liao, M.; Li, X.; Alian, A.; Griner, S. L.; Juge, N.; Yu, Y.; Mergel, C. M.; Chaparro-Riggers, J.; Strop, P.; Tampé, R.; Edwards, R. H.; Stroud, R. M.; Craik, C. S.; Cheng, Y. Fabs Enable Single Particle CryoEM Studies of Small Proteins. *Structure* **2012**, *20* (4), 582–592.
- (64) Zhou, M.; Robinson, C. V. When Proteomics Meets Structural Biology. *Trends Biochem. Sci.* **2010**, *35* (9), 522–529.
- (65) El-Aneed, A.; Cohen, A.; Banoub, J. Mass Spectrometry, Review of the Basics: Electrospray, MALDI, and Commonly Used Mass Analyzers. *Appl. Spectrosc. Rev.* **2009**, *44* (3), 210–230.
- (66) Zenobi, R.; Knochenmuss, R. Ion Formation in MALDI Mass Spectrometry. *Mass Spectrom. Rev.* **1998**, *17* (5), 337–366.
- (67) Seyfried, B. K.; Siekmann, J.; Belgacem, O.; Wenzel, R. J.; Turecek, P. L.; Allmaier, G. MALDI Linear TOF Mass Spectrometry of PEGylated (Glyco)Proteins. *J. Mass Spectrom.* **2010**, *45* (6), 612–617.
- (68) Räder, H.; Schrepp, W. MALDI-TOF Mass Spectrometry in the Analysis of Synthetic Polymers. *Acta Polym.* **1998**, *49* (6), 272–293.
- (69) Chen, F.; Gülbakan, B.; Weidmann, S.; Fagerer, S. R.; Ibáñez, A. J.; Zenobi, R. Applying Mass Spectrometry to Study Non-Covalent Biomolecule Complexes. *Mass Spectrom. Rev.* **2016**, *35* (1), 48–70.
- (70) Kebarle, P.; Verkerk, U. H. Electrospray: From Ions in Solution to Ions in the Gas Phase, What We Know Now. *Mass Spectrom. Rev.* **2009**, *28* (6), 898–917.
- (71) Loo, J. A. Studying Noncovalent Protein Complexes by Electrospray Ionization Mass Spectrometry. *Mass Spectrom. Rev.* **1997**, *16* (1), 1–23.
- (72) Sobott, F.; Robinson, C. V. Characterising Electrosprayed Biomolecules Using Tandem-MS—the Noncovalent GroEL Chaperonin Assembly. *Int. J. Mass Spectrom.* **2004**, *236* (1), 25–32.
- (73) Collier, R. J. Membrane Translocation by Anthrax Toxin. *Mol. Asp. Med.* **2009**, *30* (6), 413–422.
- (74) Petosa, C.; Collier, R. J.; Klimpel, K. R.; Leppla, S. H.; Liddington, R. C. Crystal Structure of the Anthrax Toxin Protective Antigen. *Nature* **1997**, *385* (6619), 833–838.

- (75) Kintzer, A. F.; Thoren, K. L.; Sterling, H. J.; Dong, K. C.; Feld, G. K.; Tang, I. I.; Zhang, T. T.; Williams, E. R.; Berger, J. M.; Krantz, B. A. The Protective Antigen Component of Anthrax Toxin Forms Functional Octameric Complexes. *J. Mol. Biol.* **2009**, *392* (3), 614–629.
- (76) Kintzer, A. F.; Sterling, H. J.; Tang, I. I.; Abdul-Gader, A.; Miles, A. J.; Wallace, B. A.; Williams, E. R.; Krantz, B. A. Role of the Protective Antigen Octamer in the Molecular Mechanism of Anthrax Lethal Toxin Stabilization in Plasma. *J. Mol. Biol.* **2010**, *399* (5), 741–758.
- (77) Gabelica, V.; Marklund, E. Fundamentals of Ion Mobility Spectrometry. *Curr. Opin. Chem. Biol.* **2018**, *42*, 51–59.
- (78) Bush, M. F.; Hall, Z.; Giles, K.; Hoyes, J.; Robinson, C. V.; Ruotolo, B. T. Collision Cross Sections of Proteins and Their Complexes: A Calibration Framework and Database for Gas-Phase Structural Biology. *Anal. Chem.* **2010**, *82* (22), 9557–9565.
- (79) Canzani, D.; Laszlo, K. J.; Bush, M. F. Ion Mobility of Proteins in Nitrogen Gas: Effects of Charge State, Charge Distribution, and Structure. *J. Phys. Chem. A* **2018**, *122* (25), 5625–5634.
- (80) Lee, J. W.; Davidson, K. L.; Bush, M. F.; Kim, H. I. Collision Cross Sections and Ion Structures: Development of a General Calculation Method via High-Quality Ion Mobility Measurements and Theoretical Modeling. *Analyst* **2017**, *142* (22), 4289–4298.
- (81) Ewing, S. A.; Donor, M. T.; Wilson, J. W.; Prell, J. S. Collidoscope: An Improved Tool for Computing Collisional Cross-Sections with the Trajectory Method. *J. Am. Soc. Mass Spectrom.* **2017**, *28* (4), 587–596.
- (82) Rolland, A. D.; Prell, J. S. Computational Insights into Compaction of Gas-Phase Protein and Protein Complex Ions in Native Ion Mobility-Mass Spectrometry. *TrAC Trends Anal. Chem.* **2019**, *116*, 282–291.
- (83) Prell, J. S.; Barceló, D. Modelling Collisional Cross Sections. *Compr. Anal. Chem.* **2019**, *83*, 1–22. <https://doi.org/https://doi.org/10.1016/bs.coac.2018.08.001>.
- (84) Calabrese, A. N.; Radford, S. E. Mass Spectrometry-Enabled Structural Biology of Membrane Proteins. *Methods* **2018**, *147*, 187–205.
- (85) Bolla, J. R.; Agasid, M. T.; Mehmood, S.; Robinson, C. V. Membrane Protein–Lipid Interactions Probed Using Mass Spectrometry. *Annu. Rev. Biochem.* **2019**, *88* (1), 85–111.

- (86) Pukala, T. Importance of Collision Cross Section Measurements by Ion Mobility Mass Spectrometry in Structural Biology. *Rapid Commun. Mass Spectrom.* **2019**, *33* (S3), 72–82.
- (87) Cleary, S. P.; Thompson, A. M.; Prell, J. S. Fourier Analysis Method for Analyzing Highly Congested Mass Spectra of Ion Populations with Repeated Subunits. *Anal. Chem.* **2016**, *88* (12), 6205–6213.
- (88) Cleary, S. P.; Prell, J. S. Liberating Native Mass Spectrometry from Dependence on Volatile Salt Buffers by Use of Gábor Transform. *ChemPhysChem* **2019**, *20* (4), 519–523.
- (89) Marty, M. T.; Hoi, K. K.; Gault, J.; Robinson, C. V. Probing the Lipid Annular Belt by Gas-Phase Dissociation of Membrane Proteins in Nanodiscs. *Angew. Chemie-International Ed.* **2016**, *55* (2), 550–554.
- (90) Keener, J. E.; Zambrano, D. E.; Zhang, G.; Zak, C. K.; Reid, D. J.; Deodhar, B. S.; Pemberton, J. E.; Prell, J. S.; Marty, M. T. Chemical Additives Enable Native Mass Spectrometry Measurement of Membrane Protein Oligomeric State within Intact Nanodiscs. *J. Am. Chem. Soc.* **2019**, *141* (2), 1054–1061.
- (91) Wilson, J. W.; Rolland, A. D.; Klausen, G. M.; Prell, J. S. Ion Mobility-Mass Spectrometry Reveals That α -Hemolysin from *Staphylococcus Aureus* Simultaneously Forms Hexameric and Heptameric Complexes in Detergent Micelle Solutions. *Anal. Chem.* **2019**, *91* (15), 10204–10211.
- (92) Testa, L.; Brocca, S.; Santambrogio, C.; D’Urzo, A.; Habchi, J.; Longhi, S.; Uversky, V. N.; Grandori, R. Extracting Structural Information from Charge-State Distributions of Intrinsically Disordered Proteins by Non-Denaturing Electrospray-Ionization Mass Spectrometry. *Intrinsically Disord. Proteins* **2013**, *1* (1), e25068.
- (93) Pagel, K.; Natan, E.; Hall, Z.; Fersht, A. R.; Robinson, C. V. Intrinsically Disordered P53 and Its Complexes Populate Compact Conformations in the Gas Phase. *Angew. Chemie Int. Ed.* **2013**, *52* (1), 361–365.
- (94) Beveridge, R.; Chappuis, Q.; Macphee, C.; Barran, P. Mass Spectrometry Methods for Intrinsically Disordered Proteins. *Analyst* **2013**, *138* (1), 32–42.
- (95) Sinz, A.; Arlt, C.; Chorev, D.; Sharon, M. Chemical Cross-Linking and Native Mass Spectrometry: A Fruitful Combination for Structural Biology. *Protein Sci.* **2015**, *24* (8), 1193–1209.
- (96) Wittig, S.; Haupt, C.; Hoffmann, W.; Kostmann, S.; Pagel, K.; Schmidt, C. Oligomerisation of Synaptobrevin-2 Studied by Native Mass Spectrometry and Chemical Cross-Linking. *J. Am. Soc. Mass Spectrom.* **2019**, *30* (1), 149–160.

- (97) Liu, F.; Lössl, P.; Rabbitts, B. M.; Balaban, R. S.; Heck, A. J. R. The Interactome of Intact Mitochondria by Cross-Linking Mass Spectrometry Provides Evidence for Coexisting Respiratory Supercomplexes. *Mol. & Cell. Proteomics* **2018**, *17* (2), 216 LP – 232.
- (98) Ruotolo, B. T.; Giles, K.; Campuzano, I.; Sandercock, A. M.; Bateman, R. H.; Robinson, C. V. Evidence for Macromolecular Protein Rings in the Absence of Bulk Water. *Science (80-.)*. **2005**, *310* (5754), 1658–1661.
- (99) Li, H.; Nguyen, H. H.; Ogorzalek Loo, R. R.; Campuzano, I. D. G.; Loo, J. A. An Integrated Native Mass Spectrometry and Top-down Proteomics Method That Connects Sequence to Structure and Function of Macromolecular Complexes. *Nat. Chem.* **2018**, *10* (2), 139–148.
- (100) D’Antona, A. M.; Xie, G. F.; Sligar, S. G.; Oprian, D. D. Assembly of an Activated Rhodopsin-Transducin Complex in Nanoscale Lipid Bilayers. *Biochemistry* **2014**, *53* (1), 127–134.
- (101) Albanese, P.; Tamara, S.; Saracco, G.; Scheltema, R. A.; Pagliano, C. How Paired PSII–LHCII Supercomplexes Mediate the Stacking of Plant Thylakoid Membranes Unveiled by Structural Mass-Spectrometry. *Nat. Commun.* **2020**, *11* (1), 1361.
- (102) Barrera, N. P.; Di Bartolo, N.; Booth, P. J.; Robinson, C. V. Micelles Protect Membrane Complexes from Solution to Vacuum. *Science (80-.)*. **2008**, *321* (5886), 243–246.
- (103) Allison, T. M.; Landreh, M.; Benesch, J. L. P.; Robinson, C. V. Low Charge and Reduced Mobility of Membrane Protein Complexes Has Implications for Calibration of Collision Cross Section Measurements. *Anal. Chem.* **2016**, *88* (11), 5879–5884.
- (104) Reading, E.; Liko, I.; Allison, T. M.; Benesch, J. L. P.; Laganowsky, A.; Robinson, C. V. The Role of the Detergent Micelle in Preserving the Structure of Membrane Proteins in the Gas Phase. *Angew. Chemie Int. Ed.* **2015**, *54* (15), 4577–4581.
- (105) Pliotas, C.; Dahl, A. C. E.; Rasmussen, T.; Mahendran, K. R.; Smith, T. K.; Marius, P.; Gault, J.; Banda, T.; Rasmussen, A.; Miller, S.; Robinson, C. V.; Bayley, H.; Sansom, M. S. P.; Booth, I. R.; Naismith, J. H. The Role of Lipids in Mechanosensation. *Nat. Struct. Mol. Biol.* **2015**, *22*, 991–998.
- (106) Marcoux, J.; Wang, S. C.; Politis, A.; Reading, E.; Ma, J.; Biggin, P. C.; Zhou, M.; Tao, H.; Zhang, Q.; Chang, G.; Morgner, N.; Robinson, C. V. Mass Spectrometry Reveals Synergistic Effects of Nucleotides, Lipids, and Drugs Binding to a Multidrug Resistance Efflux Pump. *Proc. Natl. Acad. Sci.* **2013**, *110* (24), 9704 LP – 9709.

- (107) Liu, Y.; Cong, X.; Liu, W.; Laganowsky, A. Characterization of Membrane Protein–Lipid Interactions by Mass Spectrometry Ion Mobility Mass Spectrometry. *J. Am. Soc. Mass Spectrom.* **2017**, *28* (4), 579–586.
- (108) Patrick, J. W.; Boone, C. D.; Liu, W.; Conover, G. M.; Liu, Y.; Cong, X.; Laganowsky, A. Allostery Revealed within Lipid Binding Events to Membrane Proteins. *Proc. Natl. Acad. Sci.* **2018**, *115* (12), 2976–2981.
- (109) Hopper, J. T. S.; Yu, Y. T. C.; Li, D. F.; Raymond, A.; Bostock, M.; Liko, I.; Mikhailov, V.; Laganowsky, A.; Benesch, J. L. P.; Caffrey, M.; Nietlispach, D.; Robinson, C. V. Detergent-Free Mass Spectrometry of Membrane Protein Complexes. *Nat. Methods* **2013**, *10* (12), 1206–1208.
- (110) Hoi, K. K.; Robinson, C. V.; Marty, M. T. Unraveling the Composition and Behavior of Heterogeneous Lipid Nanodiscs by Mass Spectrometry. *Anal. Chem.* **2016**, *88* (12), 6199–6204.
- (111) Marty, M. T.; Zhang, H.; Cui, W. D.; Gross, M. L.; Sligar, S. G. Interpretation and Deconvolution of Nanodisc Native Mass Spectra. *J. Am. Soc. Mass Spectrom.* **2014**, *25* (2), 269–277.
- (112) Townsend, J. A.; Keener, J. E.; Miller, Z. M.; Prell, J. S.; Marty, M. T. Imidazole Derivatives Improve Charge Reduction and Stabilization for Native Mass Spectrometry. *Anal. Chem.* **2019**, *91* (22), 14765–14772.
- (113) Chorev, D. S.; Baker, L. A.; Wu, D.; Beilsten-Edmands, V.; Rouse, S. L.; Zeev-Ben-Mordehai, T.; Jiko, C.; Samsudin, F.; Gerle, C.; Khalid, S.; Stewart, A. G.; Matthews, S. J.; Grünewald, K.; Robinson, C. V. Protein Assemblies Ejected Directly from Native Membranes Yield Complexes for Mass Spectrometry. *Science* (80-.). **2018**, *362* (6416), 829 LP – 834.
- (114) Chorev, D. S.; Tang, H.; Rouse, S. L.; Bolla, J. R.; von Kügelgen, A.; Baker, L. A.; Wu, D.; Gault, J.; Grünewald, K.; Bharat, T. A. M.; Matthews, S. J.; Robinson, C. V. The Use of Sonicated Lipid Vesicles for Mass Spectrometry of Membrane Protein Complexes. *Nat. Protoc.* **2020**.
- (115) Allison, T. M.; Reading, E.; Liko, I.; Baldwin, A. J.; Laganowsky, A.; Robinson, C. V. Quantifying the Stabilizing Effects of Protein–Ligand Interactions in the Gas Phase. *Nat. Commun.* **2015**, *6*, 8551.
- (116) Cong, X.; Liu, Y.; Liu, W.; Liang, X.; Russell, D. H.; Laganowsky, A. Determining Membrane Protein–Lipid Binding Thermodynamics Using Native Mass Spectrometry. *J. Am. Chem. Soc.* **2016**, *138* (13), 4346–4349.

- (117) Wörner, T. P.; Snijder, J.; Bennett, A.; Agbandje-McKenna, M.; Makarov, A. A.; Heck, A. J. R. Resolving Heterogeneous Macromolecular Assemblies by Orbitrap-Based Single-Particle Charge Detection Mass Spectrometry. *Nat. Methods* **2020**, *17* (4), 395–398.
- (118) Cleary, S. P.; Li, H.; Bagal, D.; Loo, J. A.; Campuzano, I. D. G.; Prell, J. S. Extracting Charge and Mass Information from Highly Congested Mass Spectra Using Fourier-Domain Harmonics. *J. Am. Soc. Mass Spectrom.* **2018**, *29* (10), 2067–2080.
- (119) Stengel, F.; Baldwin, A. J.; Bush, M. F.; Hilton, G. R.; Lioe, H.; Basha, E.; Jaya, N.; Vierling, E.; Benesch, J. L. P. Dissecting Heterogeneous Molecular Chaperone Complexes Using a Mass Spectrum Deconvolution Approach. *Chem. Biol.* **2012**, *19* (5), 599–607.
- (120) Katayama, H.; Wang, J.; Tama, F.; Chollet, L.; Gogol, E. P.; Collier, R. J.; Fisher, M. T. Three-Dimensional Structure of the Anthrax Toxin Pore Inserted into Lipid Nanodiscs and Lipid Vesicles. *Proc. Natl. Acad. Sci. U. S. A.* **2010**, *107* (8), 3453–3457.
- (121) Akkaladevi, N.; Hinton-Chollet, L.; Katayama, H.; Mitchell, J.; Szerszen, L.; Mukherjee, S.; Gogol, E. P.; Pentelute, B. L.; Collier, R. J.; Fisher, M. T. Assembly of Anthrax Toxin Pore: Lethal-Factor Complexes into Lipid Nanodiscs. *Protein Sci.* **2013**, *22* (4), 492–501.
- (122) Hardenbrook, N. J.; Liu, S.; Zhou, K.; Ghosal, K.; Hong Zhou, Z.; Krantz, B. A. Atomic Structures of Anthrax Toxin Protective Antigen Channels Bound to Partially Unfolded Lethal and Edema Factors. *Nat. Commun.* **2020**, *11* (1), 840.
- (123) Goodsell, D. S.; Olson, A. J. Structural Symmetry and Protein Function. *Annu. Rev. Biophys. Biomol. Struct.* **2000**, *29* (1), 105–153.
- (124) Forrest, L. R. Structural Symmetry in Membrane Proteins. *Annu. Rev. Biophys.* **2015**, *44* (1), 311–337.
- (125) Levy, E. D.; Pereira-Leal, J. B.; Chothia, C.; Teichmann, S. A. 3D Complex: A Structural Classification of Protein Complexes. *PLOS Comput. Biol.* **2006**, *2* (11), e155.
- (126) Levy, E. D.; Teichmann, S. A. Chapter Two - Structural, Evolutionary, and Assembly Principles of Protein Oligomerization. In *Progress in Molecular Biology and Translational Science*; Giraldo, J., Ciruela, F., Eds.; Academic Press, 2013; Vol. 117, pp 25–51.

- (127) van Breukelen, B.; Barendregt, A.; Heck, A. J. R.; van den Heuvel, R. H. H. Resolving Stoichiometries and Oligomeric States of Glutamate Synthase Protein Complexes with Curve Fitting and Simulation of Electrospray Mass Spectra. *Rapid Commun. Mass Spectrom.* **2006**, *20* (16), 2490–2496.
- (128) Spinozzi, F.; Mariani, P.; Mičetić, I.; Ferrero, C.; Pontoni, D.; Beltramini, M. Quaternary Structure Heterogeneity of Oligomeric Proteins: A SAXS and SANS Study of the Dissociation Products of Octopus Vulgaris Hemocyanin. *PLoS One* **2012**, *7* (11), e49644.
- (129) Beam, M.; Silva, M. C.; Morimoto, R. I. Dynamic Imaging by Fluorescence Correlation Spectroscopy Identifies Diverse Populations of Polyglutamine Oligomers Formed in Vivo. *J. Biol. Chem.* **2012**, *287* (31), 26136–26145.
- (130) Kintzer, A. F.; Thoren, K. L.; Sterling, H. J.; Dong, K. C.; Feld, G. K.; Tang, I. I.; Zhang, T. T.; Williams, E. R.; Berger, J. M.; Krantz, B. A. The Protective Antigen Component of Anthrax Toxin Forms Functional Octameric Complexes. *J. Mol. Biol.* **2009**, *392*, 614–629.
- (131) Berube, J. B.; Wardenburg, B. J. Staphylococcus Aureus α -Toxin: Nearly a Century of Intrigue. *Toxins (Basel)*. **2013**, *5* (6), 1140–1166.
- (132) Tong, S. Y. C.; Davis, J. S.; Eichenberger, E.; Holland, T. L.; Fowler, V. G. Staphylococcus Aureus Infections: Epidemiology, Pathophysiology, Clinical Manifestations, and Management. *Clin Microbiol Rev* **2015**, *28* (3), 603–661.
- (133) Lubkin, A.; Torres, V. The Ever-Emerging Complexity of α -Toxin's Interaction with Host Cells. *Proc. Natl. Acad. Sci. U. S. A.* **2015**, *112* (46), 201519766.
- (134) Popov, L. M.; Marceau, C. D.; Starkl, P. M.; Lumb, J. H.; Shah, J.; Guerrero, D.; Cooper, R. L.; Merakou, C.; Bouley, D. M.; Meng, W.; Kiyonari, H.; Takeichi, M.; Galli, S. J.; Bagnoli, F.; Citi, S.; Carette, J. E.; Amieva, M. R. The Adherens Junctions Control Susceptibility to Staphylococcus Aureus α -Toxin. *Proc. Natl. Acad. Sci.* **2015**, *112* (46), 14337–14342.
- (135) Ayub, M.; Bayley, H. Engineered Transmembrane Pores. *Curr. Opin. Chem. Biol.* **2016**, *34*, 117–126.
- (136) Gu, L.-Q.; Braha, O.; Conlan, S.; Cheley, S.; Bayley, H. Stochastic Sensing of Organic Analytes by a Pore-Forming Protein Containing a Molecular Adapter. *Nature* **1999**, *398* (6729), 686–690.
- (137) Kasianowicz, J. J.; Brandin, E.; Branton, D.; Deamer, D. W. Characterization of Individual Polynucleotide Molecules Using a Membrane Channel. *Proc. Natl. Acad. Sci.* **1996**, *93* (24), 13770–13773.

- (138) Deamer, D. W.; Branton, D. Characterization of Nucleic Acids by Nanopore Analysis. *Acc. Chem. Res.* **2002**, *35* (10), 817–825.
- (139) Bayley, H. Nanopore Sequencing: From Imagination to Reality. *Clin. Chem.* **2015**, *61* (1), 25–31.
- (140) Qing, Y.; Ionescu, S. A.; Pulcu, G. S.; Bayley, H. Directional Control of a Processive Molecular Hopper. *Science (80-.)*. **2018**, *361* (6405), 908–912.
- (141) Arbuthnott, J. P.; Freer, J. H.; Bernheimer, A. W. Physical States of Staphylococcal Alpha-Toxin. *J. bacteriol.* **1967**, *94* (4), 1170–1177.
- (142) Olofsson, A.; Kavéus, U.; Thelestam, M.; Hebert, H. The Projection Structure of α -Toxin from Staphylococcus Aureus in Human Platelet Membranes as Analyzed by Electron Microscopy and Image Processing. *J. Ultrastruct. Mol. Struct. Res.* **1988**, *100* (2), 194–200.
- (143) Ward, R. J.; Leonard, K. The Staphylococcus Aureus α -Toxin Channel Complex and the Effect of Ca²⁺ Ions on Its Interaction with Lipid Layers. *J. Struct. Biol.* **1992**, *109* (2), 129–141.
- (144) Czajkowsky, D. M.; Sheng, S.; Shao, Z. Staphylococcal α -Hemolysin Can Form Hexamers in Phospholipid Bilayers. *J. Mol. Biol.* **1998**, *276* (2), 325–330.
- (145) Furini, S.; Domene, C.; Rossi, M.; Tartagni, M.; Cavalcanti, S. Model-Based Prediction of the α -Hemolysin Structure in the Hexameric State. *Biophys. J.* **2008**, *95* (5), 2265–2274.
- (146) Bhakdi, S.; Füssle, R.; Tranum-Jensen, J. Staphylococcal Alpha-Toxin: Oligomerization of Hydrophilic Monomers to Form Amphiphilic Hexamers Induced through Contact with Deoxycholate Detergent Micelles. *Proc. Natl. Acad. Sci.* **1981**, *78* (9), 5475–5479.
- (147) Gouaux, J. E.; Braha, O.; Hobaugh, M. R.; Song, L.; Cheley, S.; Shustak, C.; Bayley, H. Subunit Stoichiometry of Staphylococcal Alpha-Hemolysin in Crystals and on Membranes: A Heptameric Transmembrane Pore. *Proc. Natl. Acad. Sci.* **1994**, *91* (26), 12828–12831.
- (148) Song, L.; Hobaugh, M. R.; Shustak, C.; Cheley, S.; Bayley, H.; Gouaux, J. E. Structure of Staphylococcal α -Hemolysin, a Heptameric Transmembrane Pore. *Science (80-.)*. **1996**, *274* (5294), 1859–1865.
- (149) Galdiero, S.; Gouaux, E. High Resolution Crystallographic Studies of α -Hemolysin–Phospholipid Complexes Define Heptamer–Lipid Head Group Interactions: Implication for Understanding Protein–Lipid Interactions. *Protein Sci.* **2004**, *13* (6), 1503–1511.

- (150) Banerjee, A.; Mikhailova, E.; Cheley, S.; Gu, L.-Q.; Montoya, M.; Nagaoka, Y.; Gouaux, E.; Bayley, H. Molecular Bases of Cyclodextrin Adapter Interactions with Engineered Protein Nanopores. *Proc. Natl. Acad. Sci.* **2010**, *107* (18), 8165–8170.
- (151) Tanaka, Y.; Hirano, N.; Kaneko, J.; Kamio, Y.; Yao, M.; Tanaka, I. 2-Methyl-2,4-Pentanediol Induces Spontaneous Assembly of Staphylococcal α -Hemolysin into Heptameric Pore Structure. *Protein Sci.* **2011**, *20* (2), 448–456.
- (152) Das, S. K.; Darshi, M.; Cheley, S.; Wallace, M. I.; Bayley, H. Membrane Protein Stoichiometry Determined from the Step-Wise Photobleaching of Dye-Labelled Subunits. *ChemBioChem* **2007**, *8* (9), 994–999.
- (153) Hammerstein, A. F.; Jayasinghe, L.; Bayley, H. Subunit Dimers of α -Hemolysin Expand the Engineering Toolbox for Protein Nanopores. *J. Biol. Chem.* **2011**, *286* (16), 14324–14334.
- (154) Otto, M. Staphylococcus Aureus Toxins. *Curr. Opin. Microbiol.* **2014**, *17*, 32–37.
- (155) Liko, I.; Allison, T. M.; Hopper, J. T. S.; Robinson, C. V. Mass Spectrometry Guided Structural Biology. *Curr. Opin. Struct. Biol.* **2016**, *40*, 136–144..
- (156) Podobnik, M.; Savory, P.; Rojko, N.; Kisovec, M.; Wood, N.; Hambley, R.; Pugh, J.; Wallace, E. J.; McNeill, L.; Bruce, M.; Liko, I.; Allison, T. M.; Mehmood, S.; Yilmaz, N.; Kobayashi, T.; Gilbert, R. J. C.; Robinson, C. V.; Jayasinghe, L.; Anderluh, G. Crystal Structure of an Invertebrate Cytolysin Pore Reveals Unique Properties and Mechanism of Assembly. *Nat. Commun.* **2016**, *7* (11598), 1–10.
- (157) Barrera, N. P.; Isaacson, S. C.; Zhou, M.; Bavro, V. N.; Welch, A.; Schaedler, T. A.; Seeger, M. A.; Miguel, R. N.; Korkhov, V. M.; van Veen, H. W.; Venter, H.; Walmsley, A. R.; Tate, C. G.; Robinson, C. V. Mass Spectrometry of Membrane Transporters Reveals Subunit Stoichiometry and Interactions. *Nat. Methods* **2009**, *6* (8), 585–587.
- (158) Laganowsky, A.; Reading, E.; Hopper, J. T. S.; Robinson, C. V. Mass Spectrometry of Intact Membrane Protein Complexes. *Nat. Protoc.* **2013**, *8* (4), 639–651.
- (159) Watanabe, M.; Tomita, T.; Yasuda, T. Membrane-Damaging Action of Staphylococcal Alpha-Toxin on Phospholipid-Cholesterol Liposomes. *Biochim. Biophys. Acta-Biomembranes* **1987**, *898* (3), 257–265.
- (160) Marty, M. T.; Baldwin, A. J.; Marklund, E. G.; Hochberg, G. K. A.; Benesch, J. L. P.; Robinson, C. V. Bayesian Deconvolution of Mass and Ion Mobility Spectra: From Binary Interactions to Polydisperse Ensembles. *Anal. Chem.* **2015**, *87* (8), 4370–4376.

- (161) Reid, D. J.; Diesing, J. M.; Miller, M. A.; Perry, S. M.; Wales, J. A.; Montfort, W. R.; Marty, M. T. MetaUniDec: High-Throughput Deconvolution of Native Mass Spectra. *J. Am. Soc. Mass Spectrom.* **2018**.
- (162) Seo, J.; Hoffmann, W.; Warnke, S.; Bowers, M. T.; Pagel, K.; von Helden, G. Retention of Native Protein Structures in the Absence of Solvent: A Coupled Ion Mobility and Spectroscopic Study. *Angew. Chemie Int. Ed.* **2016**, *55* (45), 14173–14176.
- (163) Hildebrand, A.; Pohl, M.; Bhakdi, S. Staphylococcus Aureus Alpha-Toxin. Dual Mechanism of Binding to Target Cells. *J. Biol. Chem.* **1991**, *266* (26), 17195–17200.
- (164) Wilke, G. A.; Wardenburg, J. B. Role of a Disintegrin and Metalloprotease 10 in Staphylococcus Aureus α -Hemolysin-Mediated Cellular Injury. *Proc. Natl. Acad. Sci.* **2010**, *107* (30), 13473–13478.
- (165) Tomita, T.; Watanabe, M.; Yasuda, T. Influence of Membrane Fluidity on the Assembly of Staphylococcus Aureus Alpha-Toxin, a Channel-Forming Protein, in Liposome Membrane. *J. Biol. Chem.* **1992**, *267* (19), 13391–13397.
- (166) Rostom, A. A.; Robinson, C. V. Detection of the Intact GroEL Chaperonin Assembly by Mass Spectrometry. *J. Am. Chem. Soc.* **1999**, *121* (19), 4718–4719.
- (167) Sobott, F.; Hernández, H.; McCammon, M. G.; Tito, M. A.; Robinson, C. V. A Tandem Mass Spectrometer for Improved Transmission and Analysis of Large Macromolecular Assemblies. *Anal. Chem.* **2002**, *74* (6), 1402–1407.
- (168) Landreh, M.; Liko, I.; Uzdavinyš, P.; Coincon, M.; Hopper, J. T. S.; Drew, D.; Robinson, C. V. Controlling Release, Unfolding and Dissociation of Membrane Protein Complexes in the Gas Phase through Collisional Cooling. *Chem. Commun.* **2015**, *51* (85), 15582–15584.
- (169) Freeke, J.; Robinson, C. V.; Ruotolo, B. T. Residual Counter Ions Can Stabilise a Large Protein Complex in the Gas Phase. *Int. J. Mass Spectrom.* **2010**, *298* (1–3), 91–98.
- (170) Gabelica, V.; Pauw, E. De. Internal Energy and Fragmentation of Ions Produced in Electrospray Sources. *Mass Spectrom. Rev.* **2005**, *24* (4), 566–587.
- (171) Krutchinsky, A. N.; Chernushevich, I. V.; Spicer, V. L.; Ens, W.; Standing, K. G. Collisional Damping Interface for an Electrospray Ionization Time-of-Flight Mass Spectrometer. *J. Am. Soc. Mass Spectrom.* **1998**, *9* (6), 569–579.

- (172) Chernushevich, I. V.; Thomson, B. A. Collisional Cooling of Large Ions in Electrospray Mass Spectrometry. *Anal. Chem.* **2004**, *76* (6), 1754–1760.
- (173) Tahallah, N.; Pinkse, M.; Maier, C. S.; Heck, A. J. R. The Effect of the Source Pressure on the Abundance of Ions of Noncovalent Protein Assemblies in an Electrospray Ionization Orthogonal Time-of-Flight Instrument. *Rapid Commun. Mass Spectrom.* **2001**, *15* (8), 596–601. <https://doi.org/10.1002/rcm.275>.
- (174) Donor, M. T.; Mroz, A. M.; Prell, J. S. Experimental and Theoretical Investigation of Overall Energy Deposition in Surface-Induced Unfolding of Protein Ions. *Chem. Sci.* **2019**, *10* (14), 4097–4106.
- (175) Zhou, M.; Jones, C. M.; Wysocki, V. H. Dissecting the Large Noncovalent Protein Complex GroEL with Surface-Induced Dissociation and Ion Mobility–Mass Spectrometry. *Anal. Chem.* **2013**, *85* (17), 8262–8267.
- (176) Bolla, J. R.; Corey, R. A.; Sahin, C.; Gault, J.; Hummer, A.; Hopper, J. T. S.; Lane, D. P.; Drew, D.; Allison, T. M.; Stansfeld, P. J.; Robinson, C. V.; Landreh, M. A Mass Spectrometry-Based Approach to Distinguish Annular and Specific Lipid Binding to Membrane Proteins. *Angew. Chemie Int. Ed.* **2020**, *59*, DOI: 10.1002/anie.201914411.
- (177) Bechara, C.; Robinson, C. V. Different Modes of Lipid Binding to Membrane Proteins Probed by Mass Spectrometry. *J. Am. Chem. Soc.* **2015**, *137* (16), 5240–5247.
- (178) Harvey, S. R.; Liu, Y.; Liu, W.; Wysocki, V. H.; Laganowsky, A. Surface Induced Dissociation as a Tool to Study Membrane Protein Complexes. *Chem. Commun.* **2017**, *53* (21), 3106–3109.
- (179) Walker, L. R.; Marzluff, E. M.; Townsend, J. A.; Resager, W. C.; Marty, M. T. Native Mass Spectrometry of Antimicrobial Peptides in Lipid Nanodiscs Elucidates Complex Assembly. *Anal. Chem.* **2019**, *91* (14), 9284–9291.
- (180) Han, L.; Kitova, E. N.; Li, J.; Nikjah, S.; Lin, H.; Pluvinage, B.; Boraston, A. B.; Klassen, J. S. Protein–Glycolipid Interactions Studied in Vitro Using ESI-MS and Nanodiscs: Insights into the Mechanisms and Energetics of Binding. *Anal. Chem.* **2015**, *87* (9), 4888–4896.
- (181) Zhang, Y. X.; Liu, L.; Daneshfar, R.; Kitova, E. N.; Li, C. S.; Jia, F.; Cairo, C. W.; Klassen, J. S. Protein-Glycosphingolipid Interactions Revealed Using Catch-and-Release Mass Spectrometry. *Anal. Chem.* **2012**, *84* (18), 7618–7621.
- (182) Liu, Y.; LoCaste, C. E.; Liu, W.; Poltash, M. L.; Russell, D. H.; Laganowsky, A. Selective Binding of a Toxin and Phosphatidylinositides to a Mammalian Potassium Channel. *Nat. Commun.* **2019**, *10* (1), 1352.

- (183) Sun, J.; Kitova, E. N.; Sun, N.; Klassen, J. S. Method for Identifying Nonspecific Protein–Protein Interactions in Nano electrospray Ionization Mass Spectrometry. *Anal. Chem.* **2007**, *79* (21), 8301–8311.
- (184) Kitova, E. N.; El-Hawiet, A.; Schnier, P. D.; Klassen, J. S. Reliable Determinations of Protein–Ligand Interactions by Direct ESI-MS Measurements. Are We There Yet? *J. Am. Soc. Mass Spectrom.* **2012**, *23* (3), 431–441.
- (185) Kitov, P. I.; Han, L.; Kitova, E. N.; Klassen, J. S. Sliding Window Adduct Removal Method (SWARM) for Enhanced Electrospray Ionization Mass Spectrometry Binding Data. *J. Am. Soc. Mass Spectrom.* **2019**, *30* (8), 1446–1454..
- (186) Landreh, M.; Costeira-Paulo, J.; Gault, J.; Marklund, E. G.; Robinson, C. V. Effects of Detergent Micelles on Lipid Binding to Proteins in Electrospray Ionization Mass Spectrometry. *Anal. Chem.* **2017**, *89* (14), 7425–7430.
- (187) Roscioli, J. R.; McCunn, L. R.; Johnson, M. A. Quantum Structure of the Intermolecular Proton Bond. *Science (80-.)*. **2007**, *316* (5822), 249–254.
- (188) Miller, Z. M.; Zhang, J. D.; Donald, W. A.; Prell, J. S. Gas-Phase Protonation Thermodynamics of Biological Lipids: Experiment, Theory, and Implications. *Anal. Chem.* **2020**, in revision.
- (189) Gupta, K.; Li, J.; Liko, I.; Gault, J.; Bechara, C.; Wu, D.; Hopper, J. T. S.; Giles, K.; Benesch, J. L. P.; Robinson, C. V. Identifying Key Membrane Protein Lipid Interactions Using Mass Spectrometry. *Nat. Protoc.* **2018**, *13* (5), 1106–1120.
- (190) Bayburt, T. H.; Sligar, S. G. Membrane Protein Assembly into Nanodiscs. *Febs Lett.* **2010**, *584* (9), 1721–1727.
- (191) Denisov, I. G.; Sligar, S. G. Nanodiscs in Membrane Biochemistry and Biophysics. *Chem. Rev.* **2017**, *117* (6), 4669–4713.
- (192) Denisov, I. G.; Grinkova, Y. V.; Lazarides, A. A.; Sligar, S. G. Directed Self-Assembly of Monodisperse Phospholipid Bilayer Nanodiscs with Controlled Size. *J. Am. Chem. Soc.* **2004**, *126* (11), 3477–3487. <https://doi.org/10.1021/ja0393574>.
- (193) Denisov, I. G.; Baas, B. J.; Grinkova, Y. V.; Sligar, S. G. Cooperativity in Cytochrome P450 3A4: LINKAGES IN SUBSTRATE BINDING, SPIN STATE, UNCOUPLING, AND PRODUCT FORMATION. *J. Biol. Chem.* **2007**, *282* (10), 7066–7076.
- (194) Sinelnikov, I.; Kitova, E. N.; Klassen, J. S. Influence of Coulombic Repulsion on the Dissociation Pathways and Energetics of Multiprotein Complexes in the Gas Phase. *J. Am. Soc. Mass Spectrom.* **2007**, *18* (4), 617–631.

- (195) Hall, Z.; Politis, A.; Bush, M. F.; Smith, L. J.; Robinson, C. V. Charge-State Dependent Compaction and Dissociation of Protein Complexes: Insights from Ion Mobility and Molecular Dynamics. *J. Am. Chem. Soc.* **2012**, *134* (7), 3429–3438.
- (196) Cong, X.; Liu, Y.; Liu, W.; Liang, X.; Russell, D. H.; Laganowsky, A. Determining Membrane Protein–Lipid Binding Thermodynamics Using Native Mass Spectrometry. *J. Am. Chem. Soc.* **2016**, *138* (13), 4346–4349. <https://doi.org/10.1021/jacs.6b01771>.
- (197) Salbo, R.; Bush, M. F.; Naver, H.; Campuzano, I.; Robinson, C. V.; Pettersson, I.; Jørgensen, T. J. D.; Haselmann, K. F. Traveling-Wave Ion Mobility Mass Spectrometry of Protein Complexes: Accurate Calibrated Collision Cross-Sections of Human Insulin Oligomers. *Rapid Commun. Mass Spectrom.* **2012**, *26* (10), 1181–1193.